ANALYSIS AND MODELLING OF A NOVEL APPROACH FOR THE INTERROGATION UNIT OF FIBER BRAGG GRATING SENSORS USING OPTICAL FREQUENCY DOMAIN REFLECTOMETRY TECHNIQUES

A Thesis Submitted to
the Graduate School of Engineering and Sciences of
İzmir Institute of Technology
in Partial Fulfillment of the Requirements for the Degree of

MASTER OF SCIENCE

in Electronics and Communication Engineering

by
Deniz PALA

July 2014
İZMİR

We approve the thesis of **Deniz PALA**

Examining Committee Members:

Assist. Prof. Dr. Kıvılcım YÜKSEL ALDOĞAN
Department of Electrical and Electronics Engineering
Izmir Institute of Technology

Prof. Dr. M. Salih DİNLEYİCİ
Department of Electrical and Electronics Engineering
Izmir Institute of Technology

Assoc. Prof. Dr. Metin SABUNCU
Department of Electrical and Electronics Engineering
Dokuz Eylül University

9 July 2014

Assist. Prof. Dr. Kıvılcım YÜKSEL ALDOĞAN
Supervisor, Department of Electrical and Electronics Engineering
Izmir Institute of Technolog

Prof. Dr. M. Salih DİNLEYİCİ
Head of the Department of
Electrical and Electronics Engineering

Prof. Dr. R. Tuğrul SENGER
Dean of the Graduate School of
Engineering and Sciences

ACKNOWLEDGEMENTS

I would like to express my gratitude to my supervisor Assist. Prof. Dr. Kıvılcım YÜKSEL ALDOĞAN for her scientific guidance, support and motivation during this study and preparation of this thesis.

I would also like to express my gratitude to my committee members Prof. Dr. M. Salih DİNLEYİCİ and Assoc. Prof. Dr. Metin SABUNCU for their contributions.

There are too many people that I want to express my positive feelings and thankfulness. Firstly, I want to thank my lovely husband Arda for his never-ending love, support and understanding. Without him, this study would be more and more difficult. I would like to thank my parents Muzaffer, Dilek, Melis, Cenk, Atlas, Nuray and Halil for their patience and support throughout my master. I would also like to thank all my colleagues Oktay Karakuş, İlhan Baştürk, Göksenin Bozdağ, Başak Esin Köktürk, Esra Aycan, Tufan Bakırcıgil, Burçin Güzel for their support and friendship.

ABSTRACT

ANALYSIS AND MODELLING OF A NOVEL APPROACH FOR THE INTERROGATION UNIT OF FIBER BRAGG GRATING SENSORS USING OPTICAL FREQUENCY DOMAIN REFLECTOMETRY TECHNIQUES

The main purpose of this thesis is to demonstrate the feasibility of using polarization properties of FBGs interrogated by OFDR for quasi-distributed sensing applications.

A fiber Bragg grating (FBG) is a constant and periodic refractive index value modulation within the core along an optical fiber. This modification is generally obtained by exposing the fiber core of a photosensitive optical fiber to an intense ultraviolet (UV) interference pattern. At the fabrication process of Bragg gratings, only one side of the fiber expose to UV light. As a result, refractive index change is not constant at the cross section of fiber. This non-uniformity on the refractive index gives rise to *photo-induced birefringence* which combines with the birefringence resulting from the slightly elliptical shape of the optical fiber and creates a *global birefringence* value.

In the presence of the birefringence, the reflection (transmission) spectrum of Bragg grating is degenerated into two reflection (transmission) spectra corresponding to a pair of orthogonal polarization modes (x and y modes). The ratio between maximum and minimum optical transmitted power of these modes are defined as Polarization Dependent Loss (PDL).

We analyzed the reflection spectrum, transmission spectrum and the PDL of the cascaded FBGs interrogated by an OFDR by the way of simulations. Based on the simulation results, we demonstrated the feasibility of a novel FBG interrogation method which can be implemented in quasi-distributed strain sensors embedded into composite materials.

ÖZET

FREKANS BÖLGESİNDE OPTİK YANSIMA ÖLÇÜM TEKNİKLERİ KULLANILARAK FİBER BRAGG IZGARA SENSÖRLERİNİN SORGU ÜNİTESİ İÇİN YENİ BİR YAKLAŞIMIN ANALİZ VE MODELLENMESİ

Bu çalışmanın ana hedefi, fiber Bragg ızgaraya ait (fiber Bragg grating, FBG) polarizasyon özelliklerinin, frekans bölgesinde optik yansıtıcı (Optical Frequency Domain Reflectometer, OFDR) kullanılarak sorgulanmasıyla gerçekleştirilen yeni bir sensör yaklaşımının uygulanabilirliğinin incelemektir.

Bragg ızgaralar, fiber optik çekirdek (core) kırılma indisinin kalıcı bir şekilde ve periyodik olarak değiştirilmesiyle elde edilir. Fiber çekirdek indisindeki bu modulasyon sonucu, fiber içinde aksi yönlerde ilerleyen iki mod arasında rezonans dalga boyu (Bragg wavelength) çevresinde enerji aktarımı meydana gelir. Izgaraya uygulanacak bazı fiziksel etkiler (sıcaklık, gerilme vb.) Bragg dalga boyunun değişimi ile gözlenebilir. Bragg ızgaraların fabrika üretimi boyunca fiberin yalnızca bir kısmı mor ötesi (UV) lazere maruz kalır ve bu sebeple fiberin dairesel kesiti boyunca kırılma indisi sabit değildir. Kırılma indisindeki bu düzensizlik ışıkla indüklenen çift kırınıma (*birefringence*) neden olur ve fiberin hafif eliptik şeklinden kaynaklanan çift kırınımla birleşerek genel çift kırınımı oluşturur.

Çift kırınımın varlığında Bragg ızgaranın iletim ve yansıma katsayıları iki moda ayrılır (x- ve y- modu). Bu modların maksimum ve minimum optik çıkış güçleri arasındaki oran polarizasyona bağlı kayıp (Polarization Dependent Loss, PDL) olarak tanımlanır.

Çalışmada art arda bağlanmış ve frekans bölgesinde optik yansıtıcı ile sorgulanan fiber Bragg ızgaraların iletim ve yansıma spektrumları ile polarizasyona bağlı kaybını simülasyonlar yoluyla analiz ettik. Simülasyon sonuçları, fiber Bragg ızgaranın polarizasyon özelliklerinin OFDR tarafından sorgulanabilir olduğunu göstermiştir. Nihai bir uygulama alanı olarak ise kompozit malzeme içine gömülmüş yarı-dağıtık gerinim (strain) sensörleri, önerdiğimiz test sistemi kullanılarak tasarlanabilir.

TABLE OF CONTENTS

LIST OF FIGURES

LIST OF TABLES

LIST OF ABBREVIATIONS

C-OFDR	Coherent Optical Frequency Domain Reflectometer
EMI	Electromagnetic Interference
FBGs	Fiber Bragg Gratings
FFT	Fast Fourier Transform
FMCW	Frequency Modulated Continuous Wave
FOS	Fiber Optic Sensors
IFFT	Inverse Fast Fourier Transform
NA	Numerical Aperture
OFDR	Optical Frequency Domain Reflectometer
OTDR	Optical Time Domain Reflectometer
PDL	Polarization Dependent Loss
SOP	State of Polarization
STFT	Short Time Fourier Transform
TLS	Tunable Laser Source

CHAPTER 1

INTRODUCTION

Today's industry tends to be guided ever stronger by the aims of optimal efficiency, productivity, security and cost-effectiveness. In order to achieve these objectives, many industrial sectors require the advanced technologies providing the ability to monitor the status and health of the systems. This is because the early detection of potential faults prevents serious damages of equipment, minimizes interruption of the production or service, and provides an enhanced security for people and goods. As a consequence, the market for all kinds of sensors is expanding.

In particular, fiber optic sensors (FOS) have been gaining a prominent position in this marketplace thanks to their inherent advantages compared to their conventional counterparts such as low attenuation, immunity to electromagnetic interference (EMI), high bandwidth, small dimensions, high temperature tolerance, electrically passive nature and, low fabrication cost.

Fiber Bragg gratings (FBGs) have brought about a revolutionary dimension to the fiber optic sensors. FBGs are low-cost, mass producible intrinsic sensing devices providing self-referencing and wavelength-encoded linear response to the physical parameter to be measured. Being photo-imprinted in the core of an optical fiber, FBGs not only benefit from all the advantages of FOS but they also offer an important instrumentation capability which is not possible with conventional sensors: *quasi-distributed* and *embedded* sensing. Quasi-distributed sensing involves several concatenated FBGs on a single fiber that can be analyzed with a single interrogating system. Due to this multiplexing capability, the cost per sensing element decreases. In addition, sensors including FBG arrays can be embedded and/or attached into composite materials without degrading the performance and life of the host structure. In this context, a fast, reliable and cost-effective interrogation unit that can be implemented in many application areas is of paramount importance for FBG-based sensing systems.

Optical Time Domain Reflectometry (OTDR) and coherent Optical Frequency Domain Reflectometry (OFDR) techniques are the two main candidates that can be exploited in the optical sensing. In terms of equipment availability and cost, OTDR is a standard, off-the-shelf tool with accessible prices but brings about two big limitations related to the inevitable dead-zone and the long measurement time. OFDR on the other hand tackles the disadvantages of OTDR and has been nowadays gaining a renewed interest as an interrogating tool for use in the sensing fields also reduces the length between two sensing points thanks to its high spatial resolution [3-4].

This thesis has focused on a novel interrogation approach that uses FBG sensors cascaded into optical fiber and interrogated by OFDR. The thesis contributes to the literature in terms of the simulations computing the spectral evolution of the polarization dependent properties (e.g. Polarization Dependent Loss (PDL)) of the FBGs and the corresponding OFDR demodulation results as a function of system parameters (physical grating parameters, global birefringence, wavelength range, …).

The ultimate application area of the proposed interrogation scheme would be structural health monitoring of composite materials by the way of strain measurements in a distributed and/or quasi-distributed manner.

1.1. Thesis Outline

This thesis is organized in five chapters. In chapter two, basic principles of the optical fibers and fiber Bragg gratings are presented. It provides a detailed explanation about the spectral characteristics of uniform fiber Bragg gratings.

In chapter three, interrogation schemes of fiber Bragg gratings based on reflectometry techniques are provided. It mainly focuses on the two reflectometry techniques; Optical Time Domain Reflectometry (OTDR) and Optical Frequency Domain Reflectometry (OFDR).

Chapter four first summarizes the main concepts of light polarization in optical fibers and then focuses on the polarization phenomena that can be observed in uniform fiber Bragg gratings.

Chapter five investigates the response of uniform FBGs which are interrogated by (polarization sensitive) OFDR. A numerical model of the measurement system is built by using Transfer Matrix Method. Our model takes into account the global birefringence effect of fiber Bragg gratings. Implementing the proposed model, the Polarization Dependent Loss is simulated based on the demodulated transmission spectra of the fiber gratings.

Simulation results show a good agreement between the theoretical PDL spectra (obtained by the analytical formula based on the coupled-mode theory) and the simulated PDL spectra using our proposed model. The results confirm the feasibility of using polarization properties of FBGs and OFDR for strain sensing in structural health monitoring applications.

In chapter six, the conclusion and future aspects are discussed.

CHAPTER 2

GENERAL CONSIDERATIONS ON FIBER BRAGG GRATINGS: BASICS, PROPERTIES AND SENSING ASPECTS

2.1. Introduction

This chapter summarizes the main concepts of optical fibers, classification of optical fiber sensors and most important properties of fiber Bragg gratings. There are several types of fiber gratings like apodized, chirped, tilted, and long period gratings which are suitable for many interesting sensor implementations. Nevertheless, the analysis realized in the framework of this thesis is uniquely based on uniform fiber Bragg gratings. Therefore this chapter focuses on the principles and properties of uniform FBGs related to FBG-based sensors.

2.2. Basic Principle of Optical Fiber

Optical fiber has a simple structure which acts as a waveguide and allows the propagation of light along it. Optical fiber consists of two concentric cylinders called core and cladding. The core and cladding have different refractive indices; the index of the core is always greater than the refractive index of the cladding.

The core is the inner cylinder with a diameter of 8 and 10 micrometers for a standard single mode fiber. Optical fiber can be also multimode then it has a core diameter of about 50-62.5 micrometers and carries more than one mode of electromagnetic waves.

The cladding is surrounding the core has a diameter of about 125 micrometers for a standard fiber.

Optical fibers are commonly manufactured by means of pure silica glasses. The use of dopants like germanium, nitrogen and phosphorus in the core composition slightly increases the refractive index value and creates the required difference between core and cladding refractive indices to have the *total internal reflection* condition.

On the core-cladding interface, the incident angles which are greater than critical angle, light rays are reflected to the core and the light is guided through the core without refraction [5]. If the inclination to the fiber axis is greater, light rays are not guided through the core because they lose their power at each reflection into the cladding.

From the Snell's law of refraction maximum acceptance angle θ_a's value can be found as:

$$n_0 \sin(\theta_a) = n_1 \sin(\pi/2 - \theta_c) = n_1 \cos(\theta_c) \quad (2.1)$$

$$n_1 \sin(\theta_c) = n_2 \sin(\pi/2) = n_2 \quad (2.2)$$

n_0 is the refractive index of surrounding medium, n_1 is the core refractive index and n_2 is the cladding refractive index.

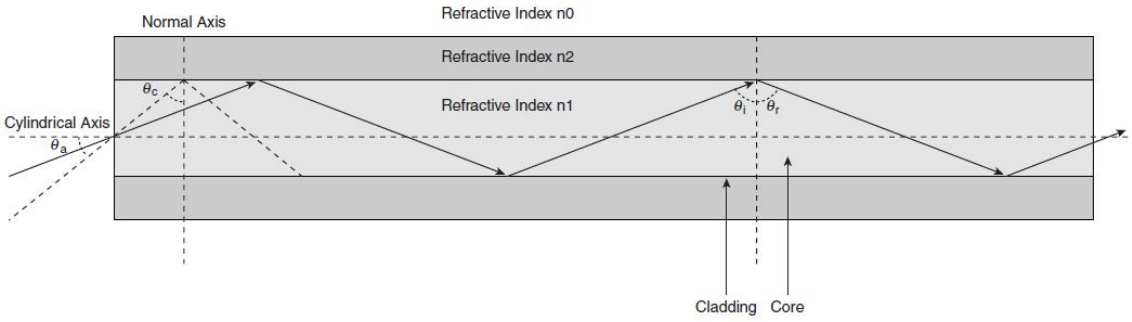

Figure 2.1. Total internal reflection in fiber geometry [6]

In order to travel inside the fiber, light rays make an angle to the fiber axis when it enters inside the fiber. This angle called *acceptance angle*. Angle equal or smaller than the acceptance angle are guided to the fiber and continue its way in it. However angles greater than acceptance angle will be lost in the cladding.

Finding an expression between refractive indices of core, cladding and surrounding medium will take us to the numerical aperture term. *Numerical aperture* shows the light gathering capability of the fiber. A fiber's numerical aperture can be express as,

$$NA = \sin(\theta_a) = \sqrt{(n_1^2 - n_2^2)} \quad (2.3)$$

For a light ray, $\theta_a > \theta_c$ condition is not sufficient to propagate inside the fiber as one can associate a plane wave to each ray. Therefore, interference effect between the plane waves should be taken into account. In other words, all points situated on the same wave front should be in phase to avoid destructive interference. This implies that light rays which have only limited number of θ_a values can propagate in the fiber. The light propagation is then possible through discrete *modes* which can be analyzed by solving Maxwell's equations for optical fibers (mode analysis in optical fibers is beyond the scope of this thesis) [7], [8].

2.3. Fiber Optic Sensors

Optical fiber sensors take few steps forward against conventional electronic sensors at the areas that require immunity to electromagnetic interference, small size to easily embed the sensor into the structures, and resistance to harsh conditions. Optical fiber is the most important part for an optical sensor system. Based on fiber optics lots of physical quantities can be sensed. Some of them are temperature, strain, pressure, vibration, acceleration, displacement etc.

A basic sensor system that measures these physical parameters (*measurands*) generally consists of an optical source, an optical fiber, a modulator (or a sensing element) and a detector. The light sent by the source is guided inside the optical fiber and during its propagation some properties of light (e.g. polarization, wavelength …) are modulated due to external effects. An optical detector converts the light into electrical form and finally some signal processing electronics like optical spectrum analyzer help to obtain the changes on the physical parameter to be sensed [9].

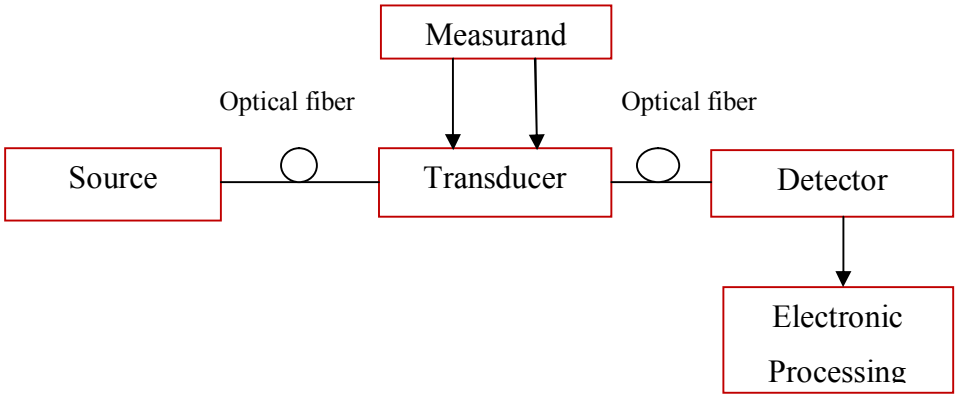

Figure 2.2. Basic components of an optical fiber sensor system

2.3.1. Classification of Fiber Optic Sensors

Table 2.1. Fiber optic sensors classification

Spatial Distribution			Sensing Location	
Point Sensors	Distributed Sensors	Quasi- Distributed Sensors	Extrinsic Sensors	Intrinsic Sensors

Fiber optic sensors can be classified with respect to their spatial distribution as *point* sensors, *distributed* sensors and *quasi-distributed* sensors [10].

In point sensors, sensor is generally placed at the end or near the end of an optical fiber to provide a connection between the interrogator and the sensing element.

These types of sensors are especially used at the implementations where it is more interesting to use multiplexing techniques (capability of interrogating several different -more than 10-20- sensor points along the same optical fiber).

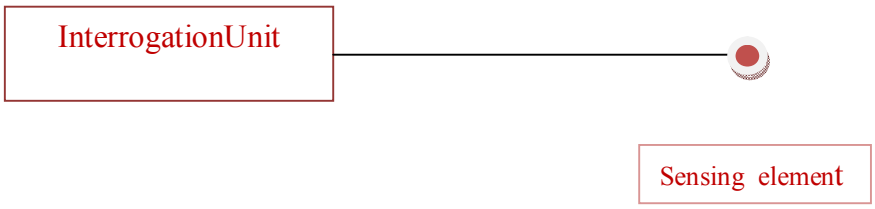

Figure 2.3. Point sensing

Distributed sensors can be defined as a sensor where the whole optical fiber itself acts as the sensing medium. Rather than using wide number of connecting cables distributed sensors only need a single connection cable to transmit the information to the reading unit.

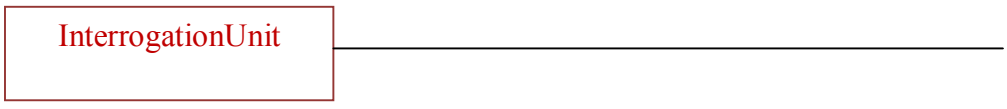

Figure 2.4. Distributed sensing

In quasi distributed sensors, a single fiber includes lots of sensors in series along the fiber to monitor the physical effects. In quasi distributed sensors monitoring of measurand is not continuous along the fiber length, however it is realized at a finite number of locations [11]. This means that it will be able to analyze a set of concatenated point sensors with one interrogating unit.

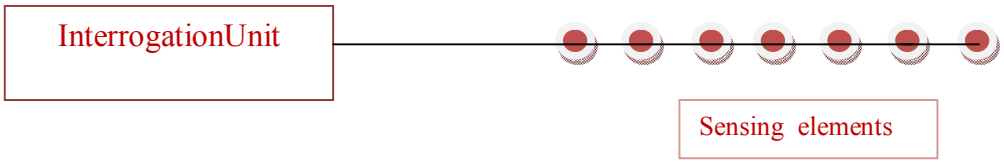

Figure 2.5. Quasi- Distributed sensing

Optical fiber sensors can also be classified depending on the sensing location as extrinsic and intrintsic. In an extrinsic fiber optic sensor, the modulation of light takes place outside of the fiber. The fiber is used only to carry light from the source to the sensing medium and from the sensing medium to the detector.

Another type of sensors is intrinsic fiber optic sensors. This type of sensors can also be called as *all fiber sensors*. The modulation of light totally occurs inside the optical fiber. By applying the physical effect to be measured, fiber's geometrical, physical and optical properties are influenced giving rise to the modulation of light during its propagation inside the fiber. Fiber Bragg grating sensors are categorized under this sensor group.

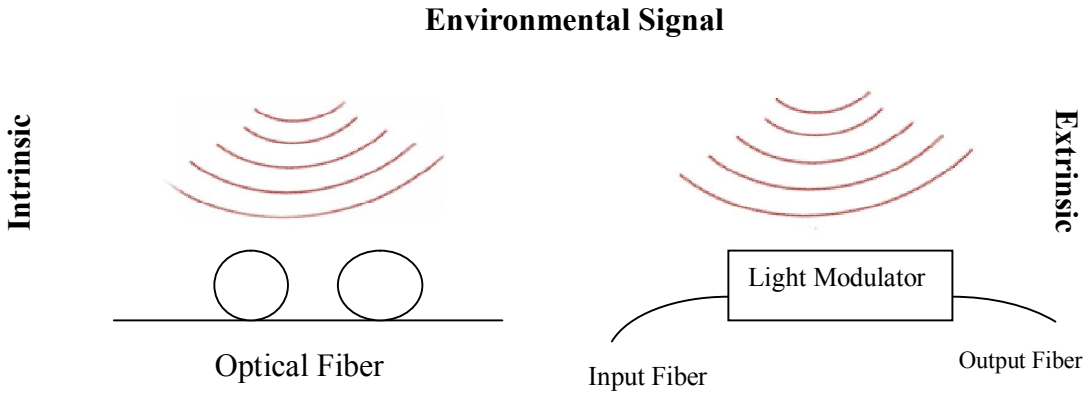

Figure 2.6. Extrinsic and Intrinsic sensing schemes

2.4. Basic Principle of Fiber Bragg Gratings

A fiber Bragg grating is a constant and periodic refractive index value modulation within the core along an optical fiber. To obtain this modification a photosensitive optical fiber is used and the core of this optical fiber is illuminated by a ultraviolet pattern of interference [12]. The parameters describing a fiber Bragg grating can be listed as follows:

- The *length* L over which the variation on refractive index is achieved. It ranges from a few mm up to a few tens of cm.
- The *periodicity* Λ, also called the *grating pitch*, ranging from 200 nm to 800 nm.
- The magnitude δn of the n_{eff} modulation. n_{eff} is the effective refractive index (i.e. the refractive index seen by the fiber core at the Bragg wavelength before the grating inscription). This modulation δn typically ranges from 10^{-5} to 10^{-3}.

The modulation of fiber core refractive index results in the coupling between modes propagating in opposite directions [13]. Mode coupling grows for some wavelengths around so called *Bragg wavelength* (λ_{Bragg}) which can be described by,

$$\lambda_{Bragg} = 2n_{eff}\,\Lambda \tag{2.4}$$

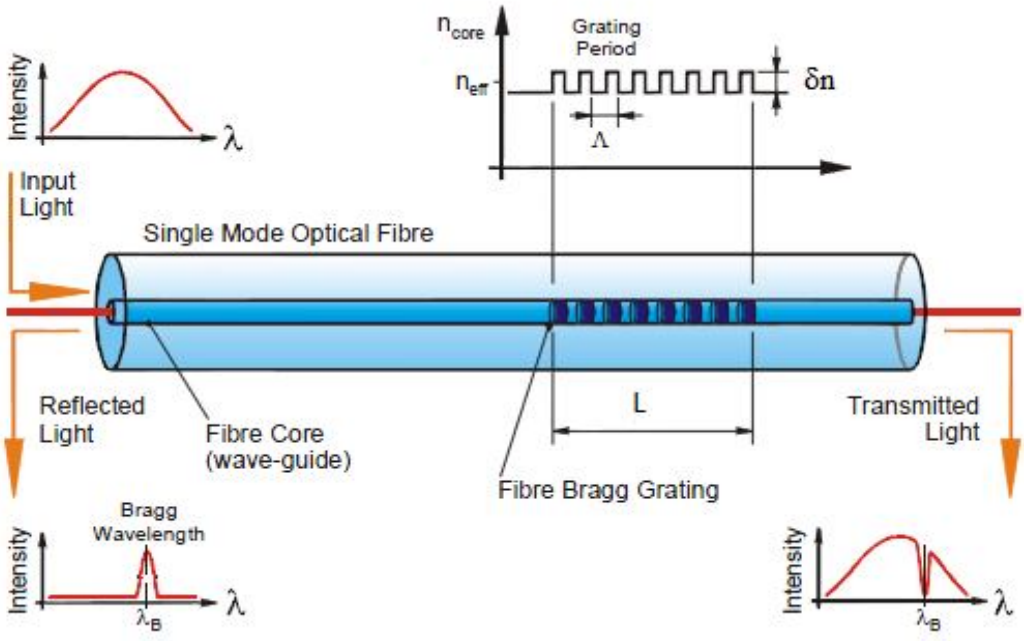

Figure 2.7. Fiber Bragg grating [14]

Physically the refractive index variation of the fiber Bragg grating give rise to a weak Fresnel reflection with each period of the grating (Λ). The weak contributions are added in phase and created a strong reflection for the Bragg wavelength. Therefore, a fiber Bragg grating can be defined as a selective mirror around the Bragg wavelength as schematically represented in Figure 2.7.

2.4.1. Model of the Uniform Bragg Grating

In uniform fiber Bragg gratings phase fronts is perpendicular along the fiber longitudinal axis and plane of the grating has constant periodic refractive index modulation. This kind of grating works as narrow-band reflective optical filter that reflects a portion of the spectrum around the wavelength which satisfies Bragg condition.

If the Bragg condition is not satisfied, light reflecting from the consecutive planes will be out of phase and finally be canceled out. When the Bragg condition is satisfied, contribution of light reflected from the each grating plane overlaps constructively to the backward creating a reflected peak at the central wavelength which is determined by the grating parameters.

Therefore, around the Bragg wavelength, FBG couples the light from the forward propagating guided modes to backward propagating guided modes.

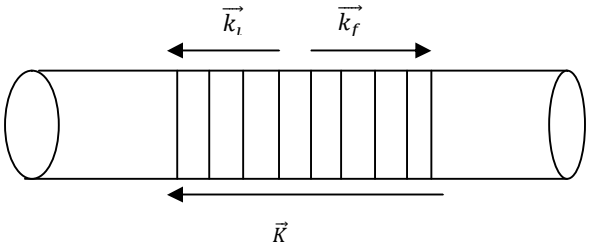

Figure 2.8. Wave vectors of uniform Bragg grating for Bragg condition

Bragg grating condition satisfies the conservation of energy and momentum. To satisfy energy conservation, frequencies of both reflected and incident radiation need to be equal [12].

$$h\,\omega_f = h\,\omega_i \qquad (2.5)$$

where h is the Planck constant (6.626 10^{-34} J.s) and ω_i and ω_f are the frequencies of the incident radiation and the reflected radiation, respectively.

To satisfy momentum conservation, wavevector of incident wave $\overrightarrow{k_i}$ and grating $\vec{K}$ should be equal to the wavevector of scattered radiation $\overrightarrow{k_f}$. Here, grating wavevector has a magnitude of $\frac{2\pi}{\Lambda}$ and perpendicular to the grating planes (see Fig. 2.8).

$$\overrightarrow{k_i} + \vec{K} = \overrightarrow{k_f} \tag{2.6}$$

The diffracted wavevector is equal in magnitude, but opposite in direction, to the incident wavevector. The conservation of momentum simplifies to the first order Bragg equation and can be expressed as,

$$\lambda_{Bragg} = 2\, n_{eff}\, \Lambda \tag{2.7}$$

where λ_{Bragg} is the Bragg wavelength, n_{eff} effective refractive index of the fiber core at the center wavelength, Λ grating periodicity.

2.4.2. Implementation of Transfer Matrix Method

To determine reflection and transmission spectra of an FBG in the presence of mode coupling, coupled mode theory is used. This theory provides us an accurate analytical solution for uniform fiber Bragg gratings.

In the framework of this thesis, the analytical solutions provided by the coupled mode theory have been used as a starting point without demonstrating the whole steps of the theory (these steps are given in Appendix A, Coupled Mode Theory).

The analytical results of the coupled-mode theory can be implemented in an efficient way to model the reflection and transmission spectra of the grating in a distributed manner all along the grating. **Transfer matrix method** is a simple and precise technique which is easy to integrate into coupled mode equations [1].

In this method, grating is divided into N cascaded sections and each section is affecting succeeding section. For instance, (N-1) th section's matrix outputs are used as the N^{th} section matrix inputs [13].

In this approach, the FBG can be considered as a 4-port device as shown in Figure 2.9,

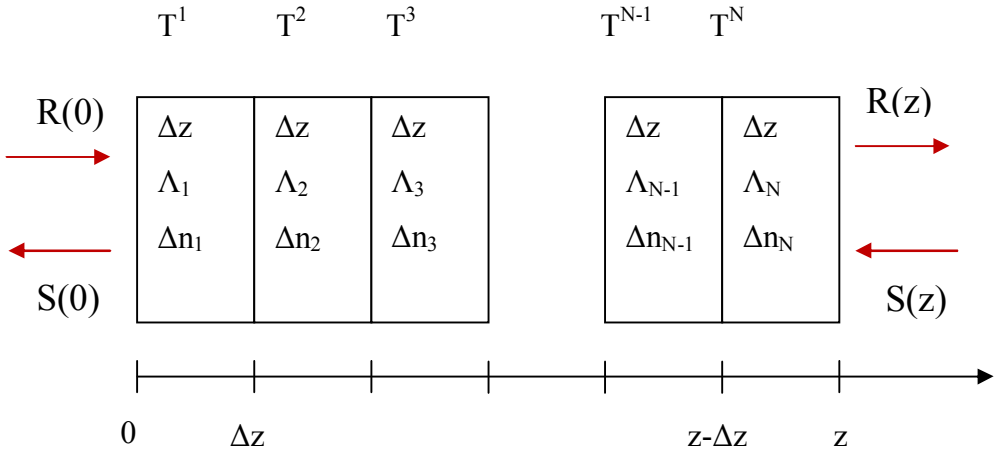

Figure 2.9. Input and output fields of Bragg grating

The forward-propagating fields R(0) and R(z), backward-propagating waves S(0) and S(z), and the section length, $\Delta z = \frac{z}{N}$ are represented in Figure 2.9. Transfer matrix of the grating (T) comprises both the amplitude and phase information.

By the help of transfer matrix, input and output fields are connected to each other as:

$$\begin{bmatrix} R(0) \\ S(0) \end{bmatrix} = [T] \begin{bmatrix} R(z) \\ S(z) \end{bmatrix} \tag{2.8}$$

In the case of *reflection grating* the reflected amplitude at input field of grating R(0) is normalized to unity and output field amplitude S(z) is zero (i.e. backward-going field does not exist further than the grating length as there is no perturbation away from the end of the grating). Equation 2.8 is revised in the light of boundary conditions and the relation is written as:

$$\begin{bmatrix} 1 \\ S(0) \end{bmatrix} = \begin{bmatrix} T_{11} & T_{12} \\ T_{21} & T_{22} \end{bmatrix} \begin{bmatrix} R(z) \\ 0 \end{bmatrix} \tag{2.9}$$

$$R(z) = \frac{1}{T_{11}} \tag{2.10}$$

$$S(0) = \frac{T_{21}}{T_{11}} \tag{2.11}$$

The entire grating after the N^{th} section can be defined as:

$$\begin{bmatrix} 1 \\ S(0) \end{bmatrix} = [T^N].....[T^3][T^2][T^1] \begin{bmatrix} R(z) \\ 0 \end{bmatrix} \quad (2.12)$$

The transfer matrix for the whole Bragg grating is the multiplication of all individual section transfer matrices.

$$[T] = \prod_{j=1}^{N} T^j \quad (2.13)$$

Solving the couple mode theory equations given in Appendix A, elements of transfer matrix are determined as,

$$T_{11} = \cosh(\alpha z) - \frac{i\delta \sinh(\alpha z)}{\alpha} \quad (2.14)$$

$$T_{12} = -\frac{i\kappa \sinh(\alpha z)}{\alpha} \quad (2.15)$$

$$T_{21} = \frac{i\kappa \sinh(\alpha z)}{\alpha} \quad (2.16)$$

$$T_{22} = \cosh(\alpha z) + \frac{i\delta \sinh(\alpha z)}{\alpha} \quad (2.17)$$

The parameters in equations from 2.14 to 2.17 are defined by the following relationships,

Self-coupling coefficient $$\hat{\sigma} = \delta + \sigma \quad (2.18)$$

AC coupling coefficient $$\kappa = \frac{\pi}{\lambda} \upsilon \delta n \quad (2.19)$$

Tuning rate $$\delta = \beta - \frac{\pi}{\Lambda} = 2\pi n_{eff}\left(\frac{1}{\lambda} - \frac{1}{\lambda Bragg}\right) \quad (2.20)$$

DC coupling coefficient $$\sigma = \frac{2\pi}{\lambda} \delta n \quad (2.21)$$

$$\alpha = \sqrt{\kappa^2 - \hat{\sigma}^2} \quad (2.22)$$

- The amplitude (r) and power (R) reflection coefficients of Bragg grating are defined as

$$r = \frac{S(0)}{R(0)} = \frac{T_{21}}{T_{11}} \tag{2.23}$$

$$r = \frac{-\kappa \sinh(\alpha z)}{\hat{\sigma}\sinh(\alpha z) + j\alpha\cosh(\alpha z)} \tag{2.24}$$

$(R = |r|^2)$ $$R = \frac{\kappa^2 \sinh^2(\alpha z)}{\kappa^2\cosh^2(\alpha z) - \hat{\sigma}^2} \tag{2.25}$$

- The amplitude (t) and power (T) transmission coefficients of Bragg grating are defined as

$$t = (1 - r) = \frac{R(z)}{R(0)} = \frac{1}{T_{11}} \tag{2.26}$$

$$t = \frac{i\alpha}{\hat{\sigma}\sinh(\alpha z) + j\alpha\cosh(\alpha z)} \tag{2.27}$$

$(T = |t|^2)$ $$T = \frac{\alpha^2}{\kappa^2\cosh^2(\alpha z) - \hat{\sigma}^2} \tag{2.28}$$

2.4.3. Amplitude Spectral Response of Uniform FBG: Some Examples

In this paragraph, the interesting features of fiber Bragg gratings is presented. The numerical simulations for the evolution of power reflection coefficient R depending on fiber length, average refractive index modulation and periodic refractive index modulation have been plotted versus normalized wavelength defined by λ / λ_{max}.

$$\lambda_{max} = \left(1 + \frac{\delta n}{n_{eff}}\right) \lambda_{Bragg} \tag{2.29}$$

$$\lambda_{max} = 2\,(n_{eff} + \delta n)\,\Lambda \tag{2.30}$$

where λ_{max} is wavelength at where the maximum reflectivity occurs. In figure 2.10 the relation between the reflected and transmitted spectra are observed as,

$$R(\lambda) + T(\lambda) = 1 \tag{2.31}$$

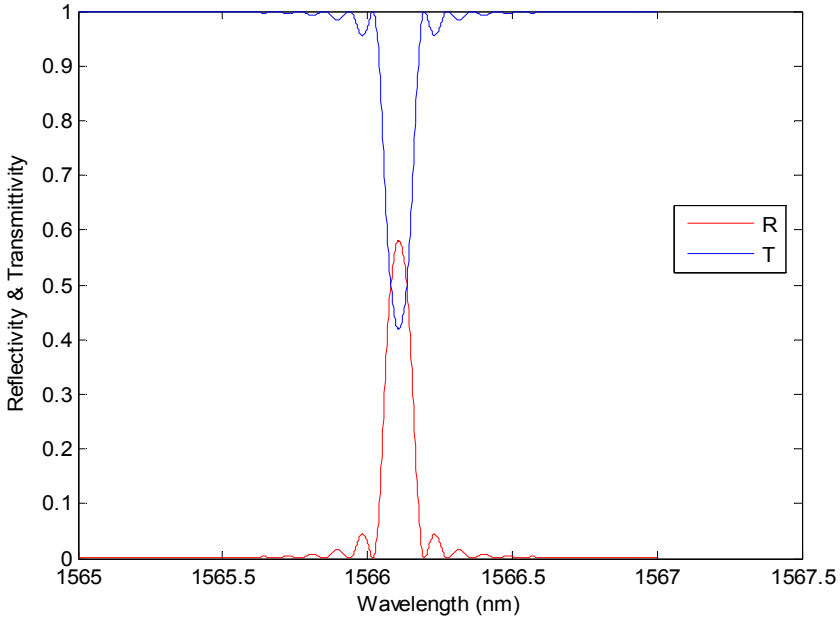

Figure 2.10. Reflection and transmission spectra of a uniform fiber Bragg grating. Parameters used for the simulation: as ν=0.5; δn=1x10^{-4}; Λ=540 nm; L=1cm

In figures 2.11, 2.12 and 2.13, the effect of grating length (L), average refractive index modulation (δn) and periodic refractive index modulation (Λ) on the reflection spectrum are presented, respectively.

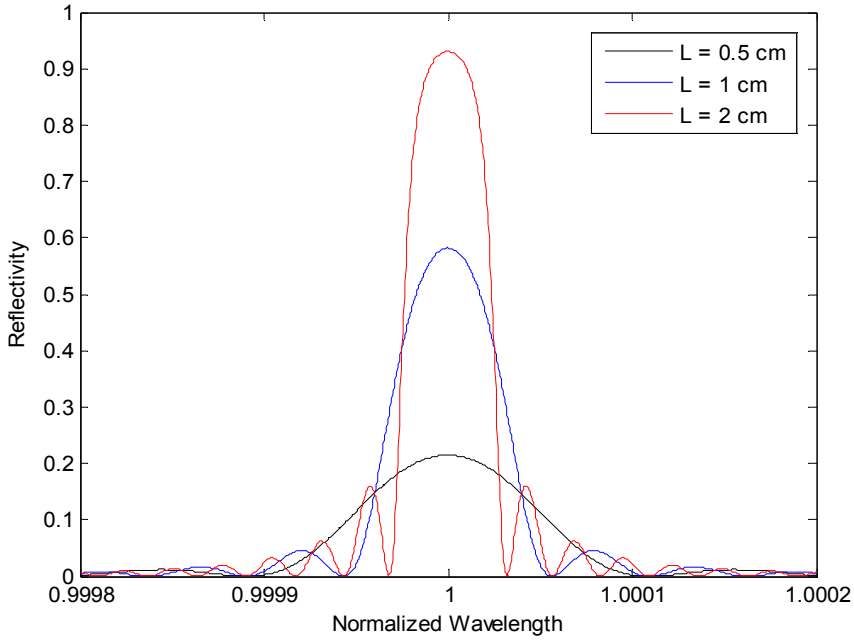

Figure 2.11. The power reflection coefficient variation as a function of grating length in uniform fiber Bragg gratings. The parameters are ν=0.5; Λ=540 nm; δn= 1x10^{-4}

It is seen from figure 2.11 that when the Bragg length increases, reflectivity of the grating also increases. There is a direct proportionality among them.

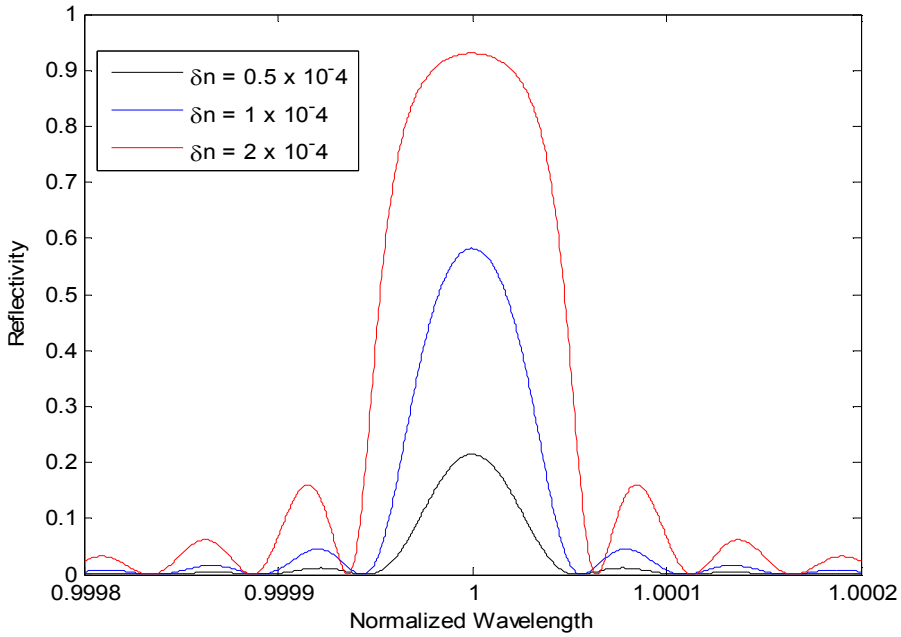

Figure 2.12. The power reflection coefficient variation as a function of average refractive index modulation in uniform fiber Bragg gratings. The parameters are ν=0.5; Λ=540 nm; L=1 cm

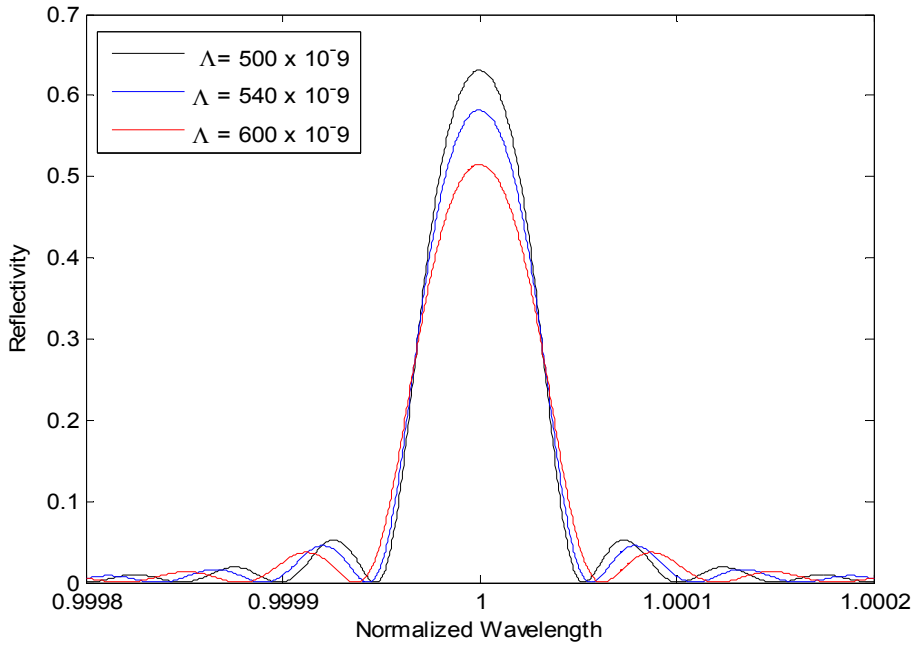

Figure 2.13. The power reflection coefficient variation as a function of periodic refractive index modulation in uniform fiber Bragg gratings. The parameters are ν=0.5; L=1 cm; δn=1 10^{-4}

In Figure 2.12 the effect of the core refractive index modulation on the reflection spectrum is observed. It is obvious from the figure that reflectivity increases when the refractive index modulation increases.

Figure 2.11 and 2.12 also show that the spectral bandwidth between first zeros increases when δn increases and/or when L decreases.

The evolution of the power reflectivity (R) with respect to periodic refractive index variation (Λ) is shown in Figure 2.13. Contrary to L and δn variation, an increase on the periodic refractive index value decreases the reflectivity of FBG.

2.4.4. Advantages of Fiber Bragg Gratings

Fiber optic sensors (FOS) have been gaining a remarkable position in marketplace thanks to their advantages compared to conventional sensors that are listed as follows:

- The information of the measurand is **wavelength-encoded.** This property makes the sensor self-referencing and independent from the fluctuations of light power levels that might rise on the system. Therefore the system is unaffected from the source power fluctuations, detector sensitivity changes, connector losses, or by the presence of other FBGs at different wavelengths. This property is the main advantage of the FBG-based sensors.
- **Multiplexing** is one of the most important advantages of optical fibers. Sensing points can be placed in series on the same optical fiber. The multiplexing ability provide us monitoring different types of sensors along the same fiber like strain sensors and thermal sensors.
- **Linear response** to the physical parameter to be measured over large ranges.
- Optical fibers have **low attenuation,** so it is easy to monitor sensing locations from a remote interrogation station at large distance (the interrogation unit can be placed tens of kilometers away from the sensing points).
- **Easy to install:** just one optical fiber is required to bond to the structure and connected to the interrogator.
- Because of their **small size and geometric versatility** FBG sensors can easily be embedded into various structures to provide damage or strain detection and offer the best option in hard-to-reach and space-limited environments.

- Optical fibers are **safe, passive** because they don't need to use electricity to work. That is why there will be no risk of fires or explosions. This is an important issue for the nuclear or chemical applications.
- They have long **durability,** as they are composed of rugged passive components.

In addition to above advantages, FBGs are also immune to electromagnetic interference and low in price [15], [16].

2.4.5. Applications of Fiber Bragg Gratings

Application areas of fiber Bragg gratings are several. Some of them are listed as,

- **Aerospace:** Structural health monitoring, maintenance of safety and integrity in aerospace structural system [17].
- **Medical:** Used as pressure sensor to measure muscular strength of hands or weight profile of patients [18].
- **Renewable wind energy:** Monitoring strain distribution along the wind turbine wing [19].
- **Civil structures:** Implementation of fiber Bragg gratings array in to the bridges, tunnels, buildings, and dams to monitor structural health.
- **Automotive:** Frame stress detection to increase safety.
- **Transportation and Rail:** Monitoring deformation on the rail, imbalance or strain on the wheels in high-speed railways or trains carrying overloads [20].
- **Marine:** Monitoring fast military vessels, racing yachts, and sub-sea vessels [21].
- **Oil and Gas:** Humidity and hydrogen detection, monitoring oil, gas, water and waste pipelines.
- **Power:** Vibration and temperature monitoring on the nuclear power plants [22].

CHAPTER 3

FIBER BRAGG GRATING INTERROGATION TECHNIQUES

3.1. Introduction

This chapter describes detection schemes for fiber Bragg grating sensors. All interrogation types are differing in system performance as well as in system complexity, robustness, and costs.

As already presented in the previous chapter, fiber Bragg gratings are intrinsic optical sensors where the wavelength of the reflected (or transmitted) spectrum is shifted as a function of external parameter to be measured.

To interrogate the FBGs, a straightforward approach might be the wavelength interrogation of the reflected or transmitted spectral components. General principle of the wavelength measurement is to convert wavelength shift to some measurable parameters such as amplitude, phase or frequency.

Since this thesis focuses on one of the optical reflectometry technique which is optical frequency domain reflectometry, the other interrogation techniques are summarized briefly.

3.2. Wavelength Detection Techniques

In all wavelength detection techniques, the set-up contains broadband light source to illuminate the fiber Bragg grating. Light coming from this source is coupled to the optical fiber and reflected light from fiber Bragg grating sensor is analyzed by a wavelength detection scheme.

Linearly wavelength dependent optical filter; In this type of detection scheme, Bragg wavelength shift is monitored depending on power variation. Although this method has a simple scheme, it is not easy to apply multiplexed FBGs to this scheme. Moreover, the measurements are affected by the power fluctuations. The set-up of measurement contains a filter, a broadband light source and fiber Bragg grating. The ratio of the reflected signal intensity between the reference arm and the filter's arm is changed linearly depending on the Bragg wavelength shift [23].

Linearly wavelength dependent optical coupler; In this method, main component of the set-up is wavelength division multiplexing (WDM) coupler. WDM coupler has a linear and opposite response in the coupling ratios between input and output ports. This coupler receives the reflected light from Bragg grating to detect the wavelength shift. This shift is achieved by computing (linear change) the ratio between sum and difference of output arms of the couplers [24].

These two methods explained above use passive components at the detection schemes.

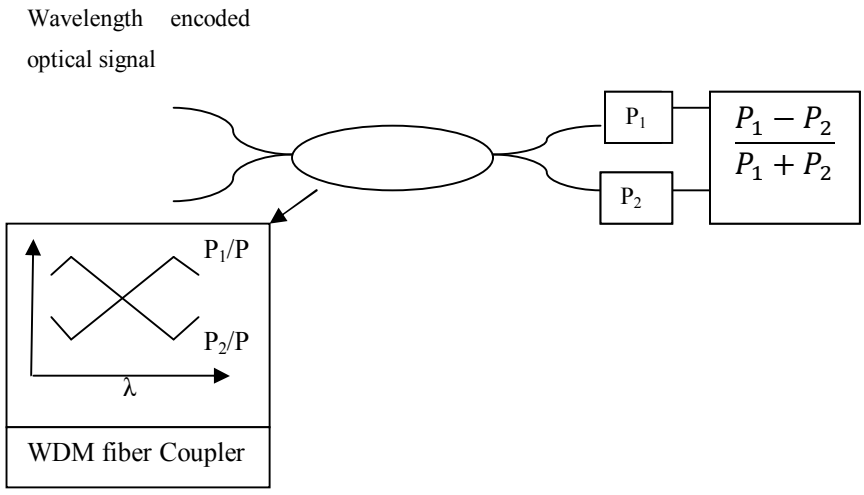

Figure 3.1. Scheme of Wavelength Division Coupler interrogation system

Detection with a scanning optical filter; One of the most attractive interrogations to measure the wavelength shift of a Bragg grating is based on the use of a tunable filter for tracking the spectrum reflected from the grating.

The filter center is tuned until the multiplication of fiber Bragg grating and scanning filter spectra match, at the match condition the system output takes its maximum. Different applications for this method are available and some of them can be found in [25], [26], [27].

Fiber Optic Interferometer; In this technique, interferometer converts the wavelength shifts at back reflected light coming from grating to the phase variation. When comparing with the other detection techniques fiber optic interferometry has more wavelength sensitivity [28]. To convert the wavelength shift to the phase variation, reflected spectrum of Bragg grating topazes through an interferometer which has a wavelength dependent transfer function with the form (1+cosø) (the ø phase term depends on the input wavelength).

3.3. Optical Reflectometry Techniques

In this paragraph, Optical Time Domain Reflectometry (OTDR) measurement technique is presented then study about the Optical Frequency Domain Reflectometry (OFDR) technique are detailed.

Optical reflectometry can be classified into two categories as direct-detection and coherent-detection. In direct detection, only the optical reflected signal is incident on the photodetector but in coherent detection reflected signal and a reference optical signal are incident on the photodetector [29].

3.3.1. Optical Time Domain Reflectometry (OTDR)

Optical Time Domain Reflectometry's basic principle is to detect and analyze the scattered light coming from small imperfections, inhomogeneities and impurities in the optical fiber. Conventional OTDRs use Rayleigh backscattering to determine the location of fiber breaks, the fiber attenuation coefficient, splice loss, and various other link characteristics. By using OTDR some parameters can be measured and provided;

- Distance to splice loss, connector loss, bend loss and their quantities.
- Reflectivity of mechanical splices, connectors
- Active monitoring on live fiber optic system
- Fiber slope and fiber attenuation

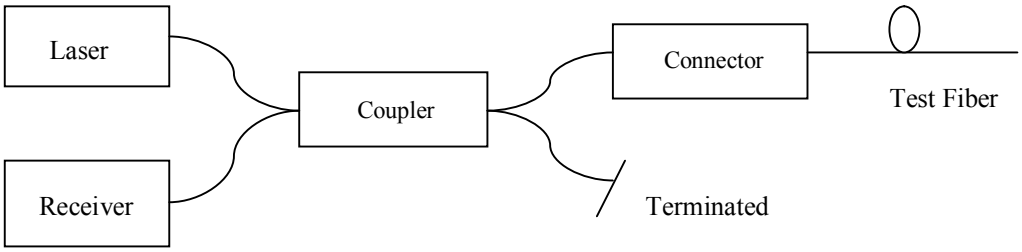

Figure 3.2. Principle diagram of an OTDR

A basic OTDR diagram is shown in Figure 3.2. Light coming from a laser is connected to a coupler. When the pulse propagates along the fiber, some of its power is lost because of Rayleigh scattering, absorption and radiation loss [30].

The most significant loss in OTDR measurements is Rayleigh scattering. The 80-90% of the total loss of light is produced by Rayleigh scattering. Microscopic inhomogeneities at the refractive index of the fiber create this scattering.

The probe signal can also be attenuated due to splices, bends or connectors at discrete locations in the fiber as shown in Figure 3.3.

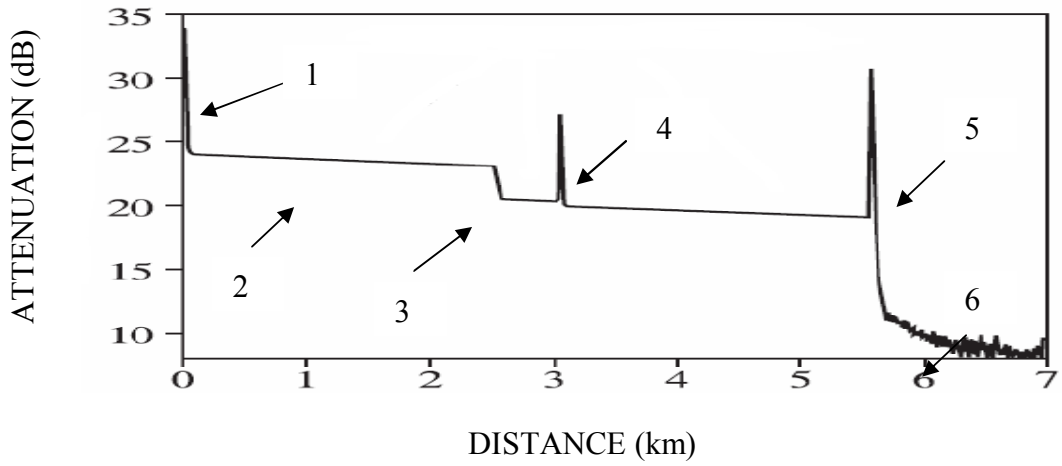

1 Reflection from Front Connector

2 Fiber Attenuation

3 Non-Reflective Loss (Fusion Splice or Bending)

4 Reflective Loss (Mechanical Splice or Connector)

5 Fiber End Reflection

6 Noise Level

Figure 3.3. Events on a typical OTDR trace

When the optical pulse is sent to the fiber and it meets with a discontinuity in the refraction index, some of the signal energy is reflected back and coupler directs it to the optical receiver. An OTDR software displays the losses on a generated graph and provides the loss value in dB as a function of distance.

The received power is measured as a function of time. Then a conversion is needed to obtain measurements in length (in km). Because of light travels forward and backward directions before reaching the receiver, it propagates twice the distance.

The OTDR software multiplies the time value by the group velocity of the light in the fiber, in order to convert time into a one-way distance. That is why optical power is computed by using $5\log_{10}$ formula not with $10\log_{10}$ formula [31].

Some key parameters are considered when investigating the performances of an OTDR.

The ***dynamic range*** of an OTDR is defined as the strength of the initial backscattering level to the noise level. It shows the maximum loss the equipment is able to measure. To increase the OTDR's dynamic range, backscatter level should be increased and noise should be decreased. (see Fig. 3.4)

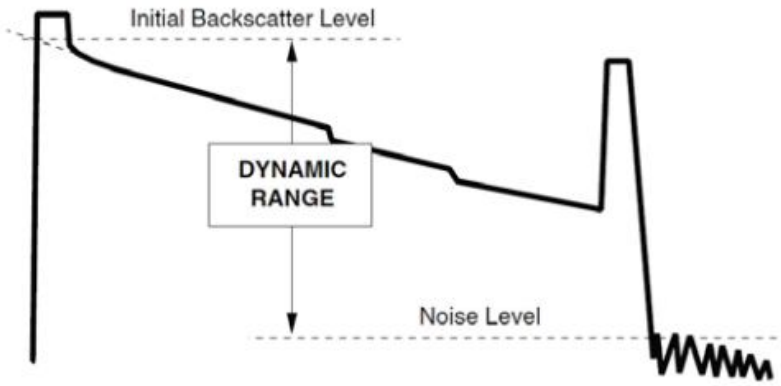

Figure 3.4. Dynamic Range

The ***spatial resolution*** parameter gives the information about capability of OTDR to resolve two close events. The spatial resolution length depends on optical pulse width (half of the pulse width).

In an OTDR measurement, there is a trade-off between spatial resolution and dynamic range. When shorter pulses (narrow pulse width) are used to provide good spatial resolution, the signal to noise ratio is worse because of the smaller backscattered power (decreasing in the pulse energy is decreasing the signal level), so the attainable dynamic range is smaller. In contrast, when the pulse width is broadened dynamic range becomes larger but spatial resolution becomes worse.

After having received a strong reflection, the OTDR receiver is blinded (saturation) during a certain time interval. There is a distance after the reflection peak where no proper measurement can be performed. This region is denoted by the term ***dead zone***.

To interrogate FBGs by OTDR, several techniques are proposed where the OTDR provides information about position, magnitude and phase of the reflective events (FBGs in this case).

To extract the wavelength shift information some signal processing is required as shown schematically in Figure 3.5.

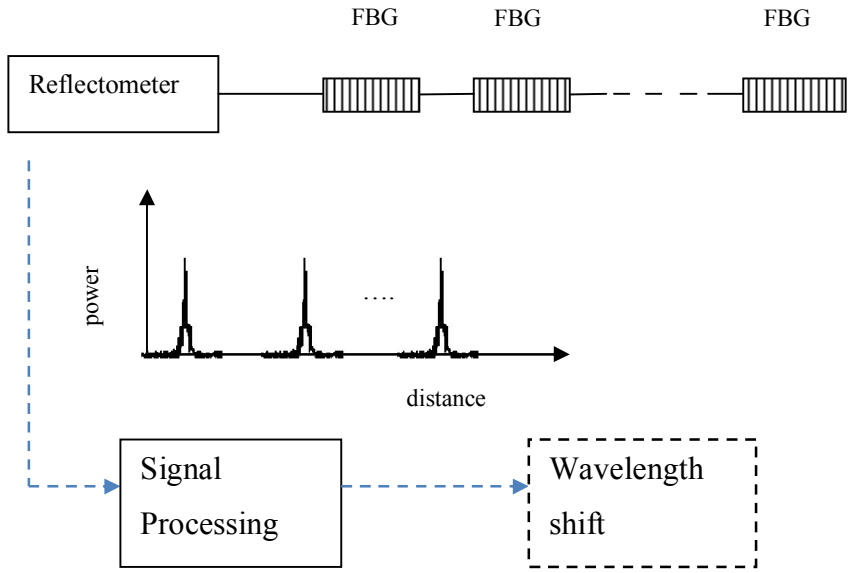

Figure 3.5. Optical reflectometry techniques for FBG interrogation

Conventional OTDR is one of the applications for interrogation of FBGs. As shown in Figure 3.6, sensor pairs are interrogated by OTDR. The physical parameters are not applied on the reference grating. The reference grating is used to compensate power fluctuations on the source. The whole range of the wavelength is used by the OTDR source and back reflected signal from the sensing grating is measured by OTDR receiver. The Bragg wavelength shift can be obtained by the linear change in the measured power according to the linear edge of the source spectrum [32].

The wavelength of the sensing grating is located at the increasing or decreasing edge of the source spectrum to obtain maximum power variation as a function of wavelength shift.

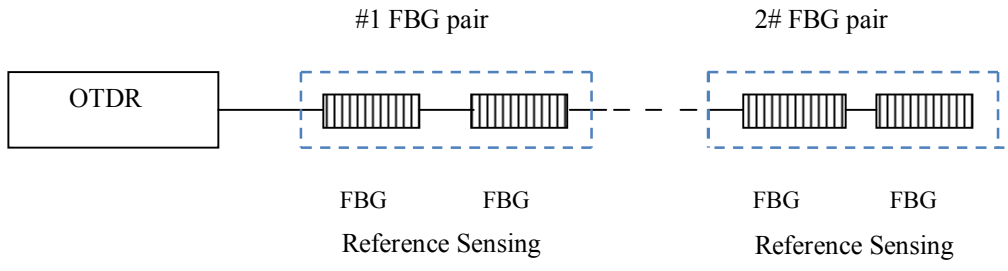

Figure 3.6. Conventional OTDR scheme

OTDR with an adjustable Fabry-Perot filter, This method is based on the association of a commercial OTDR with a band pass filter. The schematic of the proposed system is shown in figure 3.7. A concatenation of several arrays of fiber Bragg gratings (FBG_1 . . . FBG_n) is interrogated.

The FBGs in each array have got approximately the same nominal Bragg wavelengths, λ_1 . . . λ_n. The passband of the Fabry-Perot filter (1.3 nm) is slightly narrower than the FWHM of the Bragg gratings (1.5 nm). When the reflection spectrum of a given FBG coincides with the passband of the FP filter, a detectable signal will be generated at the OTDR receiver. By using low reflective gratings, several FBGs at the same nominal wavelength but at different positions (hence with different delay times) can be addressed simultaneously for a given center wavelength of the filter [33].

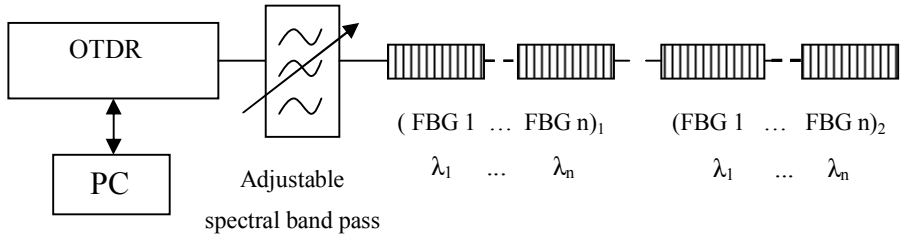

Figure 3.7. Scheme of OTDR with a spectral filtering

Wavelength Tunable OTDR: as shown in Figure 3.8 a wavelength conversion system is combined with a conventional OTDR. The optical pulses emitted from a conventional OTDR are first converted to electrical pulses and then modulate the Tunable Laser Source (TLS) at the desired wavelength [34].

Optical pulses obtained at the desired wavelength are sent to the FBGs. The reflected light from FBGs is directed to the OTDR. Tunable laser source scans the proper set of wavelength and using a set of OTDR traces obtained these wavelenghts, the reflection spectra of all FBGs are reconstructed.

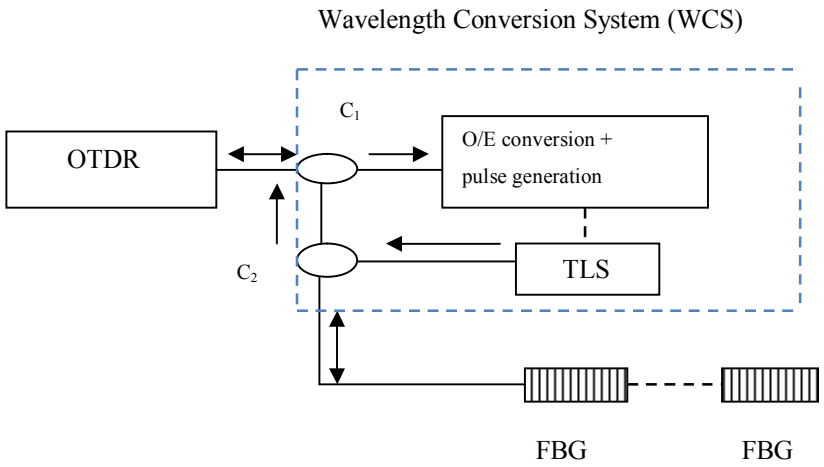

Figure 3.8. Wavelength tunable OTDR interrogation scheme

3.3.2. Coherent- Optical Frequency Domain Reflectometry (OFDR)

When the optical system under consideration is several tens of meters in length, OFDR can be used because of its millimeter resolution, high sensitivity and large dynamics. OFDR overcome the limitations of OTDR on spatial resolution, dynamic range and measurement speed for the immediate and definite detection of any structural damage.

To interrogate fiber Bragg grating spectrum, coherent-optical frequency domain reflectometry is the best suited method providing high spatial resolution between two measured point over multiple tens of meters of optical length [35].

Optical frequency domain reflectometry (OFDR) technique works with similar principle as optical time domain reflectometry (OTDR) technique and provides information about reflection and transmission spectrum on the measurand. OTDR is based on direct detection scheme but OFDR is operating in coherent detection mode.

3.3.2.1. Principle of OFDR

In its basic configuration, the optical carrier frequency of a tunable laser source (TLS) is swept linearly in time without mode hops. Then, the frequency modulated continuous-wave signal (probe signal) is split into two paths (see figure 3.9), namely the test arm and the reference arm.

The test signal which is reflected back from the reflection sites in the test arm coherently interfere at the coupler with the reference signal returning from the reference reflector. This interference signal contains the beat frequencies which appear as peaks at the network analyzer display after the Fourier transform of the time-sampled photocurrent [36].

Using a linear optical frequency sweep, the measured beat frequencies can be mapped into a distance scale (the proportionality factor between beat frequency and the corresponding distance is determined by the rate of change of the optical frequency), while the squared magnitude of the signal at each beat frequency reveals the reflectivity of each reflection site. This method is often called as coherent FMCW (Frequency-Modulated Continuous Wave) [37].

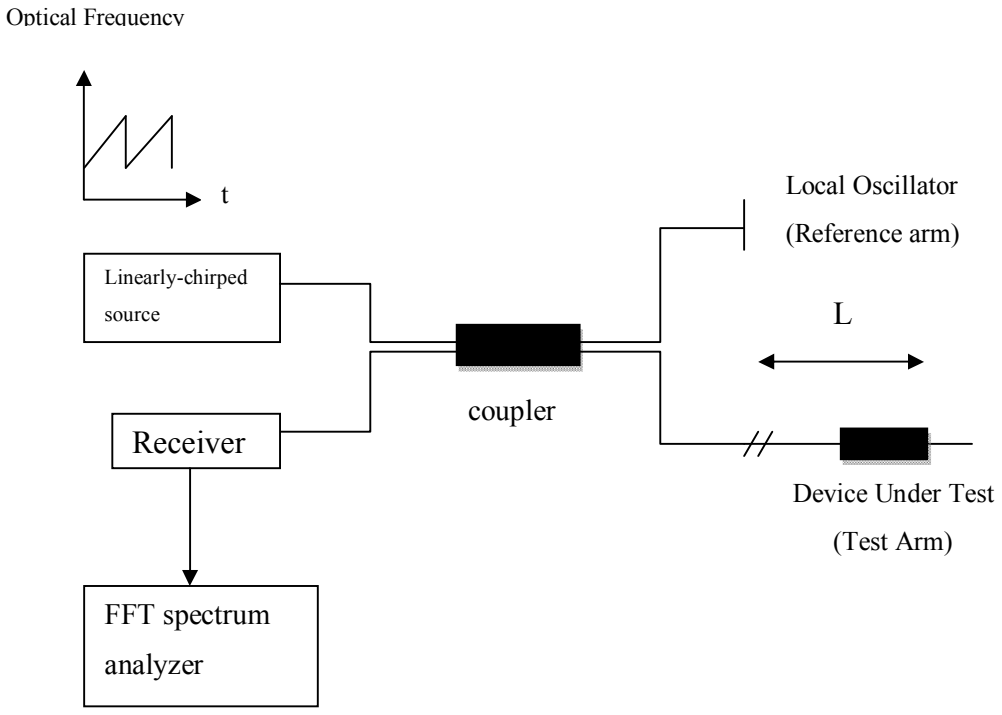

Figure 3.9. Basic configuration of distributed C-OFDR

In this thesis the formulation is described by the wavenumber of light and results of the analysis are presented in terms of wavelength of the light. The relation between wavenumber k and wavelength can be expressed as,

$$k = \frac{2\pi}{\lambda} \tag{3.1}$$

The intensity measured at the detector varies as a cosine function of the wavenumber k and can be expressed as in equation 3.2 (derived in the Appendix B [38]),

$$D = \cos\left(2n_{eff}kL\right) \tag{3.2}$$

where n_{eff} is the effective refractive index of optical fiber core.

This equation shows that light reflected from device under test and light reflected from the reference reflector have an optical path difference of $2n_{eff}L$.

Due to the linear modulation of the optical frequency, each reflection on side on the optical fiber corresponds to a beat frequency. These beat frequencies can be observed by taking the Fourier transform of the interference signal and then can be converted into distance [39].

As the laser is tuned light intensity observed by dedector varies depending on wavenumber change Δk and can be expressed as [40],

$$\Delta k = \frac{\pi}{n_{eff}L} \tag{3.3}$$

The schematic of the Fourier and Inverse Fourier Transform application can be shown in Figure 3.9 and 3.10.

The Fourier transform separates the interference signal waveform into sinusoids of different frequencies.

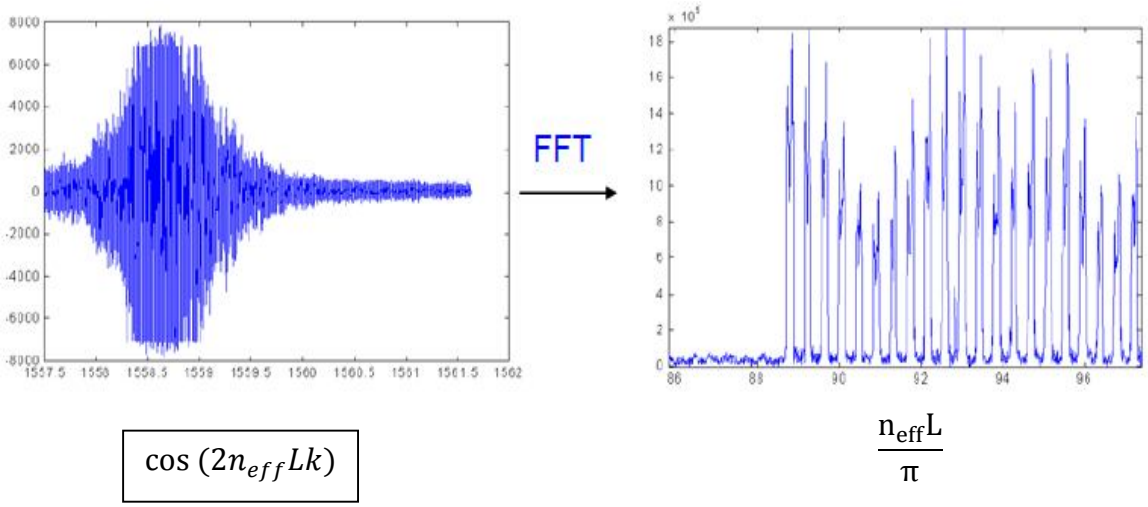

Figure 3.10. Spectral mapping between wavenumber and length [41]

By using a bandpass filter around a proper position of a reflection and by applying an inverse Fast Fourier transform to the filtered signal, the spectrum of each reflection can be obtained independently from the others.

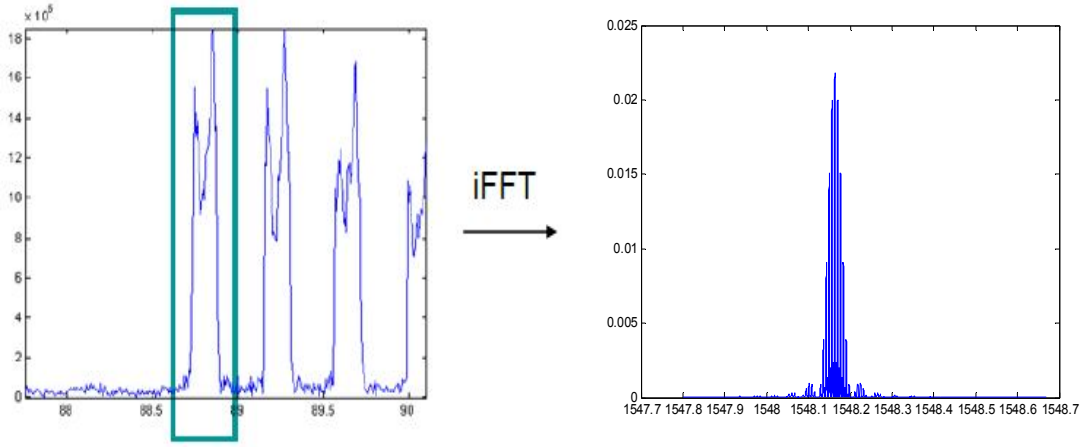

Figure 3.11. Schematic of demodulation process [41]

In summary, to obtain the reflection spectra of a reflection side (this could be a FBG or a discrete reflection) in the test arm of the OFDR, a band-pass filter (centered at a particular beat frequency, hence position) is used to extract the portion having the information related to this particular reflection.

This is followed by an inverse Fast Fourier transform to recover the complex FBG spectrum and the obtained spectrum is called as ***demodulated reflection (transmission) spectrum***. Steps to obtain demodulated spectrum can be shown in figure 3.12 where identical uniform FBGs are used as reflection points [37].

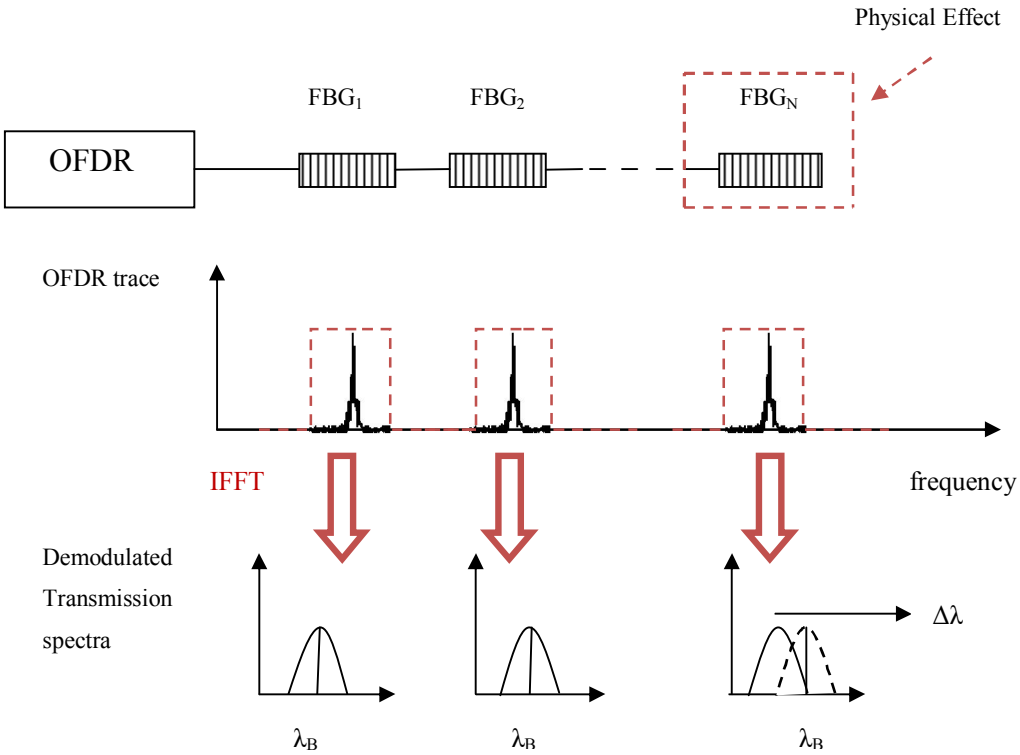

Figure 3.12. Schematic of signal processing

The flowchart belong to above explained signal process is represented in Figure 3.13 as,

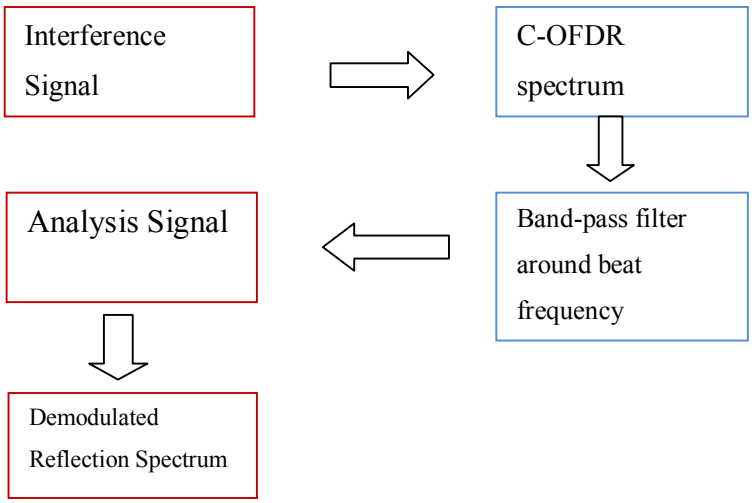

Figure 3.13. Flowchart of signal processing

- **Matlab Simulation Example**

As an example to above discussion, we simulated the OFDR trace when there is one FBG in the test arm at the position: 1.38 m. In these simulations the reflectivity of Bragg grating is derived by using equations 2.28, the interferometer signal is examined and the location information is provided by taking Fourier transform of the signal. Inverse Fourier transform of the signal allows demodulating the reflection coefficient of fiber Bragg grating. Finally theoretical reflection coefficient is compared to the demodulation result in Figure 3.15. The simulation parameters are as follows:

Table 3.1. Parameters used for Matlab simulation

Visibility	1
z (location of FBG)	1.38 m
n_{eff} (effective refractive index)	1.45
L (Fiber Bragg grating length)	200 mm
δn_{eff} (Average index change)	1.6×10^{-5}
λ_{Bragg} (Bragg wavelength)	1583.7 nm
Λ (periodic refractive index change).	547.59 nm
NoP (Number of point used in Fourier transform)	40000

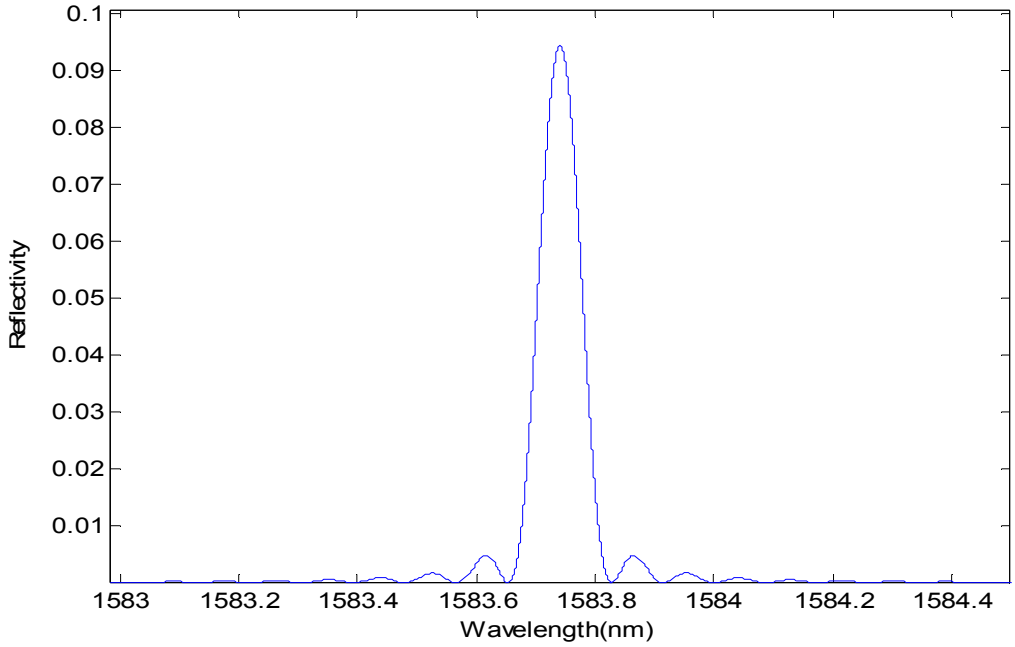

Figure 3.14. Reflectivity of FBG found by mathematical derivation (Eq.2.25)

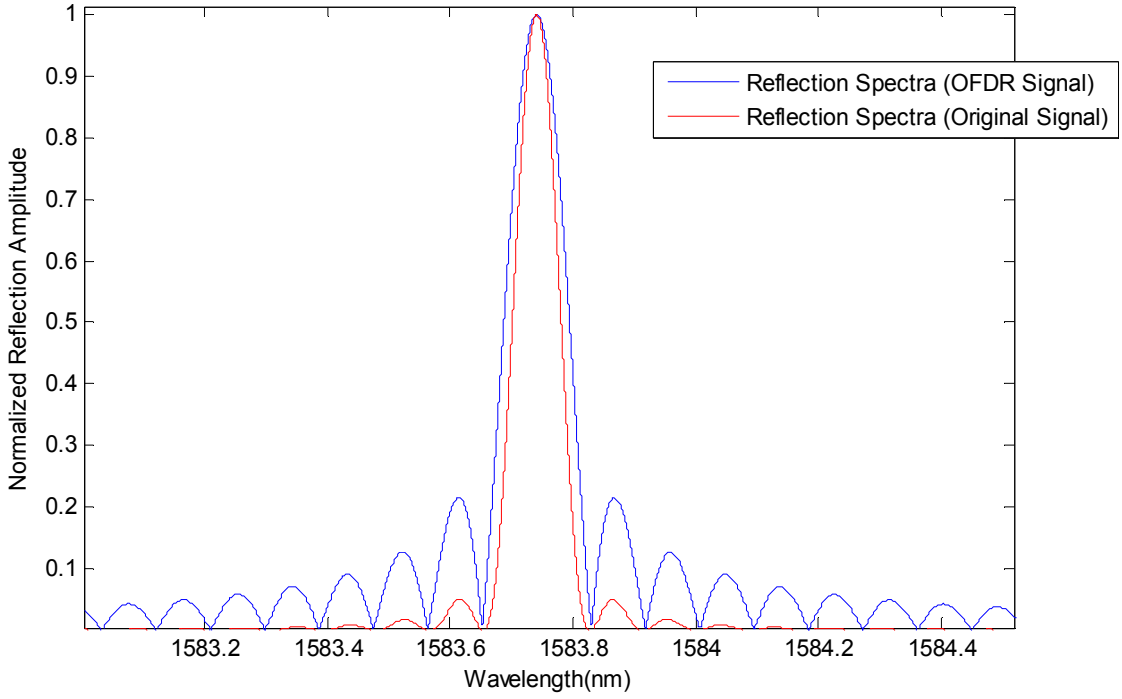

Figure 3.15. Comparison of demodulated signal with the mathematically obtained

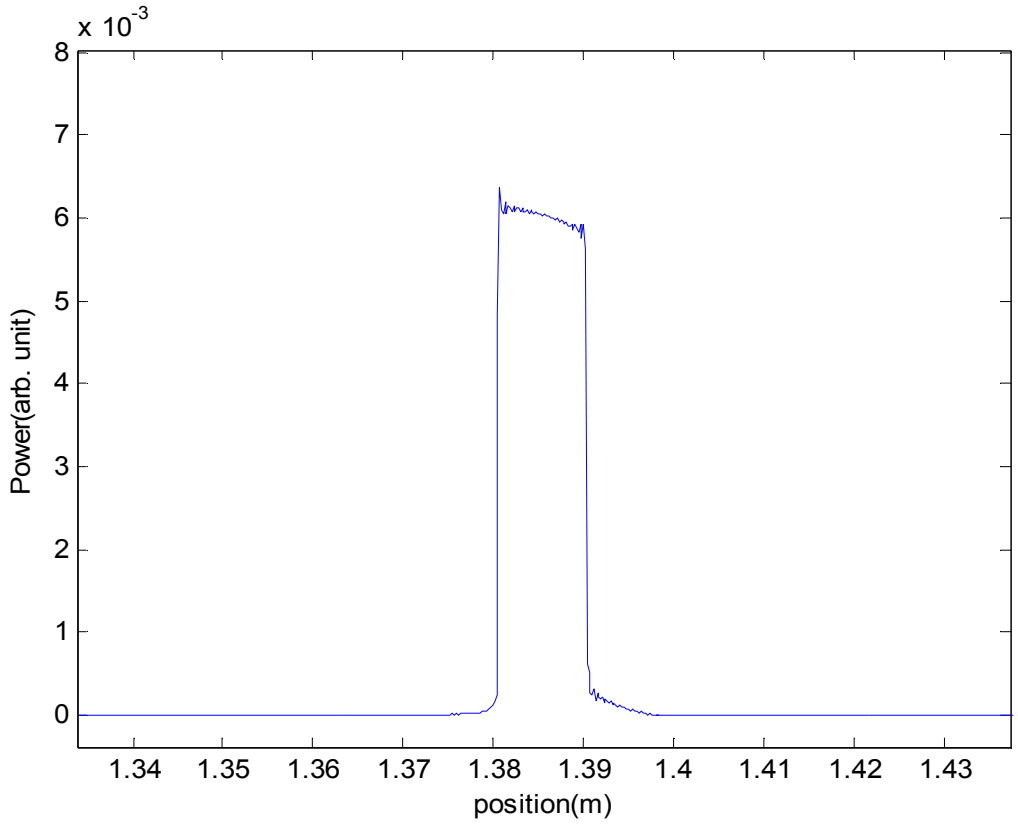

Figure 3.16. Simulated OFDR trace

3.3.2.2. OFDR Interrogation of Fiber Bragg Grating by using Transfer Matrix Method

In previous examples, the results are obtained by using the analytical approach derived in the Appendix B. This approach does not permit us to realize a distributed analysis along the length of the FBG. In this part, we implement the Transfer matrix method to model the FBG interrogated by the OFDR. In the model, there is a single FBG on the test arm of the OFDR as shown in Figure 3.17.

In order to simulate detector signal (D), FBG and mirror are modeled on the C-OFDR system. The model is determined based on transfer matrix method as mentioned in section 2.4.4. Fiber Bragg grating is divided into N uniform section and each section length is Δz long [42].

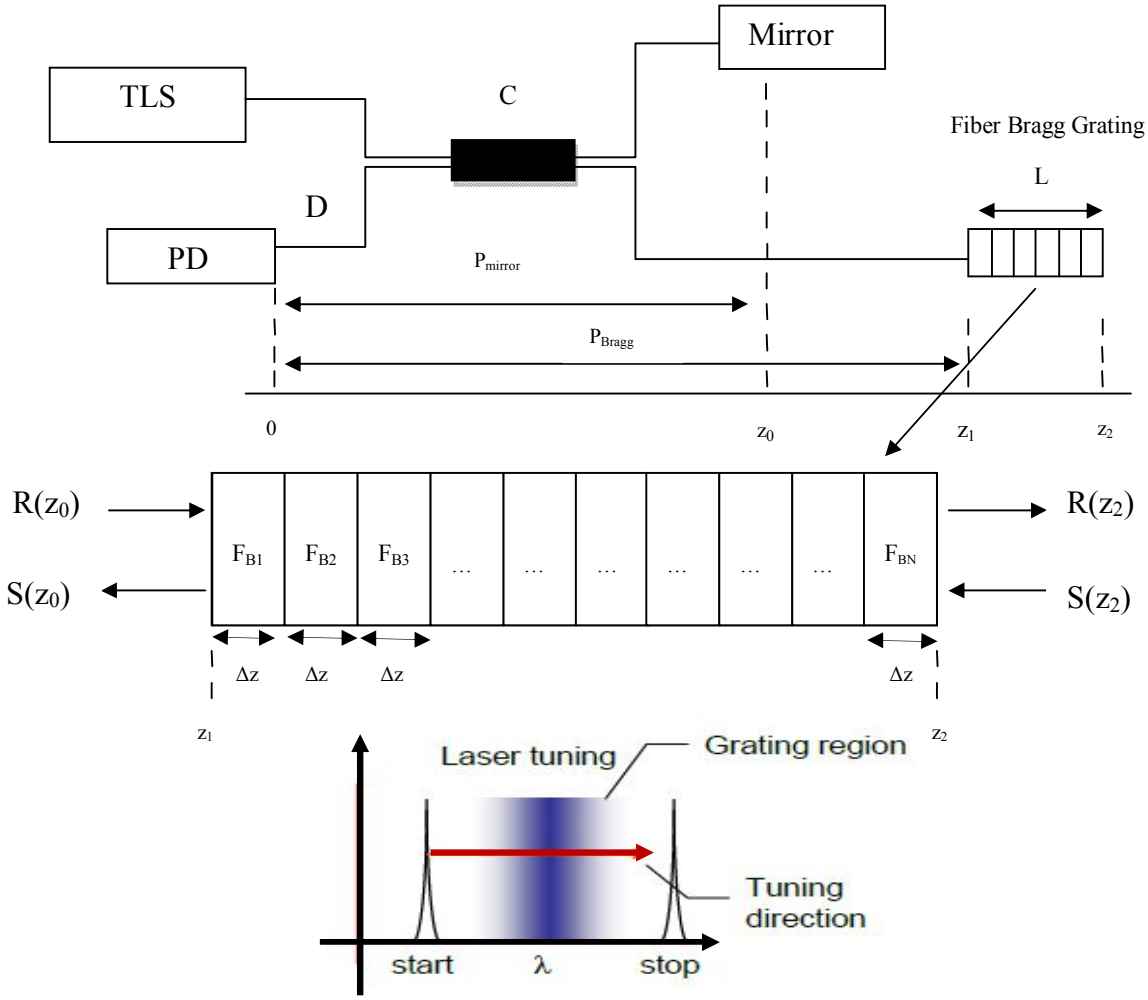

Figure 3.17. Model of FBG and mirror on C-OFDR system (TLS: Tunable Laser Source, PD: Photodetector, C: Coupler)

The elements of the grating matrices $F_{B1\ldots N}$ is formed by equations and is expressed as,

$$T_{11} = \cosh(\alpha L) - \frac{i\delta \sinh(\alpha L)}{\alpha} \quad (3.4)$$

$$T_{12} = -\frac{i\kappa \sinh(\alpha L)}{\alpha} \quad (3.5)$$

$$T_{21} = \frac{i\kappa \sinh(\alpha L)}{\alpha} \quad (3.6)$$

$$T_{22} = \cosh(\alpha L) + \frac{i\delta \sinh(\alpha L)}{\alpha} \quad (3.7)$$

$$F_B = \begin{bmatrix} \cosh(\alpha\Delta z) - \frac{i\delta \sinh(\alpha\Delta z)}{\alpha} & -\frac{i\kappa \sinh(\alpha\Delta z)}{\alpha} \\ \frac{i\kappa \sinh(\alpha\Delta z)}{\alpha} & \cosh(\alpha\Delta z) + \frac{i\delta \sinh(\alpha\Delta z)}{\alpha} \end{bmatrix} \quad (3.8)$$

The phase shift matrix P_{Mirror} and P_{Bragg} of the reflection matrices is obtained in the transfer matrix by multiplying the reflectivity of the Nth section by matrix elements only containing phase terms of reflectivity and calculated as:

$$P = \begin{bmatrix} e^{-\frac{i\phi}{2}} & 0 \\ 0 & e^{\frac{i\phi}{2}} \end{bmatrix} \quad (3.9)$$

$$\phi = \frac{4\pi}{\lambda} n_{eff} z \quad (3.10)$$

In the case of mirror side of the optical path the relation between output and input of the system is given as,

$$\begin{bmatrix} R_M(0) \\ S_M(0) \end{bmatrix} = P_{Mirror} \begin{bmatrix} R_M(z_0) \\ S_M(z_0) \end{bmatrix} \quad (3.11)$$

where R_M is the amplitude of the forward propagation mode, S_M is the amplitude of the backward propagating mode and P_M is the mirror phase shift matrix.

The phase shift matrix P_{Mirror} of the mirror reflection matrix is given as,

$$P_{Mirror} = \begin{bmatrix} e^{-\frac{i\phi}{2}} & 0 \\ 0 & e^{\frac{i\phi}{2}} \end{bmatrix} \quad (3.12)$$

$$\phi = \frac{4\pi}{\lambda} n_{eff} z_0 \quad (3.13)$$

When the boundary conditions are applied,

$$R_M(0) = 1 \quad (3.14)$$

$$S_M(z_0) = R_M(z_0) e^{i\pi} \quad (3.15)$$

$$\begin{bmatrix} 1 \\ S_M(0) \end{bmatrix} = \begin{bmatrix} P_{M11} & P_{M12} \\ P_{M21} & P_{M22} \end{bmatrix} \begin{bmatrix} R_M(z_0) \\ R_M(z_0)e^{i\pi} \end{bmatrix} \quad (3.16)$$

The mirror reflection coefficient is given as,

$$RL_{Mirror} = S_M(0) = \frac{P_{M21}+P_{M22}e^{i\pi}}{P_{M11}+P_{M12}e^{i\pi}} \quad (3.17)$$

$$RL_{Mirror} = e^{i(2n_{eff}z_0k+\pi)} \quad (3.18)$$

For the optical path contains fiber Bragg grating, the transfer matrix (T) for the whole optical path is considered as the multiplication of the transfer matrices of all the individual FBG sections and express as,

$$T=P_{Bragg}F_{B1}F_{B2}\ldots\ldots F_{BN} \quad (3.19)$$

where P_{Bragg} is Bragg phase shift matrix and given as,

$$P_{Bragg} = \begin{bmatrix} e^{-\frac{i\emptyset}{2}} & 0 \\ 0 & e^{\frac{i\emptyset}{2}} \end{bmatrix} \quad (3.20)$$

$$\emptyset = \frac{4\pi}{\lambda} n_{eff} z_1 \quad (3.21)$$

The relation between input and output of the Bragg system is defined by the equation 3.22,

$$\begin{bmatrix} R_B(0) \\ S_B(0) \end{bmatrix} = \begin{bmatrix} T_{11} & T_{12} \\ T_{21} & T_{22} \end{bmatrix} \begin{bmatrix} R_B(z_2) \\ S_B(z_2) \end{bmatrix} \quad (3.22)$$

where R_B is the amplitude of the forward propagating mode and S_B is the amplitude of the backward propagating mode.

The boundary conditions for the Bragg system is defined as,

$$R_B(0) = 1 \tag{3.23}$$

$$S_B(z_2) = 0 \tag{3.24}$$

When the boundary condition is applied on equation 3.22, the reflection coefficient for Bragg grating cab be defined as,

$$RL_{Bragg} = S_B(0) = \frac{T_{21}}{T_{11}} \tag{3.25}$$

Finally the output signal observed by detector (D) is calculated by using two-beam interference method and given by [7],

$$D = \left(RL_{Mirror} + RL_{Bragg}\right)\left(RL_{Mirror} + RL_{Bragg}\right)^{*} \tag{3.26}$$

$$D = \left|RL_{Mirror} + RL_{Bragg}\right|^{2} \tag{3.27}$$

- **Matlab Implementation**

In this part, mathematical model is verified for the above scheme (Figure 3.17) with the Matlab simulations. Figures 3.18, 3.19, 3.20, 3.21 and 3.22 are obtained by using equations from 3.4 to 3.27. The parameters used in simulations are as follows,

Table 3.2. Parameters used for the Matlab implementation of OFDR

Visibility	0.3944
z_0 (absolute location of the mirror)	1 m
z_1 (location of FBG)	4.96 m
n_{eff} (effective refractive index of fiber core)	1.45
L (Fiber Bragg grating length)	200 mm
δn_{eff} (Average index change)	3.10×10^{-6}
λ_{Bragg} (Bragg wavelength)	1548.163 nm
N (number of FBG section)	100

In figure 3.18, the reflection spectrum of a uniform fiber Bragg grating is obtained by using Transfer Matrix Method. This results that Bragg grating reflects %20 of the incident signal. Figure 3.19 shows the composite detector signal, D which is normalized by its maximum value at the Bragg wavelength (1548.163 nm)

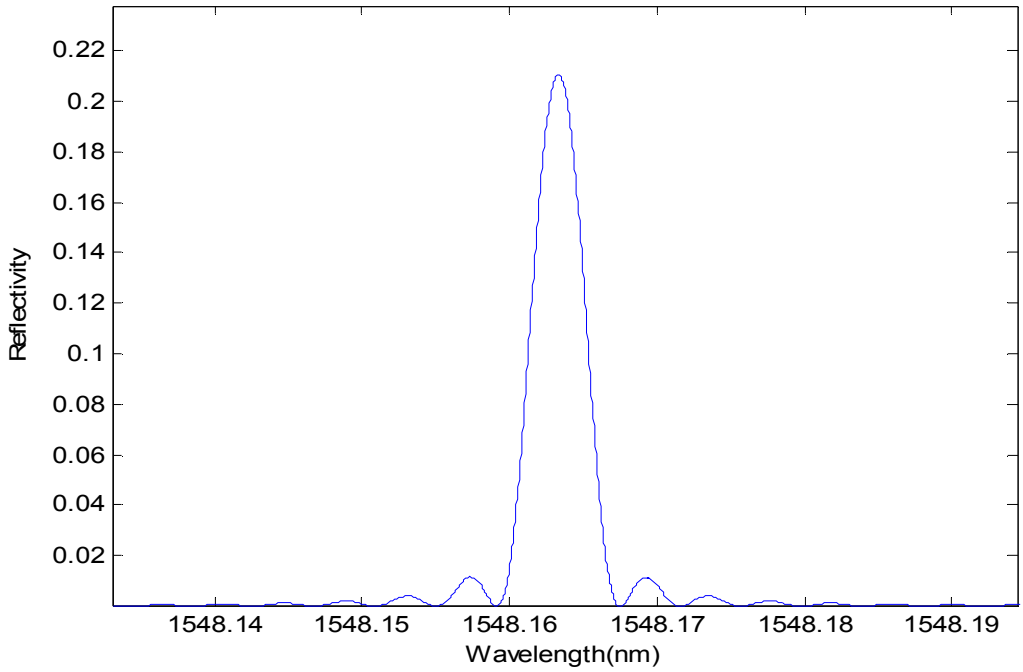

Figure 3.18. Evolution of Fiber Bragg Grating reflection spectrum by transfer matrix method

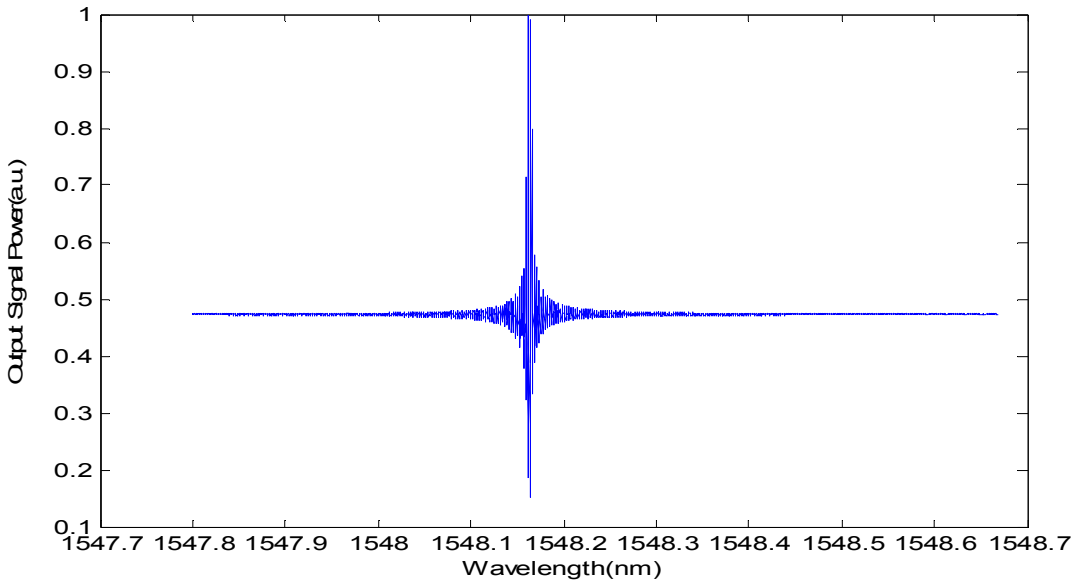

Figure 3.19. Output signal calculated by photodetector

In Figure 3.20, the Fourier transform of interference signal is taken to obtain the OFDR trace showing the power reflected from the FBG as a function of position. The reason of the power decrease along the grating length is the loss of the light when it propagates though the grating.

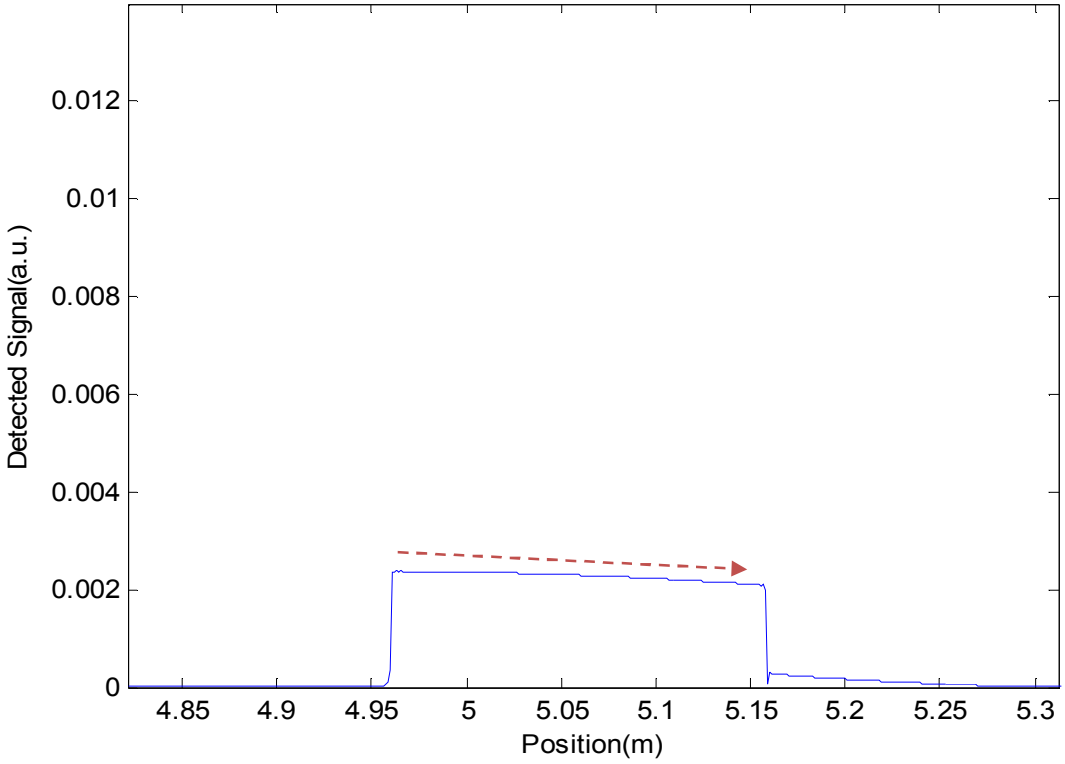

Figure 3.20. Simulated beat spectrum of the interferometer

In Figure 3.21 Inverse Fourier transform is applied on the selected position (between 4.96 m- 5.16 m) as explained before to "demodulate" the reflection spectrum of the FBG. This demodulated reflection spectrum is then compared with the original reflection spectrum where a good agreement is observed between the two approaches. This means that our demodulation process works well and our simulation results match with the theoretical values.

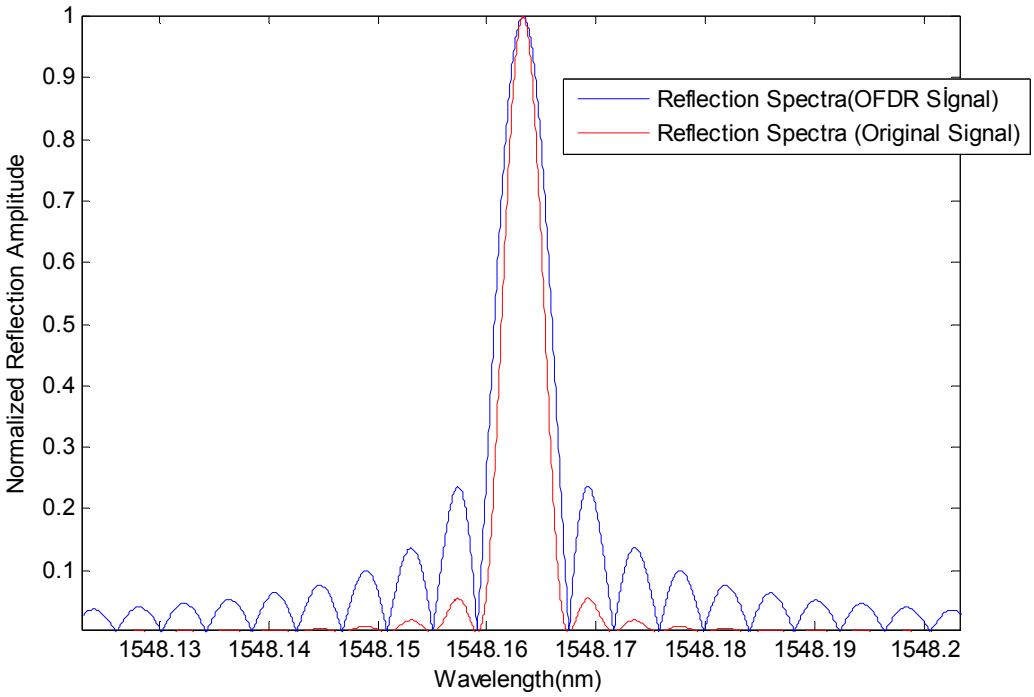

Figure 3.21. Comparison of demodulated signal with calculated reflectivity

Figure 3.22 represents the spectrogram of the output signal D. The spectrogram is obtained by applying Short Time Fourier Transform of the signal and provides the spectrum information in 3 dimensions, namely, wavelength, position and intensity.

To perform STFT, a proper window (Hanning window is used in simulations) is applied for a definite wavelength, the information about the signal around focused wavelength is obtained.

Then by using Fast Fourier Transform the extracted signal analyzed and each frequency components power in the output signal is achieved.

Sliding the window to all wavelengths and performing Fourier transform provided us three dimensional information that includes wavelength information at the x-axis, position information at the y-axis and colored part shows the power of the signal.

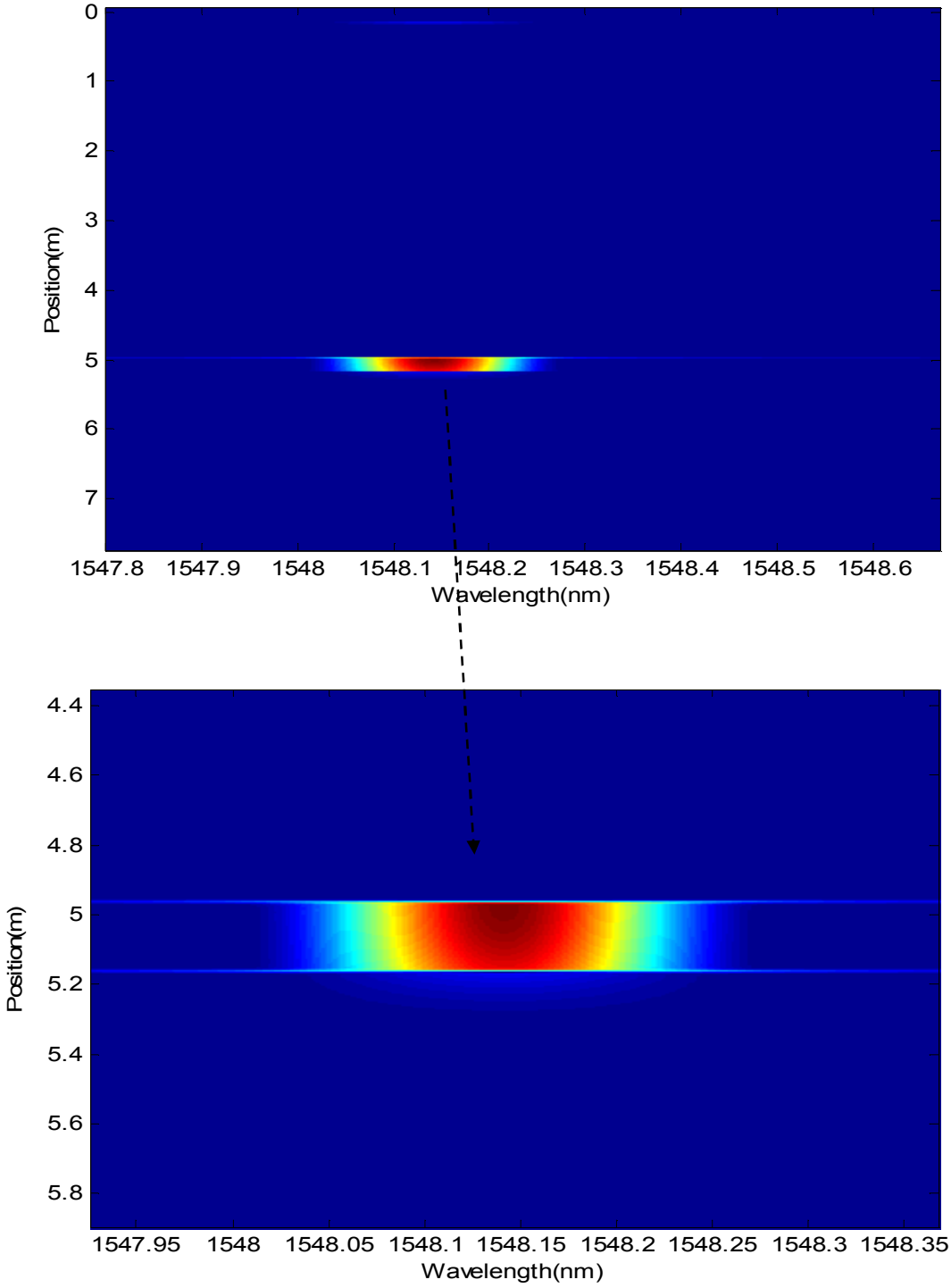

Figure 3.22 Spectrogram of interference signal

In figure 3.22 the red colored part of the spectrogram denotes the highest intensity regions from red to dark blue region the intensity of light is increase. It is logical because of the reflection is occurs at the Bragg wavelength 1548.16 for this simulation and the intensity of light is expanded around this wavelength.

Under a physical effect applied on Bragg grating, the Bragg wavelength shifts differently proportional to the applied effect. Figure 3.23 and 3.24 shows shift on the reflection coefficient of the fiber Bragg grating and shift on the detector signal under applied strain. In this simulation the Bragg wavelength shift is 0.2 nm at its center in other words it shifts from 1548.16 nm to 1548.36 nm. So the output and reflection spectrum is separated by 0.2 nm.

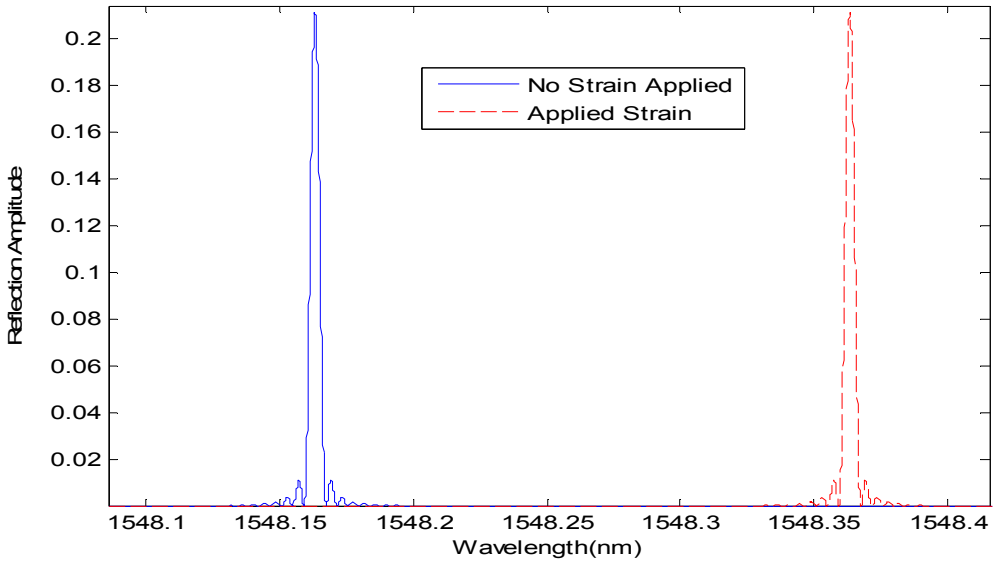

Figure 3.23. Reflection spectrum of uniform FBG for 0.2 nm shifts

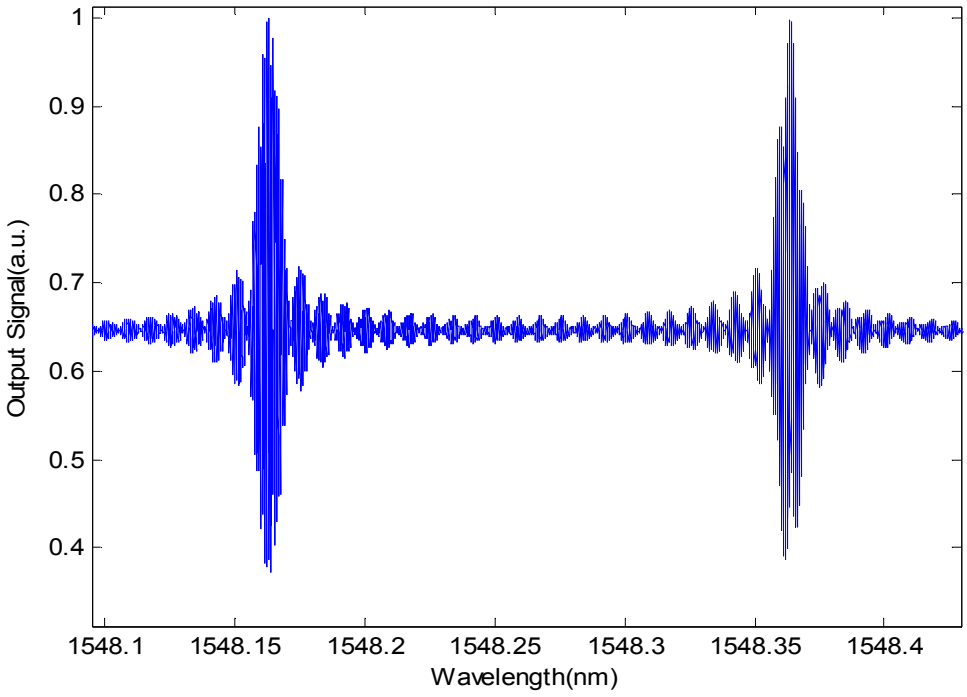

Figure 3.24. Output signals for 0.2 nm shifts

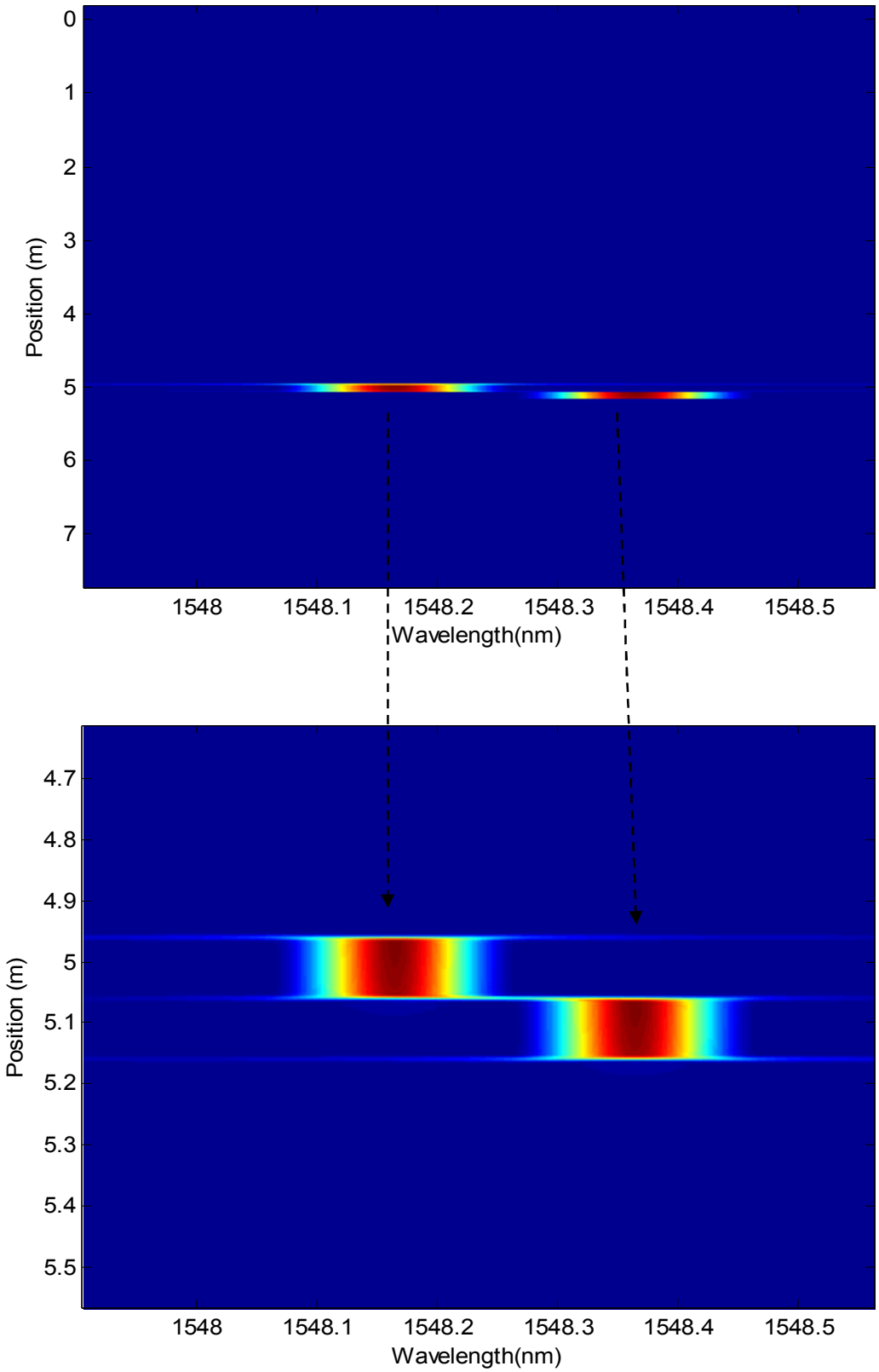

Figure 3.25. Spectrogram of the 0.2 nm shifted interference signal

In figure 3.25 the reflection center wavelength shift is obtained in spectrogram. Bragg wavelength. The spectrogram is obtained by appliying STFT on the detector signal. The reflected light is sampled by 0.14 1/m (Δk) wave number spacing. This results a 0.053 pm wavelength spacing ($\Delta\lambda$). Analysis is done by using 4000 points Hanning window and FFT is applied to 2^{14} points. Window is slided 20 points. The window length is choosed as 4000 point due to influencing distance and wavelength resolution. Here figures show that applied strain effects amount of wavelength shift on the Bragg wavelength.

CHAPTER 4

POLARIZATION CONCEPTS

4.1. Introduction

Fiber Bragg gratings that studied in Chapter 2 is manufactured by exposing one side of the optical fiber to an intense UV interference pattern. It is accepted that the writing process of the fiber leads to small amount of birefringence. This quantity combines with the intrinsic birefringence. The small birefringence values have significant polarization dependent effects on Bragg gratings. In this chapter, the basic phenomena of the polarization of light are studied. Then, the mathematical formalism to define the state of the polarization is examined. Birefringence term and the effect of this phenomenon to the uniform fiber Bragg gratings are also explained in detail. Finally, the effect of grating parameters (physical length, refractive index modulation) and the value of the birefringence on the Polarization Dependent Loss (PDL) are studied.

4.2. Polarization of Light

A polarized lightwave signal propagating in free space or in a waveguide like optical fiber can be described by electrical and magnetic field vectors perpendicular to each other in a transverse plane and perpendicular to the direction of propagation [43].

The state of polarization is presented by the pattern plotted by electrical field vector as a function of time at a fixed point in a transverse plane [44].

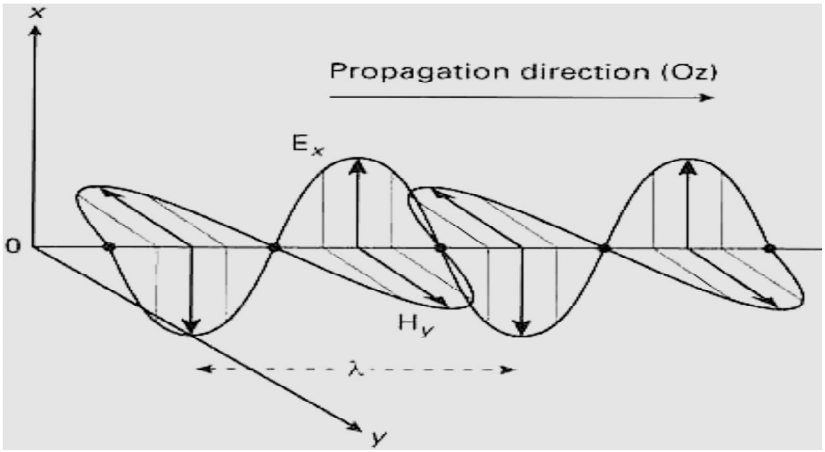

Figure 4.1. Concept of polarization of light

To present the polarized light propagating along the z direction mathematically (in terms of the x and y axis projections of electrical field vector), x and y components of the electric field at z=0 given by,

$$E_x = \varepsilon_x e^{i\omega t - kz} \quad ; \quad E_y = \varepsilon_y e^{i\omega t - kz} \tag{4.1}$$

$$\varepsilon_x = E_{0x} e^{i\delta_x} \quad ; \quad \varepsilon_y = E_{0y} e^{i\delta_y} \tag{4.2}$$

$$E_x(z,t) = E_{0x}\cos(\omega t + \delta_x - kz) \tag{4.3}$$

$$E_y(z,t) = E_{0y}\cos(\omega t + \delta_y - kz) \tag{4.4}$$

where E_{0x} and E_{0y} are the maximum amplitudes, δ_x and δ_y are the corresponding phases. The pattern drawn by electrical field is found by eliminating (ωt-kz) term from the equations 4.3 and 4.4 so the relation is define as,

$$\frac{E_x^2}{E_{0x}^2} + \frac{E_y^2}{E_{0y}^2} - 2\frac{E_x E_y}{E_{0x}E_{0y}}\cos\delta = \sin^2\delta \tag{4.5}$$

where $\delta = \delta_x - \delta_y$ is the phase difference between x and y components.

Equation 4.5 is the polarization ellipse equation trace out in the transverse plane by the tip of the electrical field vector in a fixed point of space and as a function of time [45]. Fully polarized light wave's state of polarization is elliptical by the equation it is obvious that state of polarization depends three parameters E_{0x}, E_{0y} and δ. This ellipse is presented in figure 4.2.

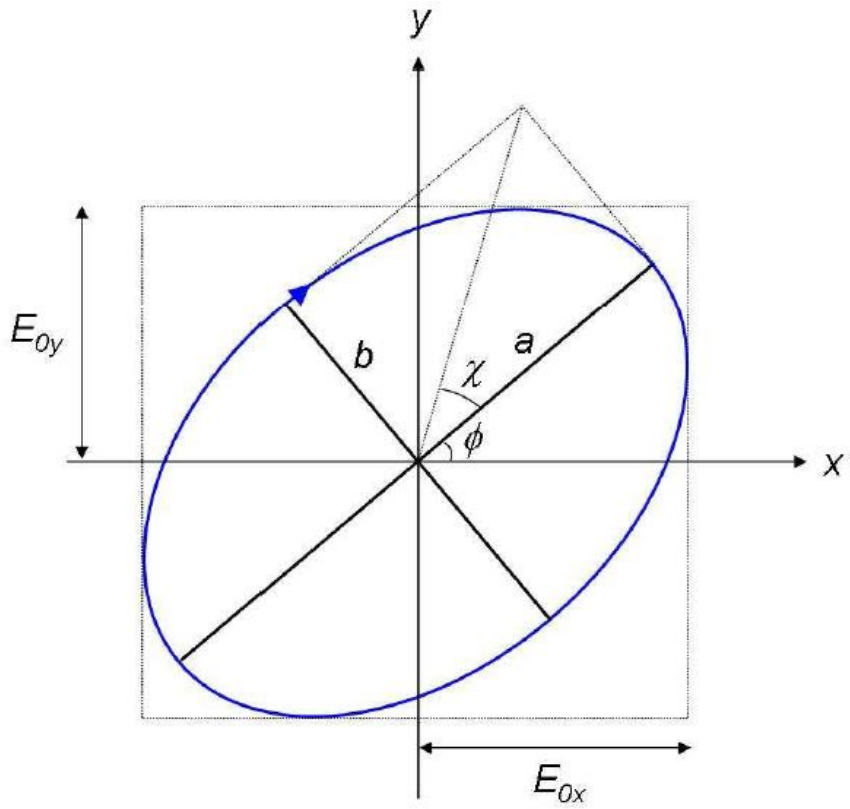

Figure 4.2. Polarization ellipse

where ø is the azimuth between the major axis and x axis of ellipse and defined as,

$$ø = \tan^{-1}\frac{E_{0x}}{E_{0y}} \tag{4.6}$$

The ellipticity e is defined as,

$$e = \tan\chi = \pm\frac{b}{a} \tag{4.7}$$

where a and b are the length of half the major and minor axis. e remains between -1 and +1. Positive/negative sign in the preceding equation represents left/right rotation of the electric field vector. If the electrical field vector in the clockwise, the state of polarization is right handed and sign of ellipticity is positive.

In the case of linear polarization state, phase difference between x and y component should be $\delta=\pm m\pi$ m=0, 1, 2,… so $\chi=0$ and the resultant state of polarization is linear.

4.2.1. Jones Vector Formalism of Polarized Light

Polarization variation of an incident wave when it passes through an optical component can be described by three formalisms:; Jones calculus, Mueller calculus, and the Poincaré sphere.

Between 1941 and 1948 Clark Jones proposed a mathematical representation of polarized light based on optical fields. This method represents a given SOP by only a two dimensional vector of complex numbers known as Jones vector and uses simple 2 × 2 matrices to calculate the effect of a polarizer or a birefringent medium for a given state of polarization (SOP) [46].

Description of the electric field vector of an arbitrarily polarized light wave in terms of two orthogonal and linearly polarized components can be written as,

$$E(z,t) = E_{0x}\cos(\omega t + \delta_x - kz)\,\hat{\boldsymbol{x}} + E_{0y}\cos(\omega t + \delta_y - kz)\hat{\boldsymbol{y}}\text{m} \tag{4.8}$$

The SOP is defined in terms of a 2 × 1 matrix as,

$$E(z,t) = \begin{bmatrix} E_x \\ E_y \end{bmatrix} = \begin{bmatrix} E_{0x}\cos(\omega t + \delta_x - kz) \\ E_{0y}\cos(\omega t + \delta_y - kz) \end{bmatrix} \tag{4.9}$$

$$E(z,t) = \begin{bmatrix} E_{0x}\mathrm{e}^{\omega t+\delta_x-kz} \\ E_{0y}e^{\omega t+\delta_y-kz} \end{bmatrix} = \mathrm{e}^{\omega t+\delta_x-kz}\begin{bmatrix} E_{0x} \\ E_{0y}\mathrm{e}^{\mathrm{i}\delta} \end{bmatrix} \tag{4.10}$$

When the common phase factor is omitted to simplify the representation of the phases, equation 4.10 is written as,

$$E(z,t) = \begin{bmatrix} E_{0x} \\ E_{0y}\mathrm{e}^{\mathrm{i}\delta} \end{bmatrix} \tag{4.11}$$

To normalize the Jones vector given by Equation 4.11, the amplitudes E_{0x} and E_{0y} are divided by $\sqrt{E_{0x}^2 + E_{0y}^2}$ and obtained as,

$$E(z,t) = \frac{1}{\sqrt{E_{0x}^2+E_{0y}^2}}\begin{bmatrix} E_{0x} \\ E_{0y}\mathrm{e}^{\mathrm{i}\delta} \end{bmatrix} \tag{4.12}$$

A linearly polarized wave of amplitude E_{0x} making an angle ø with the x axis can be described as a superposition of the x- and y polarized components. Thus, the corresponding normalized Jones vector is given by,

$$E(z,t) = \begin{bmatrix} \cos ø \\ sin ø \end{bmatrix} \tag{4.13}$$

For the different values of ø, ø = 0 or ø = π/2, a linear horizontal or vertical polarization, the Jones vectors is expressed as,

Horizantal: $$\hat{e}_x = \begin{bmatrix} 1 \\ 0 \end{bmatrix} \tag{4.14}$$

Vertical: $$\hat{e}_y = \begin{bmatrix} 0 \\ 1 \end{bmatrix} \tag{4.15}$$

The effect of any polarization component on a given SOP can be described by a 2 × 2 Jones matrix, hence, Jones matrix connects the input and the output of Jones vectors.

As shown in Figure 4.3, if a given polarization state **A** is passed through a polarizing device whose Jones matrix is J, the output polarization state **A′** will be given by as,

$$\mathbf{A}' = \mathrm{J}\ \mathbf{A}. \tag{4.16}$$

If there are two devices in a series with Jones matrices J1 and J2, respectively, the Jones matrix of the combination is given by J2 J1, and the output polarization state will be given by

$$\mathbf{A}' = \mathrm{J2\ J1}\ \mathbf{A} \tag{4.17}$$

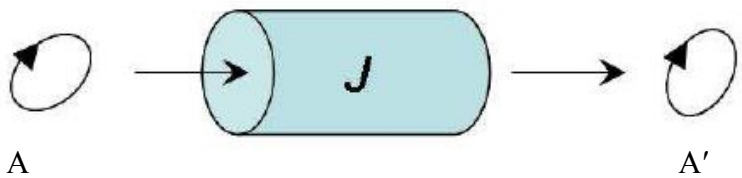

Figure 4.3. Jones matrix presentation of optical component

4.2.2. The Stokes Parameters Formalism

In previous section, the Jones vector formalism of polarized light is studied. Although Jones vector presentation is quite simple and straightforward this formalism only described polarized light. In 1852 George Gabriel Stokes was proposed Stokes parameters, to obtain a mathematical definition of the polarization state of light which can be unpolarized, partially polarized or polarized [47].

In Jones formalism, the representation of polarized light was based on optical fields and described by complex numbers. But Stokes formalism is developed for expressing polarization in terms of measured intensities and described by real numbers.

The polarization states of the electric fields is defined by four dimensional Stokes vector (S) as,

$$S = \begin{pmatrix} S_0 \\ S_1 \\ S_2 \\ S_3 \end{pmatrix} \tag{4.18}$$

$$S_0 = I_0 \tag{4.19}$$

$$S_1 = I_H - I_V \tag{4.20}$$

$$S_2 = I_{+45} - I_{-45} \tag{4.21}$$

$$S_3 = I_{RCP} - I_{LCP} \tag{4.22}$$

where S_0, S_1, S_2 and S_3 are the Stokes parameters.

S_0= Total power (Polarized + Unpolarized)

S_1= Power through Linear Horizontal Polarizer (LHP) + power through Linear Vertical Polarizer (LVP)

S_2= Power through Linear +45 deg polarizer - power through linear -45 deg polarizer

S_3= Power through Right Circular Polarizer (RCP) – power through Left Circular Polarizer (LCP) [48].

To obtain normalized Stokes parameters, Stokes parameters are divided into total power S_o and founded as,

$$s_1 = \frac{S_1}{S_0} \; ; \; s_2 = \frac{S_2}{S_0} \; ; s_3 = \frac{S_3}{S_0} \tag{4.23}$$

The new Stokes vector for the normalized Stokes parameters can be written as,

$$s = \begin{pmatrix} 1 \\ s_1 \\ s_2 \\ s_3 \end{pmatrix} \tag{4.24}$$

Thus, the range of the normalized Stokes parameters is -1 to +1. For the fully polarized light the analogy between Jones vectors and Stokes vectors can be expressed as,

$$S_0 = E_{0x}^2 + E_{0y}^2 \tag{4.25}$$

$$S_1 = E_{0x}^2 - E_{0y}^2 \tag{4.26}$$

$$S_2 = 2Re\left(E_x E_y^*\right) = 2E_{0x}E_{0y}\cos\delta \tag{4.27}$$

$$S_3 = 2Im\left(E_x E_y^*\right) = 2E_{0x}E_{0y}\sin\delta \tag{4.28}$$

4.3. Birefringence in Optical Fibers

A single-mode fiber supports two (degenerate) modes (HE_{11}^x, HE_{11}^y) to propagate simultaneously, which are orthogonally polarized. In an ideal circular-core fiber (has perfect circular symmetry); these two degenerate modes will propagate with the same phase and velocity. Practical fibers have slightly elliptical core. Furthermore, the doping concentration in the core section of optical fiber is not perfectly uniform and the fiber material can be subjected environmental factors as bend, twist, and anisotropic stress. This asymmetry in core leads to removing of degeneracy and the refractive index value will be different for the orthogonal polarization pairs called polarization modes. This property is called as birefringence.

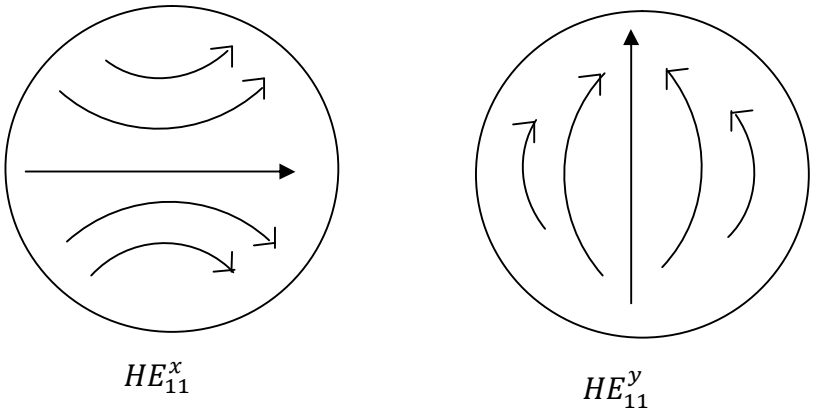

Figure 4.4. Schematic of polarization states for orthogonally polarized HE_x and HE_y modes

For a standard fiber the order of magnitude of the intrinsic birefringence is typically 10^{-7} [49], [50].

Birefringence can be defined by taking the absolute value of the difference between the polarization modes propagation constants,

$$\Delta\beta = \left|\beta_x - \beta_y\right| = \frac{2\pi}{\lambda}\left|n_{eff,x} - n_{eff,y}\right| = \frac{\omega}{c}\Delta n \qquad (4.29)$$

In equation 4.29, Δn is the refractive index difference (the degree of birefringence), c is the speed of the light in vacuum and $n_{eff,x}$ and $n_{eff,y}$ is the effective refractive indices of two polarization modes.

Optical fibers that is described by the uniform birefringence have constant difference between propagation constant of two polarization modes and phase delay between two modes is equal to $\Delta\phi = \Delta\beta L$. The birefringence property of an optical fiber which characterized by a uniform birefringence can be divided as linear birefringence and circular birefringence.

For a linear birefringence the two polarization modes are linearly polarized and orthogonal to each other. For a circular birefringence two polarization modes are circularly polarized one of them is right handed polarized and another one is left handed [46].

- The ellipticity of core that leads the geometrical anisotropy produces a linear birefringence.
- Transversal stress applied on optical fibers results proportional change on the linear birefringence.
- A transverse electric field results linear birefringence.
- An asymmetrical lateral stress on the fiber introduces linear birefringence.
- Twisting an optical fiber introduces a circular birefringence in the optical fiber.

4.4. Polarization Dependent Loss

Polarization dependent loss (PDL) can be defined as the measure of the power variation of an optical system for all possible input states of polarization. PDL can be calculated by taking the ratio of the maximum and minimum power of the output of the optical system with regard to all polarization states.

The PDL can be expressed as,

$$PDL_{dB} = 10\log_{10}\frac{P_{max}}{P_{min}} \tag{4.30}$$

where P_{max} is the maximum output power and P_{min} is the minimum output power through the test component of the system. For classical optical fibers, PDL is often very small ($\leq$ 0.1 dB for a fiber coupler) and is thus neglected. [51].

4.5. Polarization Manifestation in Uniform Fiber Bragg Gratings

Until now, the polarization concept of light in optical fibers is studied. In this part of this chapter the effect of polarization in uniform Bragg grating is investigated in order to include this effect in the model and simulations.

Exposing one side of the fiber to the UV light source, during the fabrication process of fiber Bragg grating, induces variation of refractive index along the cross section of fiber. The refractive index becomes larger at the core side which is subjected to UV laser. Refractive index variation produces photo-induced birefringence (order of magnitude varies between 10^{-6} and 10^{-5} in practice). Combination of photo-induced birefringence with the intrinsic fiber birefringence results a global birefringence value Δn.

The differences between effective refractive indices of the two polarization modes are expressed as,

$$n_{eff,x} = n_{eff} + \frac{\Delta n}{2} \tag{4.31}$$

$$n_{eff,y} = n_{eff} - \frac{\Delta n}{2} \tag{4.32}$$

where n_{eff} stands for the mean effective refractive index in the fiber core without birefringence and Δn is the global birefringence value reached at the end of the writing process.

Polarization modes propagating along the grating subjected to different coupling due to the presence of birefringence. As a result the complex reflection and transmission coefficients of Bragg grating degenerate into two (x and y) modes [2].

Writing one side of the core during the fabrication process is assumed to lead a linear birefringence, applying a transversal load can also create liner birefringence.

In a Cartesian coordinates system whose reference axes match the grating polarization modes one can therefore associate a diagonal Jones matrix to the grating and the Jones vector of the transmitted signal is then [52]:

$$\begin{pmatrix} E_{t,x} \\ E_{t,y} \end{pmatrix} = \begin{pmatrix} t_x & 0 \\ 0 & t_y \end{pmatrix} \begin{pmatrix} E_{i,x} \\ E_{i,y} \end{pmatrix} = \begin{pmatrix} t_x E_{i,x} \\ t_y E_{i,y} \end{pmatrix} \tag{4.33}$$

Jones vector of the input signal is expressed as,

$$\begin{pmatrix} E_{i,x} \\ E_{i,y} \end{pmatrix} = \begin{pmatrix} a_x e^{i\varphi_x} \\ a_y e^{i\varphi_y} \end{pmatrix} \tag{4.34}$$

where $a_{x,y}$ and $\varphi_{x,y}$ are the amplitude and phase of the polarization state of the input signal.

As obtained in equations from 2.17 to 2.25, the obtained equations by using Transfer Matrix Method are implemented for two polarization modes (x and y).

$$\alpha_j = \sqrt{\kappa^2 - \hat{\sigma}_j{}^2} \tag{4.35}$$

$$\kappa = \frac{\pi}{\lambda} \upsilon \delta n \tag{4.36}$$

$$\hat{\sigma}_j = \frac{2\pi(n_{eff,j} + \delta n)}{\lambda} - \frac{\pi}{\Lambda} \tag{4.37}$$

So the transmission coefficient is rewritten as,

$$t_{FBG(j)} = \frac{\alpha_j}{-\hat{\sigma}_j \sinh(i\alpha_j L) + \alpha_j \cosh(i\alpha_j L)} \tag{4.38}$$

If $A_j = \frac{\alpha}{i}$, the transmission coefficient of a uniform fiber Bragg grating is express as,

$$t_{FBG(j)} = \frac{-A_j}{i\hat{\sigma}_j \sin(A_j L) - A_j \cos(A_j L)} \tag{4.39}$$

Since polarization dependent loss (PDL) is defined as the measure of the power variation in transmission, PDL can be calculated by taking the ratio of the maximum and minimum transmission [53]. PDL for a uniform Bragg grating is obtained by following equation [51],

$$PDL_{dB} = 10 \log_{10} \frac{T_{FBGx}(\lambda)}{T_{FBGy}(\lambda)} \;;\; T_{FBG(j)}(\lambda) = \left| t_{FBG(j)}(\lambda) \right|^2 \tag{4.40}$$

4.5.1. Study of Polarization Properties of Uniform Fiber Bragg Gratings

Using the above equations, the impact of some fiber Bragg gratings parameters (physical length (L), refractive index modulation (δn) and birefringence value (Δn)) on the spectral evolutions of the PDL is theoretically analyzed. In all simulations following parameters are used shown in Table 4.1.

Table 4.1. Parameters used in numerical example

Visibility	0.5
n_{eff} (effective refractive index)	1.4514
L (Fiber Bragg grating length)	1 cm
δn_{eff} (Average index change)	$1x\ 10^{-4}$
Λ (periodic refractive index change)	530 nm
Δn (value of birefringence)	$5x10^{-6}$

As shown in Figure 4.5 transmission spectrum of two polarization modes split from each other because of the birefringence Δn.

The PDL evolution in Figure 4.6 can be justified from the transmitted spectra in figure 4.5 corresponding to the x and y modes. Indeed, null PDL values are reached at wavelengths λ_i for which $T_x(\lambda_i)=T_y(\lambda_i)$. In particular, it happens close to the center of the rejection band. Between two consecutive minimum values, PDL evolutions exhibit local maximum values at wavelengths λ_j corresponding to the local maximum differences of amplitude between $T_x(\lambda_j)$ and $T_y(\lambda_j)$.

The greatest PDL values are obtained at the edges of the rejection band where the difference of amplitude between $T_x(\lambda)$ and $T_y(\lambda)$ is also the largest.

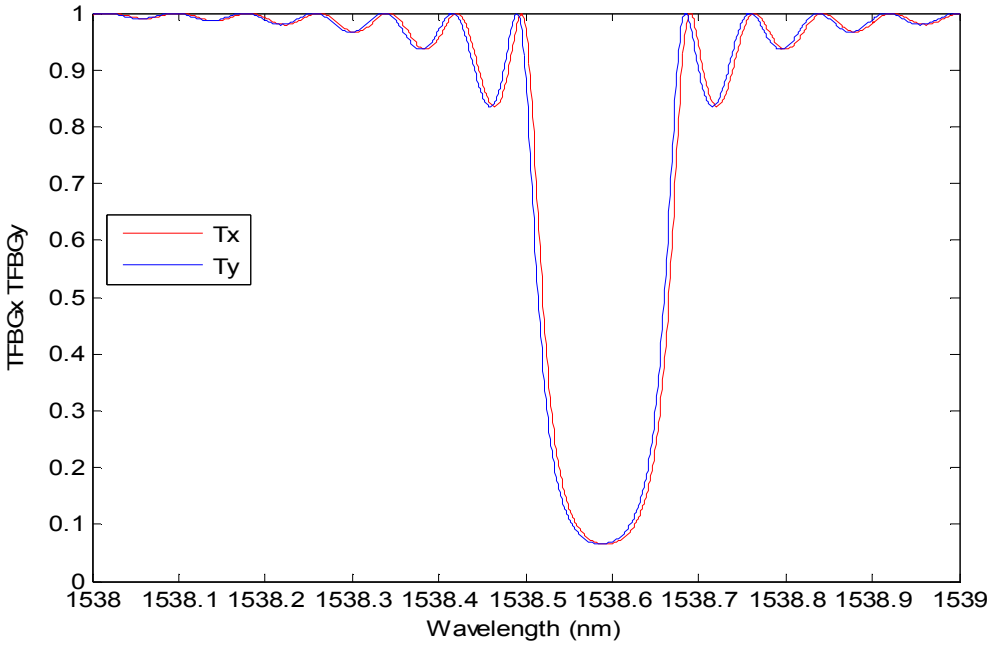

Figure 4.5. Evolution of transmission coefficient of a uniform fiber Bragg grating

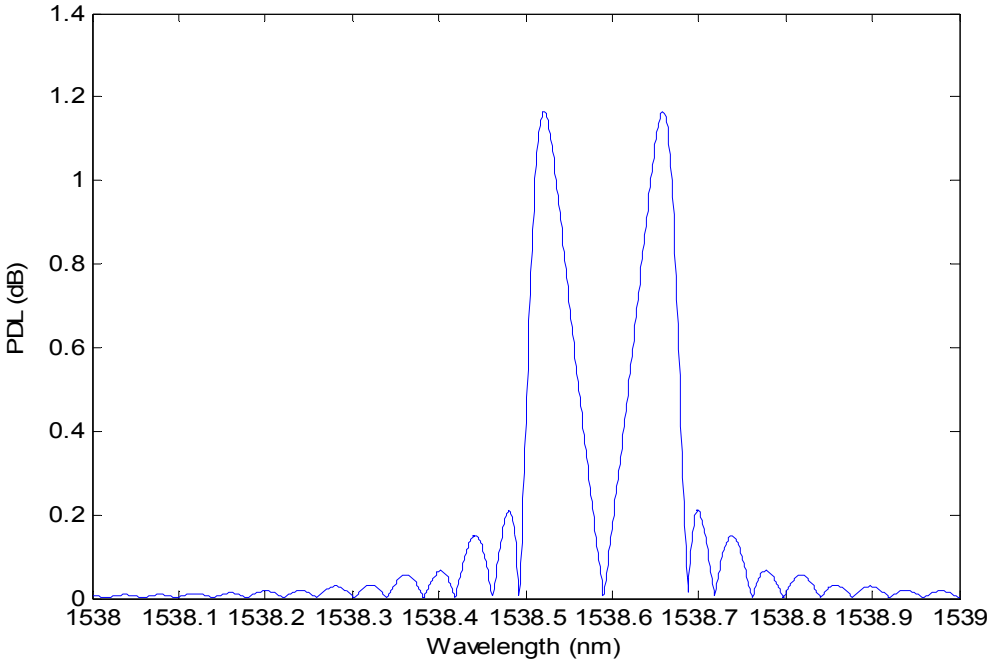

Figure 4.6. Polarization Dependent Loss of a uniform fiber Bragg grating

As shown on these figures 4.7, 4.8, 4.9, 4.10, the grating length and the refractive index modulation have similar effect on the PDL spectra, which is an increase of the peak amplitudes at wavelengths coinciding with the edges of the rejection band of the transmitted spectrum.

The transmitted spectrum is characterized by an increasing amplitude variation at the edges of the main rejection band whereas the wavelength spacing between the two polarization modes is slightly influenced. As a result, sharp PDL evolutions with important maximum values in the rejection band are obtained for gratings characterized by long physical lengths and/or high refractive index modulations.

In figures, the curves are obtained as a function of the normalized wavelength. Normalized wavelength is defined as the ratio between the working wavelength and the central wavelength λ_{max} (λ /λ_{max}).

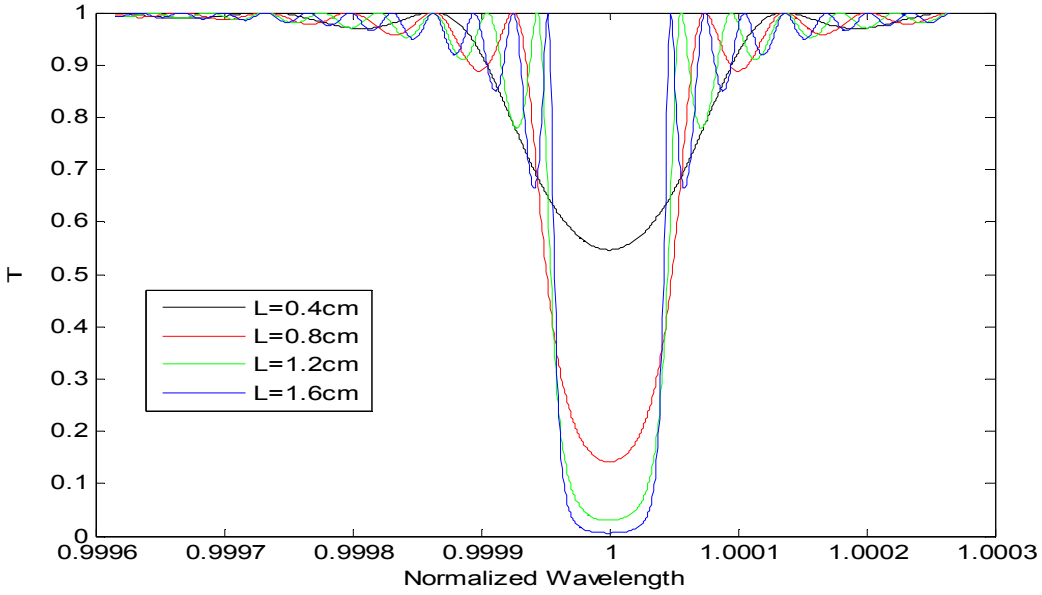

Figure 4.7. Transmitted spectrum evolution as a function of grating length

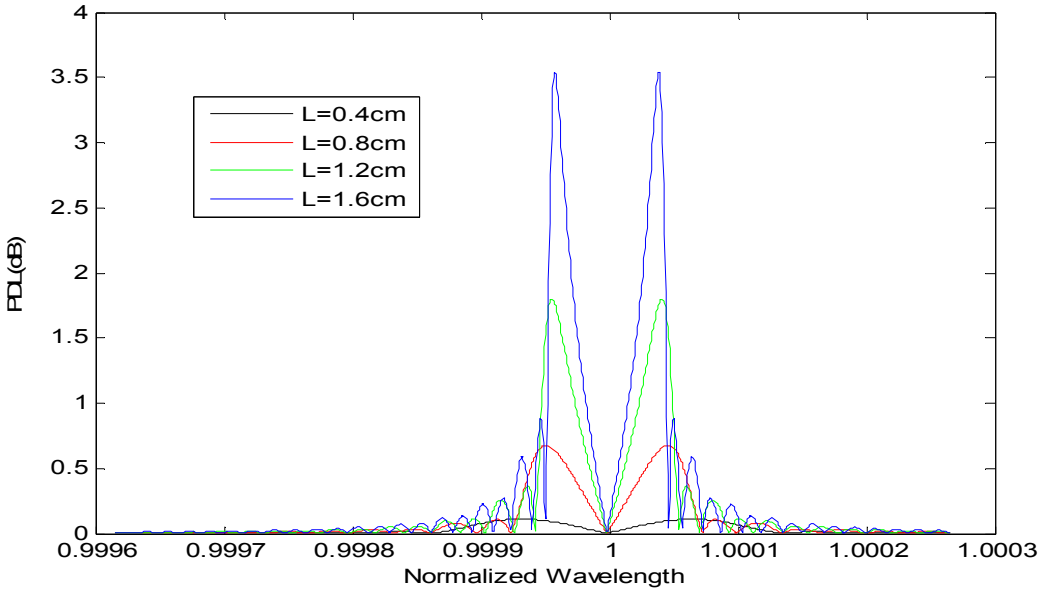

Figure 4.8. Polarization Dependent Loss spectra as a function of grating length

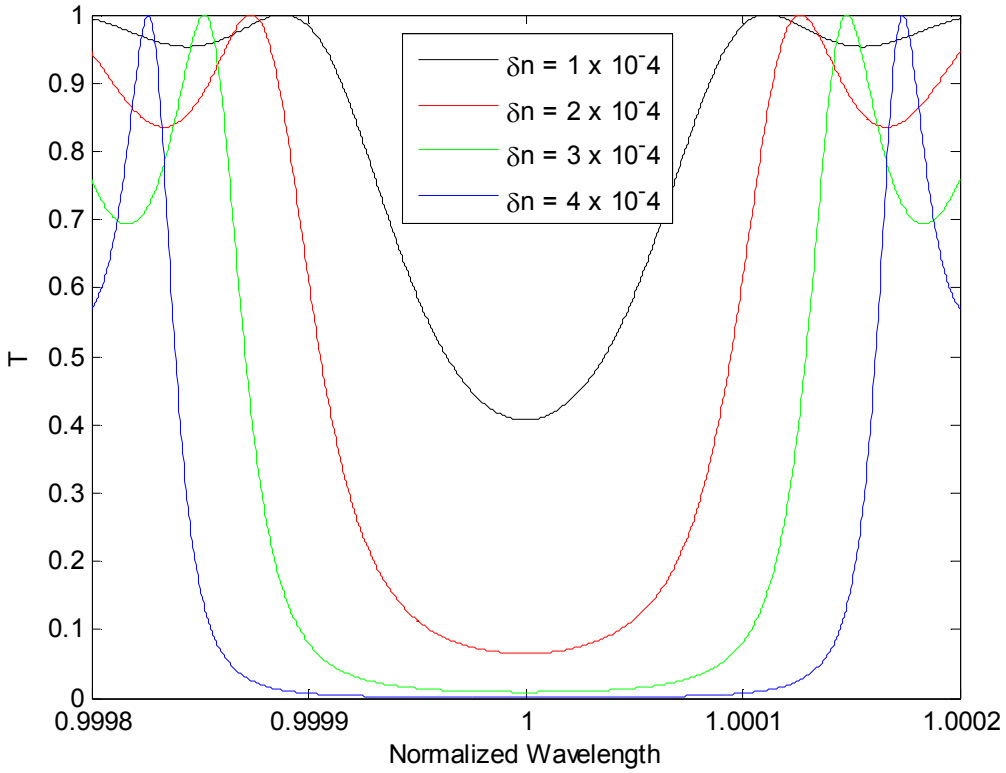

Figure 4.9. Transmitted spectrum evolution as a function of grating periodicity

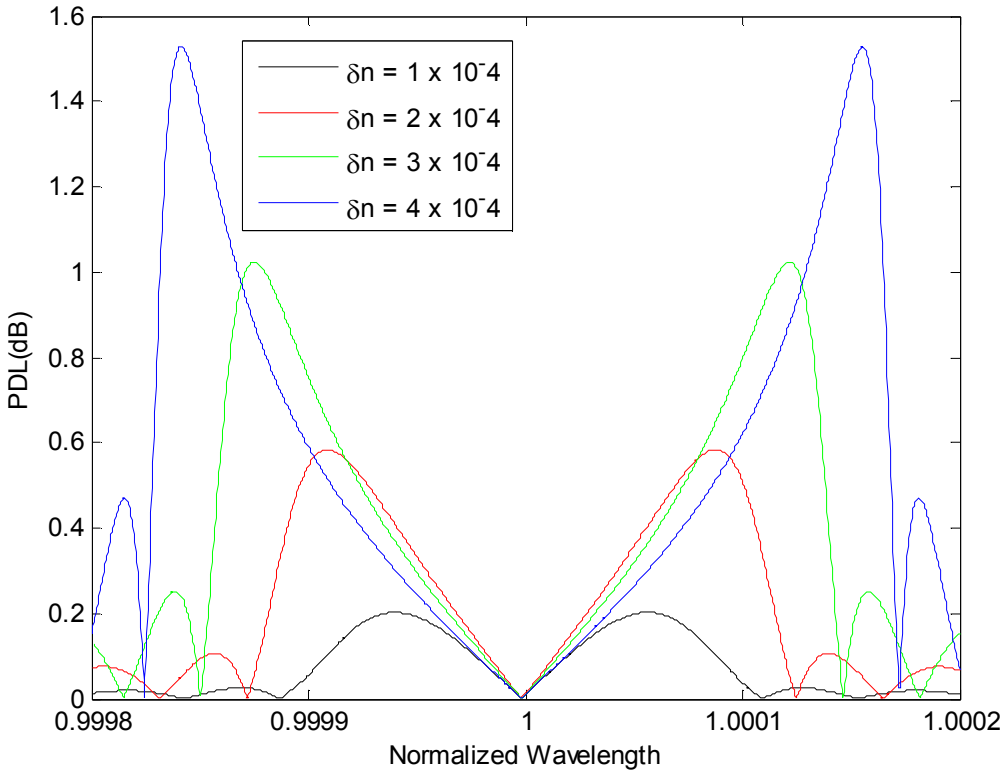

Figure 4.10. Polarization Dependent Loss spectra as a function of grating periodicity

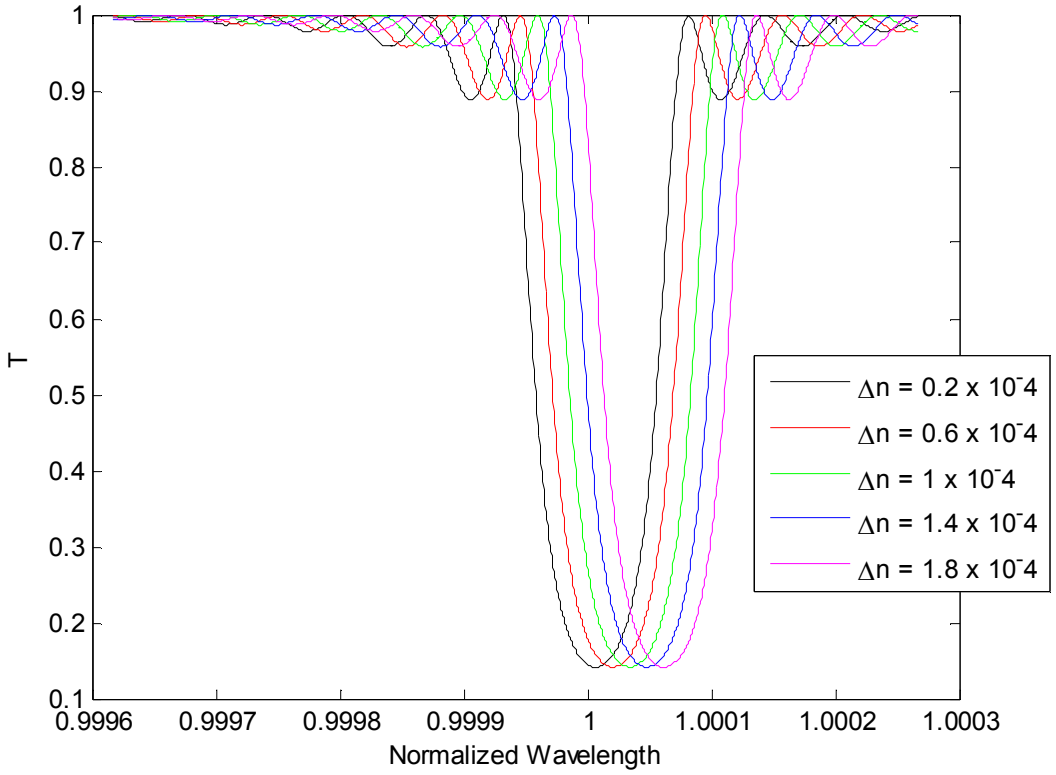

Figure 4.11. Transmitted spectrum evolution as a function of birefringence value

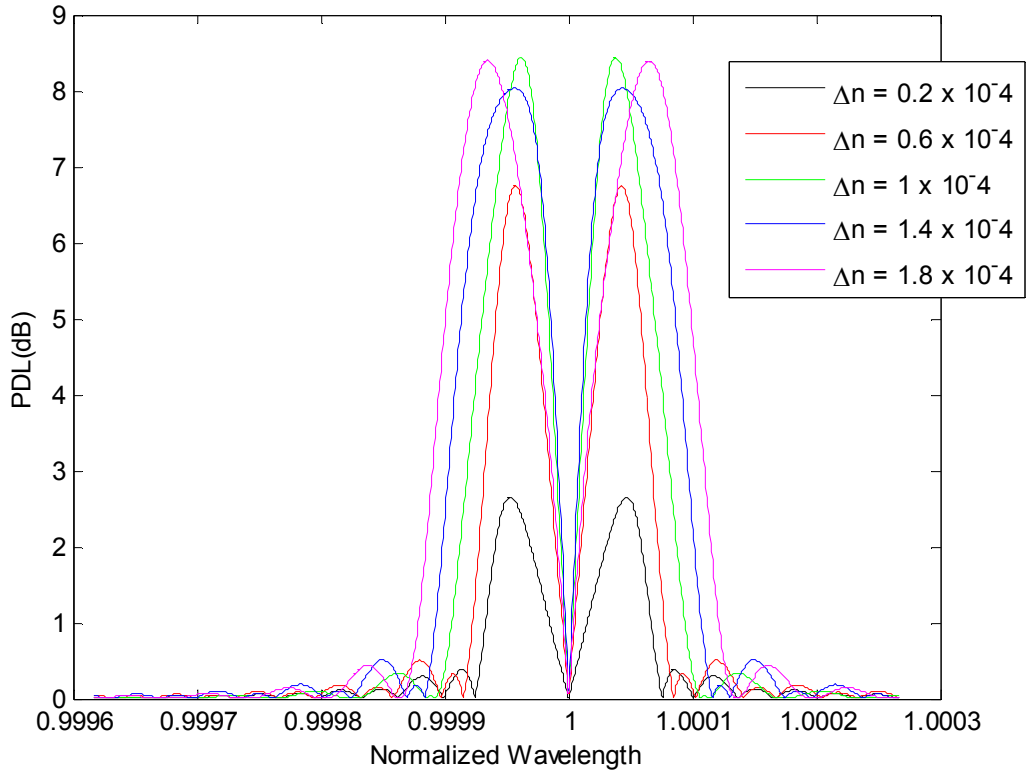

Figure 4.12. Polarization Dependent Loss spectra as a function of birefringence value

CHAPTER 5

INTERROGATION OF POLARIZATION EFFECTS IN FBG BY USING OFDR

5.1. Introduction

In this chapter, in order to understand whether the polarization properties of uniform FBGs may be interrogated by the way of OFDR, a numerical simulation model is built for the OFDR system where the FBG is modeled by implementing the transfer matrix method. This model takes into account the effect of birefringence on the FBG's spectral response. Once the signal on the photodetector of the OFDR is modeled, the signal processing steps (based on FFT and IFFT), as explained in chapter 3, are used in order to obtain ("*demodulate*") the transmission spectrum responses of the FBG. Finally, based on the demodulated transmission spectra for both polarization modes, Polarization Dependent Loss of the FBG is determined.

5.2. Numerical Simulation Model of OFDR System Considering Two Polarization Modes

Figure 5.1 represents the distributed sensing system containing C-OFDR and FBG. The main difference from the model used in section 3.3.2.2 is that two transfer matrices are assigned to each small section of the FBG [54]. Therefore, it is allowed to obtain Bragg spectra at an arbitrary position for given birefringence value.

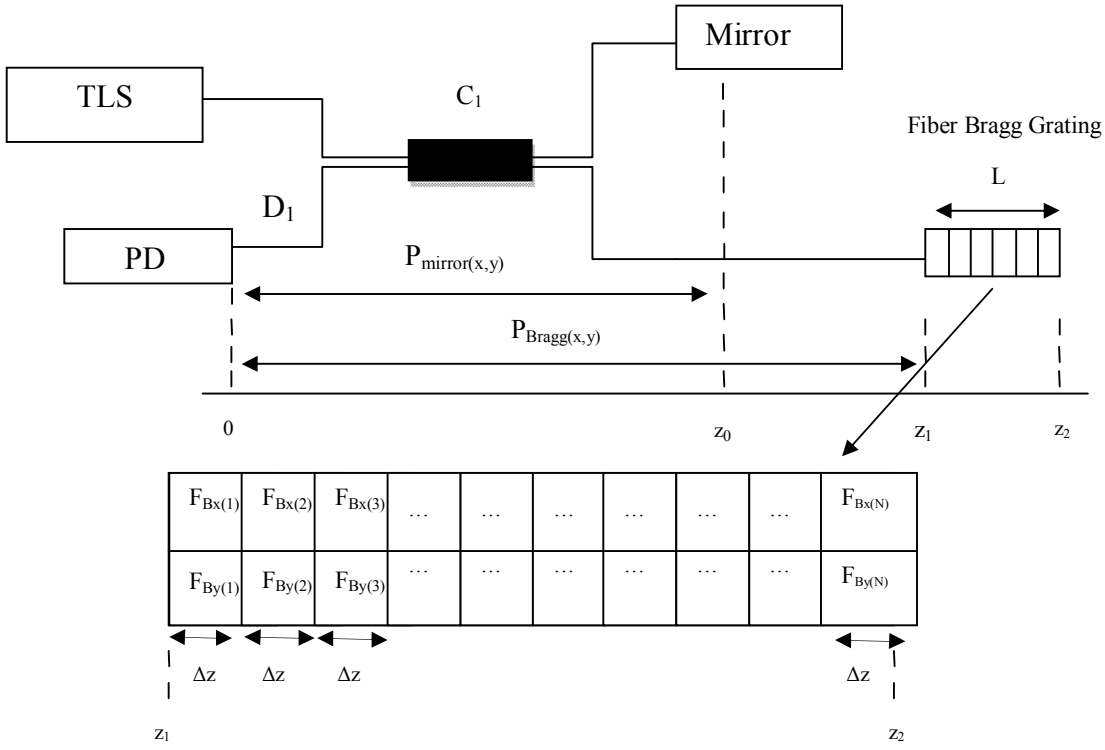

Figure 5.1. Model of FBG and mirror on C-OFDR system with two polarization modes (TLS: Tunable Laser Source, PD: Photodedector, C: Coupler)

As shown in Figure 5.1 the tunable laser source sweeps the wavelength λ of the incident light. This probe signal is split at the coupler C_1 into mirror and test arms. Reflected light from mirror and FBG interfere and observed at the detector (D_1).

The distributed spectrum of the FBG at each position all along the grating length can be obtained by applying Short Time Fourier Transform (STFT) on the detector signal (D1).

A certain range of wavenumber is extracted by window function. Fast Fourier transform is applied to the defined range to obtain the power profile of each frequency component. By sliding window function through the whole wavenumber range and by realizing proper conversions (wavenumber and frequency domains are converted to the wavelength and position, respectively), a spectrogram is constructed which shows the power profile along the FBG for each optical wavelength [55].

In the presence of birefringence, two grating matrices, phase shift matrices, and input /output fields are assigned to two polarization modes.

The elements of the grating matrices $F_{B_{j(1....N)}}$ (j=x or y) are formed in equations 5.1, 5.2, 5.3, 5.4 as,

$$T_{11} = \cosh(\alpha_j L) - \frac{i\delta_j \sinh(\alpha_j L)}{\alpha_j} \tag{5.1}$$

$$T_{12} = -\frac{i\kappa \sinh(\alpha_j L)}{\alpha_j} \tag{5.2}$$

$$T_{21} = \frac{i\kappa \sinh(\alpha_j L)}{\alpha_j} \tag{5.3}$$

$$T_{22} = \cosh(\alpha_j L) + \frac{i\delta_j \sinh(\alpha_j L)}{\alpha_j} \tag{5.4}$$

$$F_{B_j} = \begin{bmatrix} \cosh(\alpha_j \Delta z) - \frac{i\delta_j \sinh(\alpha_j \Delta z)}{\alpha_j} & -\frac{i\kappa \sinh(\alpha_j \Delta z)}{\alpha_j} \\ \frac{i\kappa \sinh(\alpha_j \Delta z)}{\alpha_j} & \cosh(\alpha_j \Delta z) + \frac{i\delta_j \sinh(\alpha_j \Delta z)}{\alpha_j} \end{bmatrix} \tag{5.5}$$

The phase shift matrices P_{Mj} and P_{Bj} (j=x or y) of the reflection matrices of two polarization modes are calculated as,

$$P_j = \begin{bmatrix} e^{-\frac{i\phi_j}{2}} & 0 \\ 0 & e^{\frac{i\phi_j}{2}} \end{bmatrix} \tag{5.6}$$

$$\phi_j = \frac{4\pi}{\lambda} n_{eff,j} z \tag{5.7}$$

In the case of mirror side of the optical path, the relation between output and input of the system is given as,

$$\begin{bmatrix} R_{Mj}(0) \\ S_{Mj}(0) \end{bmatrix} = P_{Mj} \begin{bmatrix} R_{Mj}(z_0) \\ S_{Mj}(z_0) \end{bmatrix} \tag{5.8}$$

where R_{Mj} is the amplitude of the forward propagation mode, S_{Mj} is the amplitude of the backward propagating mode and P_{Mj} is the mirror phase shift matrix.

The phase shift matrix P_{Mj} of the mirror is given as,

$$P_{Mj} = \begin{bmatrix} e^{-\frac{i\phi_j}{2}} & 0 \\ 0 & e^{\frac{i\phi_j}{2}} \end{bmatrix} \tag{5.9}$$

$$\phi_j = \frac{4\pi}{\lambda} n_{eff,j} z_0 \tag{5.10}$$

When the boundary conditions are applied,

$$R_{Mj}(0) = 1 \tag{5.11}$$

$$S_{Mj}(z_0) = R_{Mj}(z_0)e^{i\pi} \tag{5.12}$$

$$\begin{bmatrix} 1 \\ S_{Mj}(0) \end{bmatrix} = \begin{bmatrix} P_{Mj11} & P_{Mj12} \\ P_{Mj21} & P_{Mj22} \end{bmatrix} \begin{bmatrix} R_{Mj}(z_0) \\ R_{Mj}(z_0)e^{i\pi} \end{bmatrix} \tag{5.13}$$

The mirror reflection coefficient is given as,

$$\begin{aligned} RL_{Mirror} &= S_{Mx}(0).\boldsymbol{x} + S_{My}(0).\boldsymbol{y} \\ &= \frac{P_{Mx21}+P_{Mx22}e^{i\pi}}{P_{Mx11}+P_{Mx12}e^{i\pi}}.\boldsymbol{x} + \frac{P_{My21}+P_{My22}e^{i\pi}}{P_{My11}+P_{My12}e^{i\pi}}.\boldsymbol{y} \end{aligned} \tag{5.14}$$

For the optical path contains fiber Bragg grating, the transfer matrix (T_j) for the whole optical path is considered as the multiplication of the transfer matrices of all the individual FBG sections and express as,

$$T_j = P_{Bj}F_{B_j(N)} \dots \dots F_{B_j(2)}F_{B_j(1)} \tag{5.15}$$

where P_{Bj} (j=x or y) is Bragg phase shift matrix and given as,

$$P_{B_j} = \begin{bmatrix} e^{-\frac{i\emptyset_j}{2}} & 0 \\ 0 & e^{\frac{i\emptyset_j}{2}} \end{bmatrix} \tag{5.16}$$

$$\emptyset_j = \frac{4\pi}{\lambda} n_{eff,j} z_1 \tag{5.17}$$

The relation between input and output of the Bragg system for the two polarization mode is defined by the equation 5.18,

$$\begin{bmatrix} R_{B_j}(0) \\ S_{B_j}(0) \end{bmatrix} = T_j \begin{bmatrix} R_{B_j}(z_2) \\ S_{B_j}(z_2) \end{bmatrix} \tag{5.18}$$

where R_{Bj} is the amplitude of the forward propagating mode and S_{Bj} is the amplitude of the backward propagating modes.

The boundary conditions for the Bragg system will be defined as,

$$R_{B_x}(0) = a_x e^{i\varphi_x} \tag{5.19}$$

$$R_{B_y}(0) = a_y e^{i\varphi_y} \tag{5.20}$$

$$S_{B_x}(z_2) = 0 \tag{5.21}$$

$$S_{B_y}(z_2) = 0 \tag{5.22}$$

where the amplitude and the phase of the two polarization state are expressed as aj and φj (j=x or y), respectively,

When the boundary condition is applied on equation 5.18, the reflection coefficient for Bragg grating can be obtained as,

$$\begin{aligned} RL_{FBG} &= S_{B_x}(0).\boldsymbol{x} + S_{B_y}(0).\boldsymbol{y} \\ &= a_x e^{i\varphi_x} \frac{T_{x21}}{T_{x11}}.\boldsymbol{x} + a_y e^{i\varphi_y} \frac{T_{y21}}{T_{y11}}.\boldsymbol{y} \end{aligned} \tag{5.23}$$

The transmission coefficient of the Bragg grating is obtained as,

$$\begin{aligned} T_{FBG} &= R_{B_x}(z_2).\boldsymbol{x} + R_{B_y}(z_2).\boldsymbol{y} \\ &= a_x e^{i\varphi_x} \frac{1}{T_{x11}}.\boldsymbol{x} + a_y e^{i\varphi_y} \frac{1}{T_{y11}}.\boldsymbol{y} \end{aligned} \tag{5.24}$$

The obtained detector signal can be expressed as,

$$D_1 = |RL_{Mirror} + RL_{FBG}|^2 \tag{5.25}$$

- **An Example For Numerical Simulations**

For the following example, in order to obtain a clear understanding about observed signal of the birefringent FBGs in the OFDR system, the analytical signal of FBG response is studied by numerical simulations [56]. At the simulation, the fiber is written into a high birefringent fiber ($\Delta n = 1.2\ 10^{-4}$). The schematic of the system shown in Figure 5.1 is explained in detailed in the section 5.1.

In this case, the amplitude and phase of the two polarization modes equal $a_j = 1$, $\varphi_j = 0$ (j=x or y), respectively. A Hanning window with a wavelength range of 400pm is applied for the signal processing. The spatial resolution was approximately 0.6mm. The window slide was set as 5 pm. The sampling rate of the wavelength was approximately 0.0827 pm.

For the numerical simulation the parameters are as follows,

Table 5.1. Parameters used in numerical simulation

Visibility	0.394
n_{eff}	1.45
N (Number of FBG section)	100
L (Length of fiber Bragg Grating)	100mm
z_0 (absolute mirror location)	1m
z_1 (absolute FBG location)	4m
Laser sweep range	1549-1554 nm
NoP (Number of Point)	25059
κ (AC coupling coefficient)	1.42
Δn(Birefringence value)	$1.2\ 10^{-4}$

In Figure 5.2 and 5.3 reflection amplitude of x and y polarization modes and power of detector signal (D1) are presented where the split between the two polarization modes is equal to 240pm.

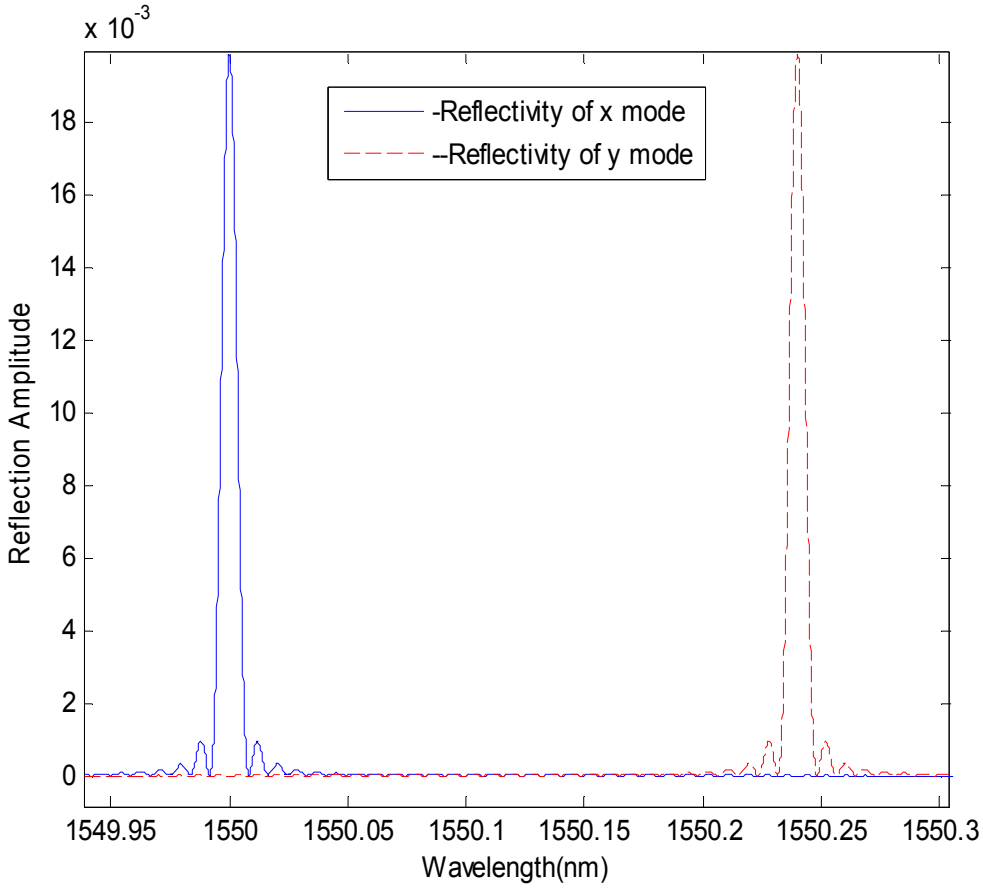

Figure 5.2. Evolution of reflection spectrum of two polarization mode

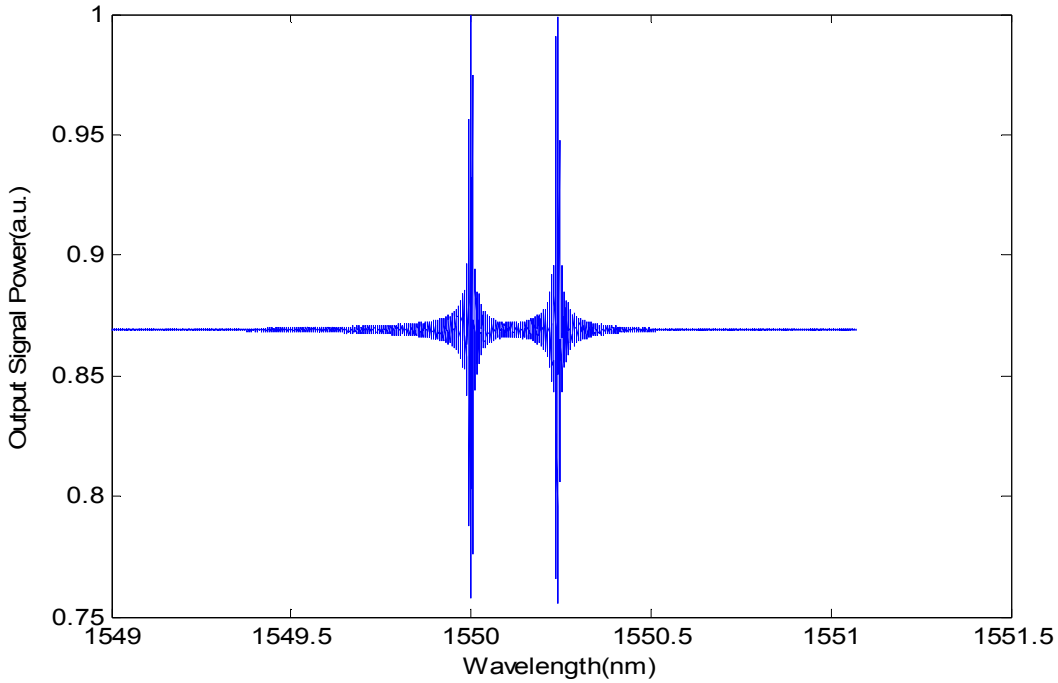

Figure 5.3. Evolution of detector signal

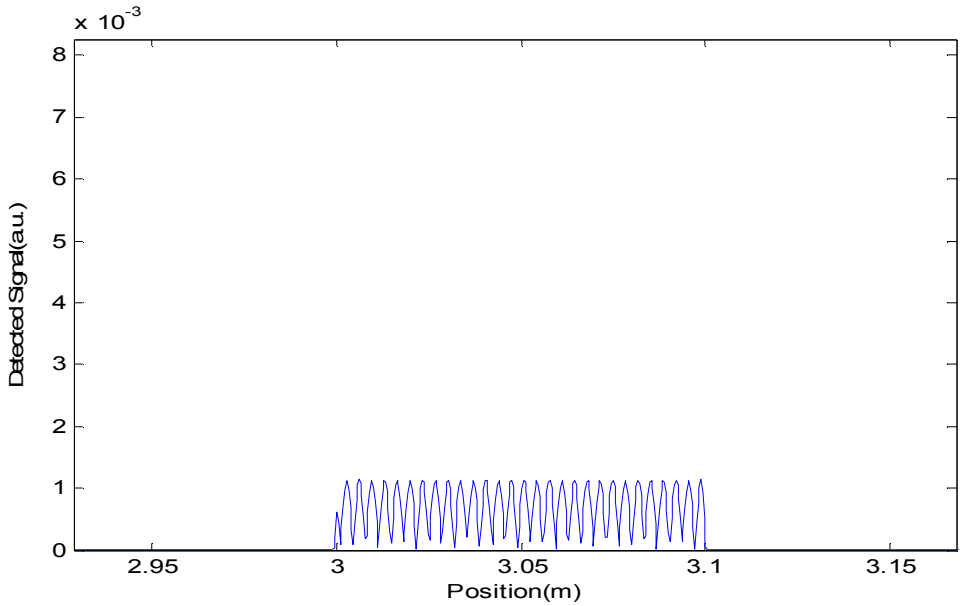

Figure 5.4. Simulated beat spectrum converted to distance scale

Simulated beat spectrum of the photodetector can be seen from the Figure 5.4. Intensity detected by the photodetector in above explained system is a wavenumber dependent sinusoidal function with a constant frequency called beat frequency. The beat frequency can be expressed as,

$$\Delta k = \frac{\pi}{n_{eff} L} \tag{5.26}$$

Figure 5.5 shows the power fluctuations when 240 pm Bragg wavelength splits are applied, the Bragg peaks of two polarization modes are district from each other The periodical power fluctuations can also be clearly observed on the spectrogram. For the 240 pm split, the Bragg peaks of the two polarization modes are rather distinct compared with the power fluctuation which is seen between the two peaks. The maximum power of the power fluctuation is approximately 50% of that of the two Bragg peaks. This indicates that birefringence is directly detectable when the Bragg wavelength split is more than 200 pm.

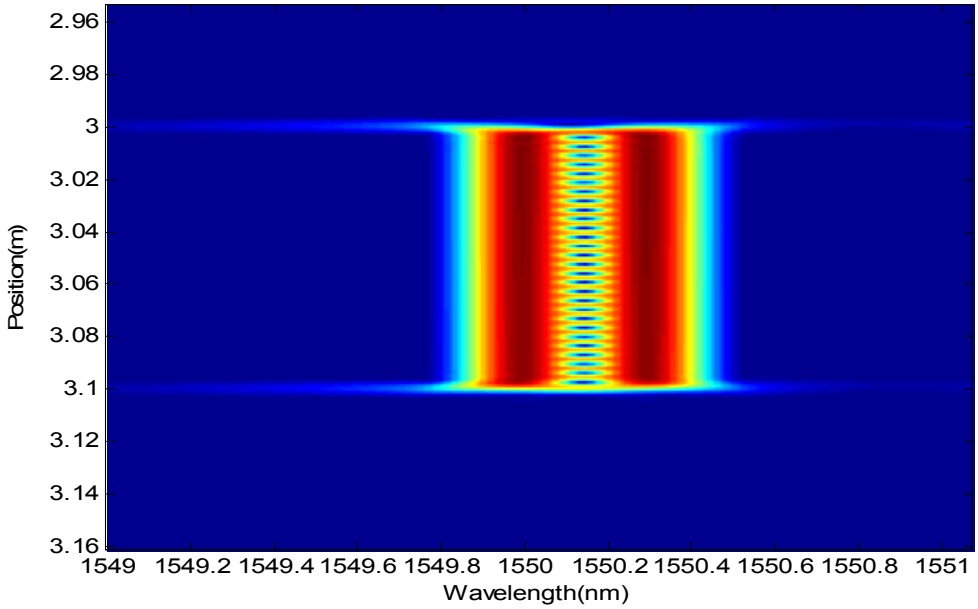

Figure 5.5. Spectrogram of FBG with 240pm wavelength splits

5.3. Original Interrogation Concept Based on Polarization Sensitive OFDR and FBGs

The main idea behind the proposed study is to interrogate polarization properties of Bragg gratings. In the framework of this thesis the study is first focused on PDL. The reason for that, the PDL has been shown as responsive to transversal strain in the literature [53]. Therefore interrogation of this parameter is promising in strain sensor applications.

The most important feature of our proposed system that distinguishes from the other systems is the capability to interrogate polarization dependent loss in quasi-distributed manner (by using OFDR).

Figure 5.6 shows the schematic of the proposed system to evaluate polarization dependent loss. In this system, a tunable laser source, a coupler, one fiber Bragg grating, a beam splitter and two OFDR units are used.

In order to obtain the polarization dependent loss, it is needed to access transmission spectrum of Bragg grating for both polarization modes. In our model the tunable laser source is swept the wavelength λ of the incident light. The modulated optical signal is then split at the coupler into mirror and test arms. Reflected light from mirror and transmitted light from FBG (optical path of reflected signal from mirror and transmitted signal from Bragg grating is equal to each other) are interfered. Two components corresponding to two polarization modes are separated by the way of polarization beam splitter. Finally, interference signals are observed on photodetector x and photodetector y, separately.

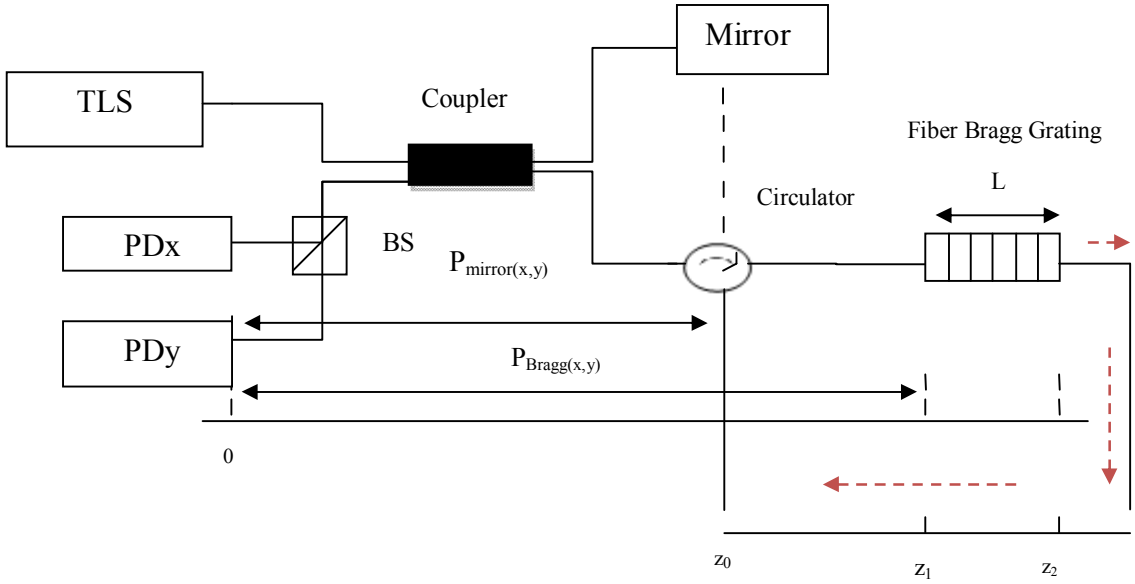

Figure 5.6. Schematic representation of proposed C-OFDR system

By using equations obtained in section 5.2, output signals calculated at detector x and detector y can be provided.

In the reference arm of the system reflected light from the mirror is calculated as,

$$RL_{Mirror,x} = \frac{P_{Mx21}+P_{Mx22}e^{i\pi}}{P_{Mx11}+P_{Mx12}e^{i\pi}}.\boldsymbol{x} \tag{5.27}$$

$$RL_{Mirror,y} = \frac{P_{My21}+P_{My22}e^{i\pi}}{P_{My11}+P_{My12}e^{i\pi}}.\boldsymbol{y} \tag{5.28}$$

where P_{Mx} and P_{My} are the phase shift matrix for the optical path contains mirror.

$$P_{Mj} = \begin{bmatrix} e^{-(in_{eff,j}z_0k)} & 0 \\ 0 & e^{(in_{eff,j}z_0k)} \end{bmatrix} \tag{5.29}$$

For the optical path with FBG, transmitted light is calculated with respected boundary conditions in section 5.2 as,

$$T_{FBG,x} = a_x e^{i\varphi_x}\frac{1}{T_{x11}}.\boldsymbol{x} \tag{5.30}$$

$$T_{FBG,y} = a_y e^{i\varphi_y}\frac{1}{T_{y11}}.\boldsymbol{y} \tag{5.31}$$

where a_j, φ_j (j=x or y) are the amplitude and phase of the polarization state of the input signal and T_{j11} denotes the elements of transfer matrix , T_j.

Finally the output signal can be expressed by taking the absolute square of coupled signals reflected from reference path and transmitted from test path. The obtained signal D_x and D_y were calculated as,

$$D_x = \left|RL_{Mirror,x} + T_{FBG,x}\right|^2 \tag{5.32}$$

$$D_y = \left|RL_{Mirror,y} + T_{FBG,y}\right|^2 \tag{5.33}$$

- **Demodulation of Transmission Spectra**

The OFDR spectrum is obtained applying Fast Fourier transform (as explained in chapter 3) on the interference signals and power profile of the frequency component converted to the corresponding distance of fiber Bragg grating.

In order to determine the demodulated transmission spectrum, inverse Fast Fourier transform steps (as represented at the chapter 3) are applied around the particular position of FBG by defining a proper window around beat frequency as shown in Figure 5.7.

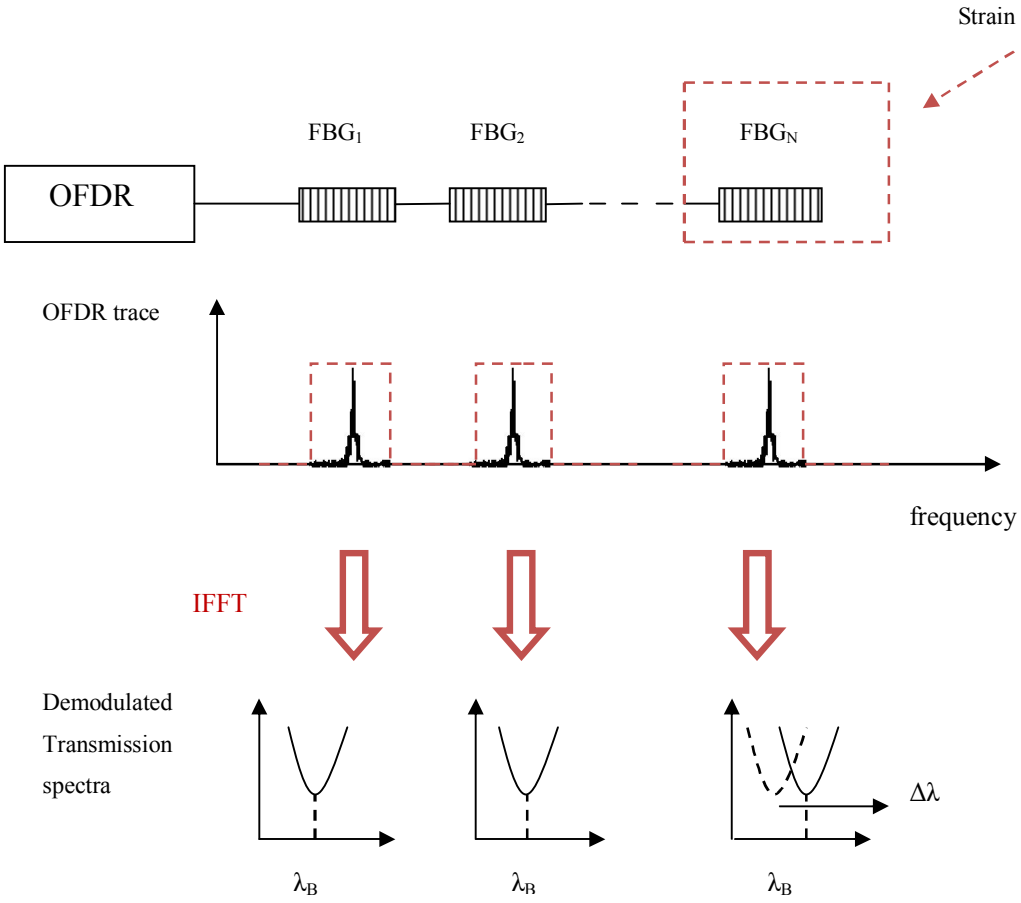

Figure 5.7. Demodulation scheme for the transmitted spectra

Extracted transmission evolution from demodulation allows computing polarization dependent loss.

$$PDL_{dB} = 10\log_{10}\frac{T_{FBGx}(\lambda)}{T_{FBGy}(\lambda)} \quad (5.34)$$

$$T_{FBG,j}(\lambda) = Demodulated\ Power\ Transmission\ Coefficients \quad (5.35)$$

5.4. Simulation Results of the Proposed System and Discussion

In the following part, numerical simulations (based on the model explained in section 5.2) are performed to obtain polarization dependent loss by using our proposed scheme represented in Figure 5.6. The simulation results are then compared with the theoretical PDL values obtained by analytical expressions as presented in Chapter 4.The parameters for the numerical simulations of C-OFDR are as follows,

The parameters for the numerical simulations of C-OFDR are as follows,

Table 5.2. The parameters used in PDL simulation

Visibility	0.5
n_{eff} (effective refractive index)	1.4514
δn (Average refractive index modulation)	$1x\ 10^{-4}$
Λ (Periodic refractive index modulation)	$530x10^{-9}$
Δn (Degree of Birefringence effect)	$5x10^{-6}$
z_0 (absolute mirror location)	1 m
z_1 (absolute FBG location)	4 m
L (Length of Bragg grating)	1 cm
N (Number of FBG section)	100
λ_{Bragg} (Bragg wavelength)	1538.5 nm
Laser sweep range	1538-1539 nm
NoP (Number of Point)	2^{14}

According to these parameters, the transmission spectrum of fiber Bragg grating with respect to two polarization modes is obtained in figure 5.9. Under low birefringence value ($5x10^{-6}$) the Bragg wavelength shift is around 10 pm.

In figure 5.10, first calculated PDL variation with calculated transfer matrix transmission coefficients are introduced and it shows that when the power transmission coefficient of two modes equal to each other than polarization dependent loss is zero.

Between two successive minimum values of power transmission coefficient the polarization dependent loss takes its maximum values at the corresponding wavelength. Second part of the figure 5.10 shows us the polarization dependent loss, calculated by power transmission coefficient achieved after demodulation process this result is matching with the calculated results.

As a result, a fiber Bragg grating transmission spectrum is demodulated and the polarization dependent information is extracted by demodulating OFDR signal.

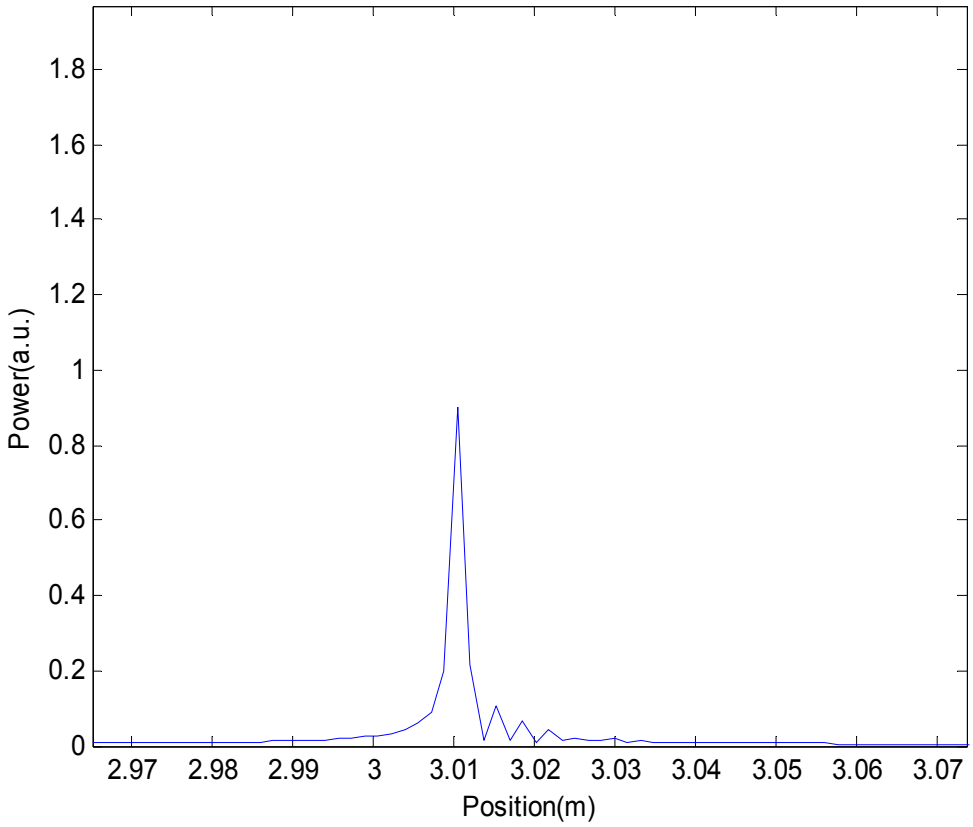

Figure 5.8. OFDR trace in frequency domain (converted into position)

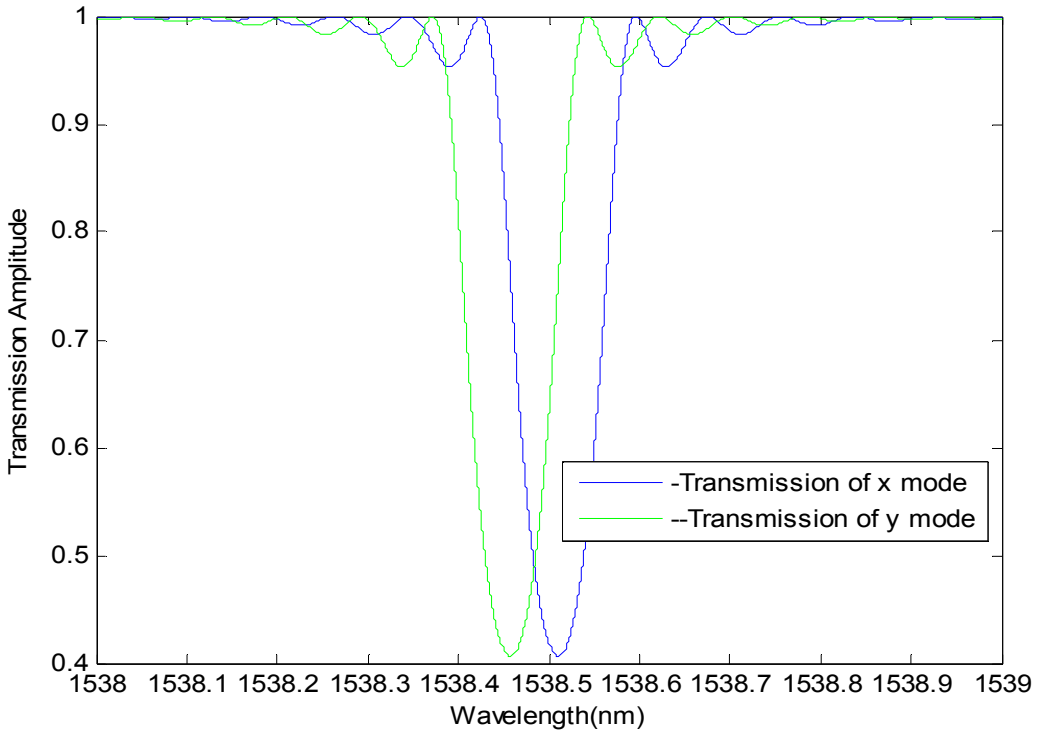

Figure 5.9. Transmitted spectrum of FBG for x and y modes

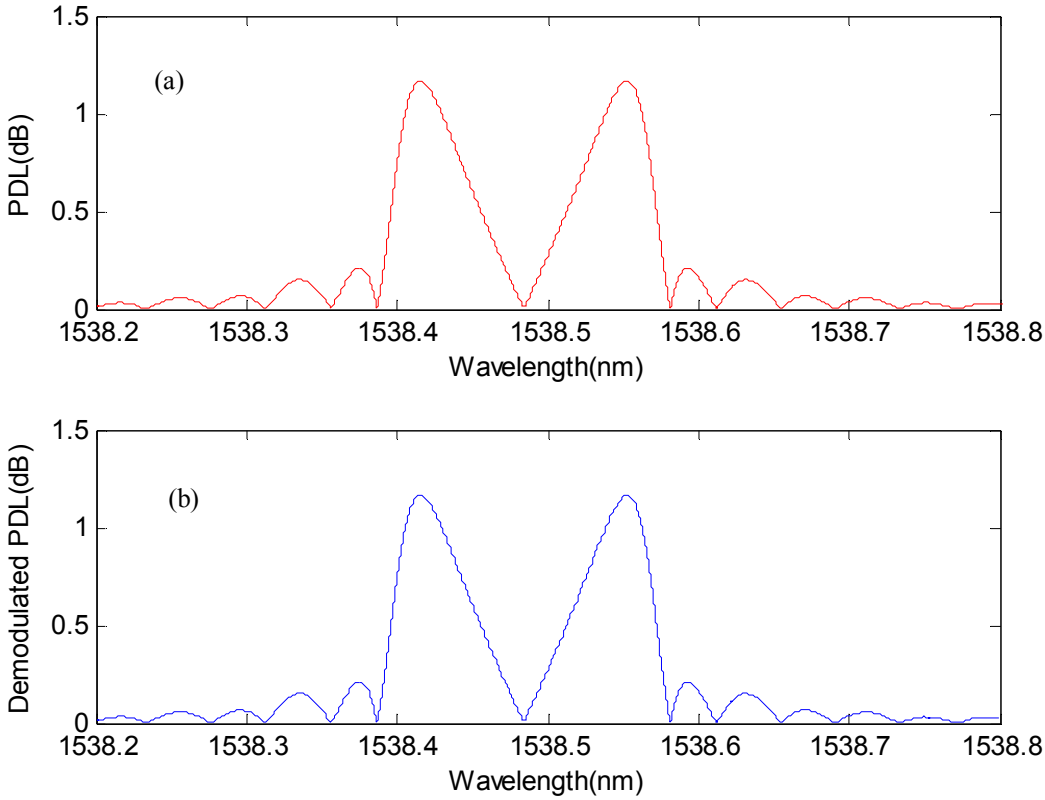

Figure 5.10. (a) PDL obtained by analytical calculations (b) simulated PDL

After that impact of Bragg grating parameters as length (L), periodic refractive index modulation (δn), and birefringence value on the spectral evaluation of polarization dependent loss is performed.

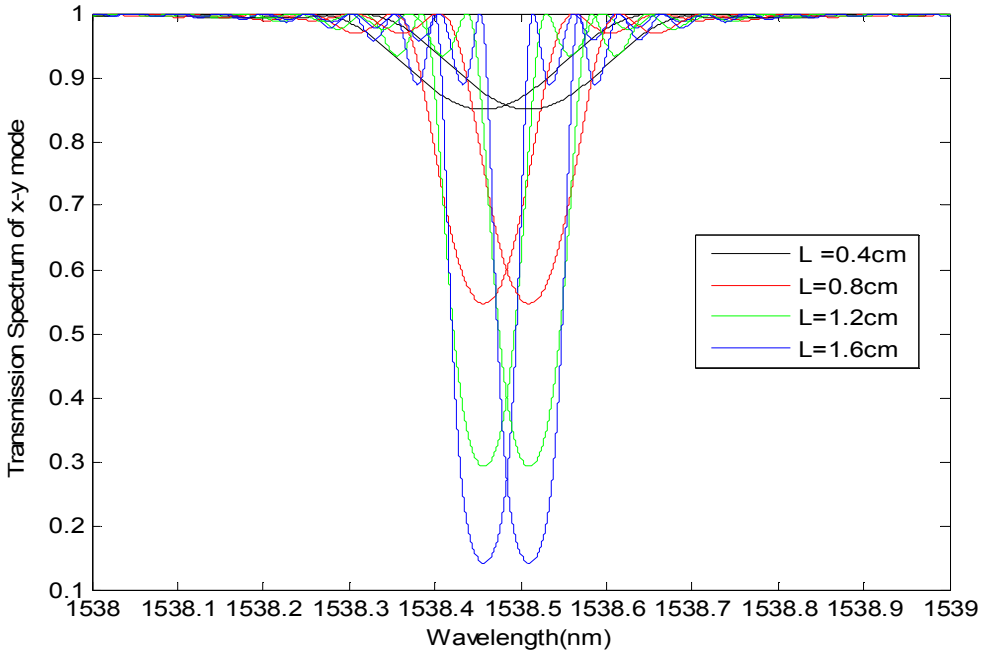

Figure 5.11. Computed transmission spectrum of x and y mode as a function of grating length

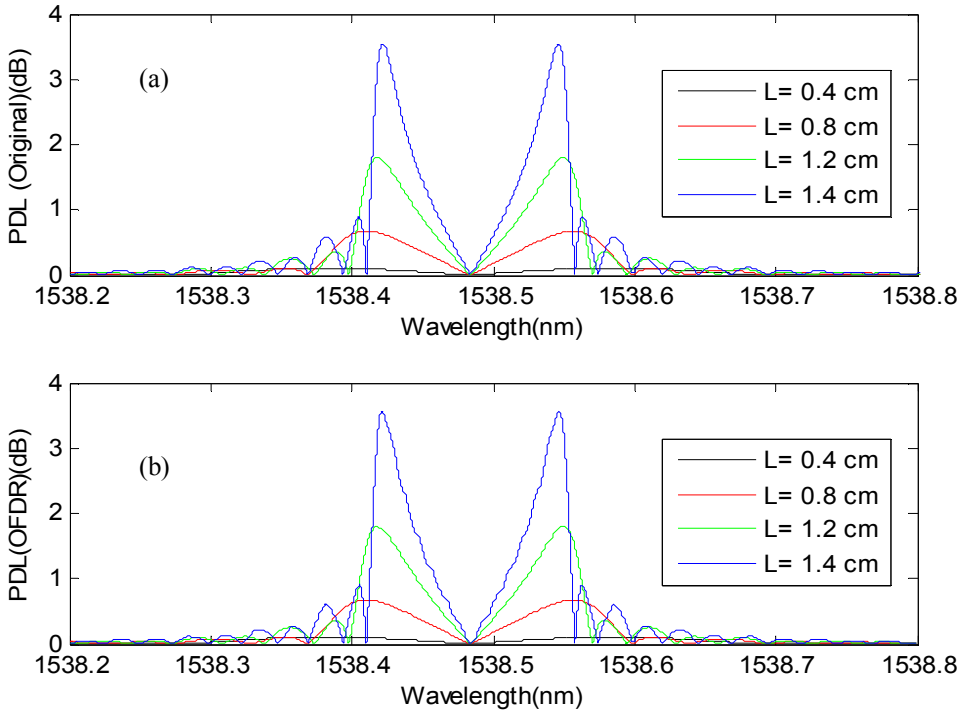

Figure 5.12. (a) PDL obtained by analytical calculations (b) simulated PDL as a function of grating length ()

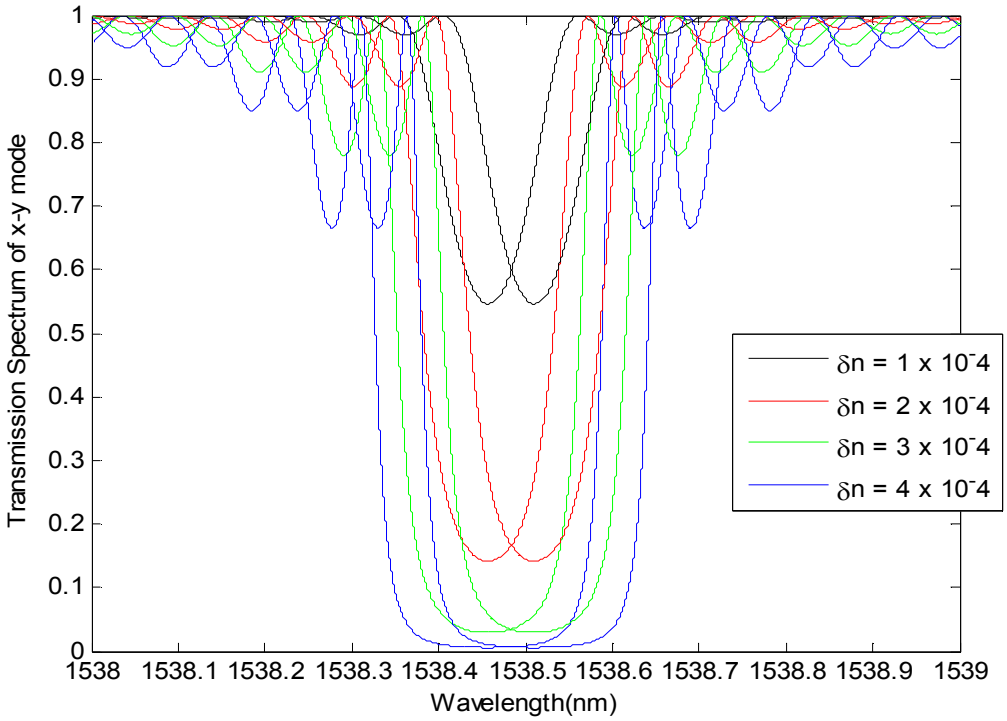

Figure 5.13. Computed transmission spectrum of x and y mode as a function of refractive index modulation

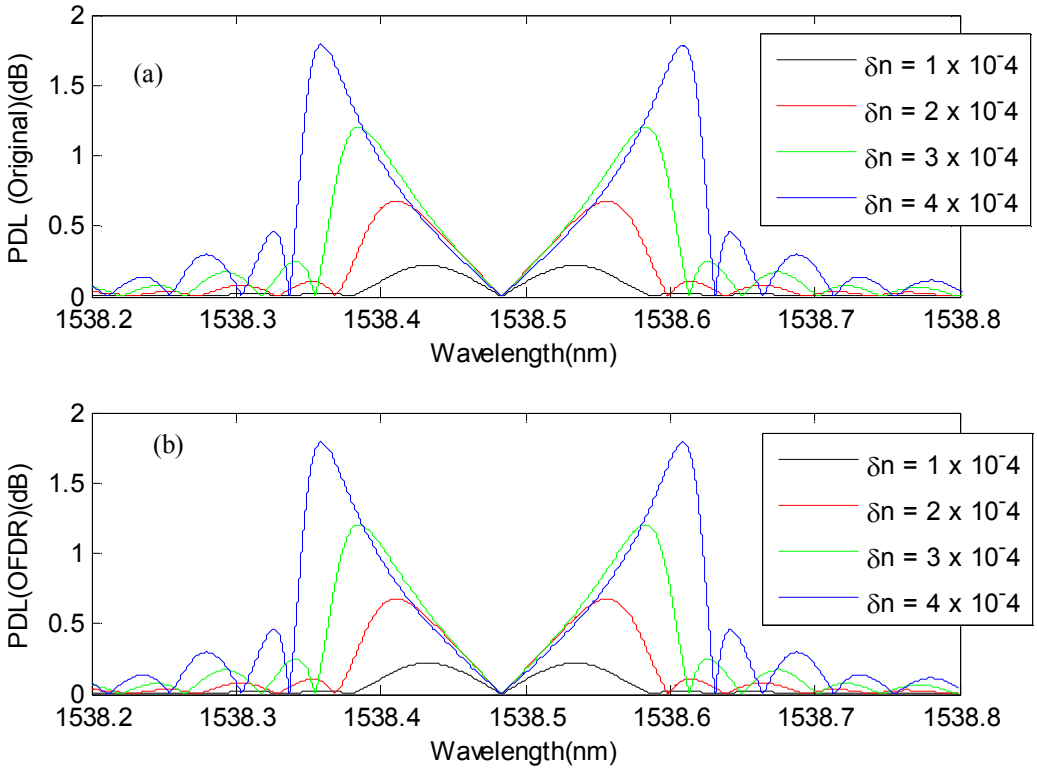

Figure 5.14. (a) PDL obtained by analytical calculations (b) simulated PDL as a function of refractive index modulation

The evolution of the transmitted spectrum and PDL with respect to the grating length is investigated in Figure 5.11 and 5.12. Figure 5.13 and 5.14 present the same evolution with respect to the refractive index modulation. The parameters used in the simulations are given in table 5.2.

As shown on figures, grating length and the refractive index modulation results in the same effect on polarization dependent loss spectra. The peak amplitude is increased at the wavelength coincidence with the edge of the rejection band of transmitted spectra. For the long grating length and high refractive index modulation values, sharp PDL evolution with maximum values in the rejection band is obtained.

The results obtained by analytical calculations is in a good agreement with the results obtained after the demodulations process for grating length variation, refractive index modulation and birefringence value variation.

The effect of the birefringence value is studied in Figure 5.15 and 5.16. For Δn values less than $1\ 10^{-4}$ which corresponds to photo-induced birefringence values, the birefringence effect is not well perceived in the transmitted spectrum as the two transmitted spectra corresponding to the x and y modes is not split well enough. For the Δn value bigger than $1.5\ 10^{-4}$ the split between the two spectra can be observed and the amplitude remains unchanged.

For Δn values up to $1x10^{-4}$, the maximum PDL values monotonically increase whereas the wavelength spacing between them slightly decreases. For Δn higher than $1x10^{-4}$, the maximum PDL saturate but the wavelength spacing between the peaks is increased.

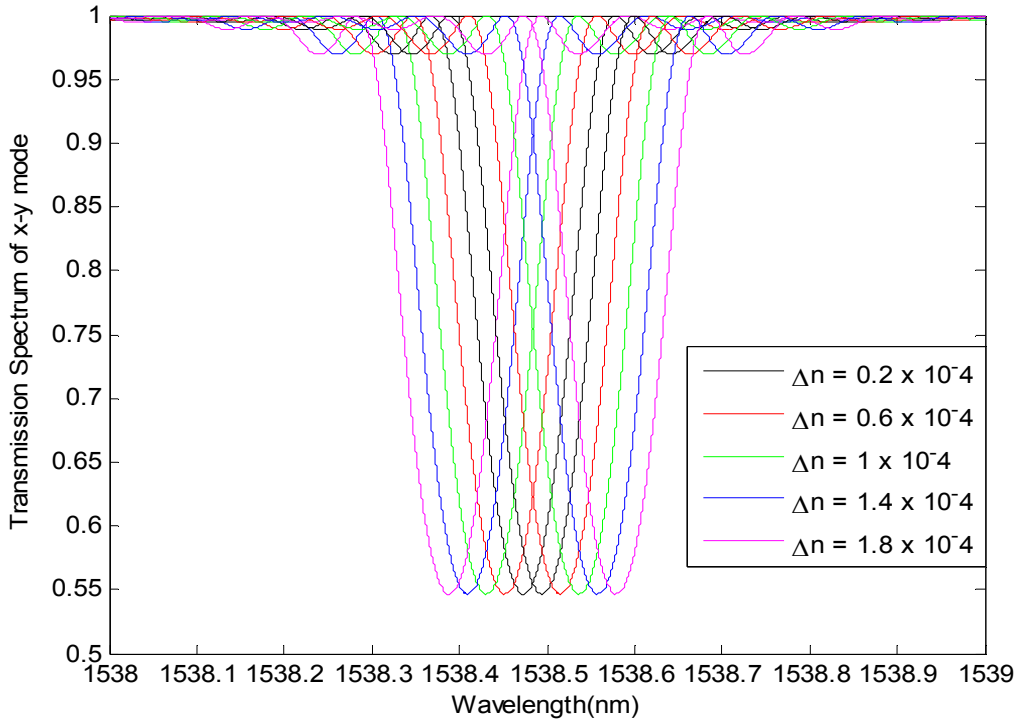

Figure 5.15. Computed transmission spectrum of x and y mode as a function of birefringence value

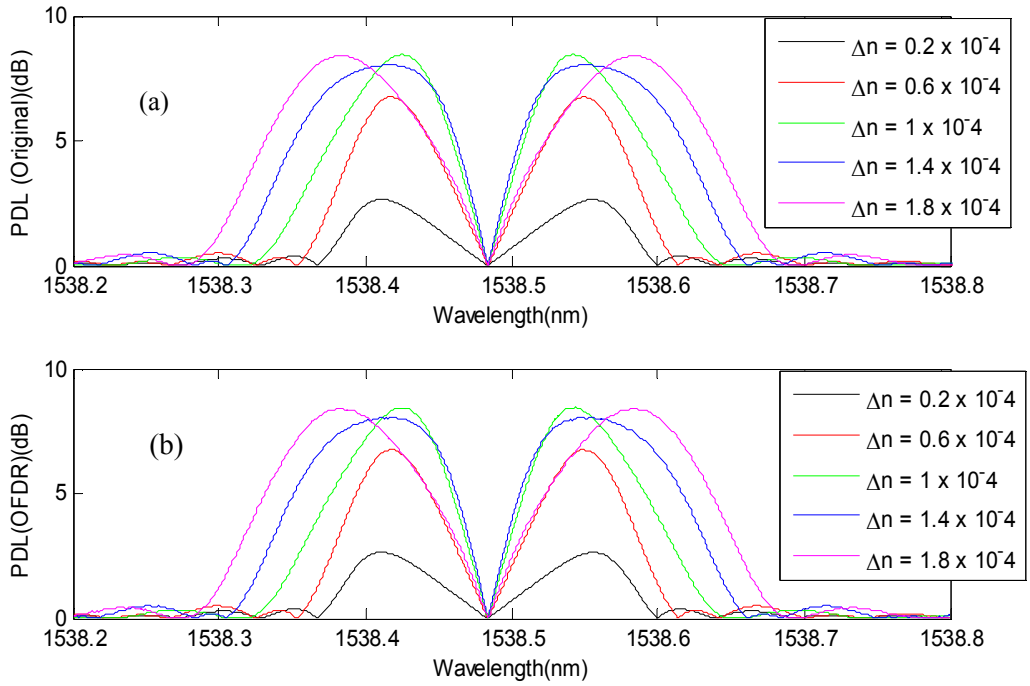

Figure 5.16. (a) PDL obtained analytical calculations (b) simulated PDL as a function of birefringence value

- **Discussion**

Birefringence in fiber Bragg gratings can be produced by combining the intrinsic birefringence with the birefringence induced by UV writing process or birefringence induced by transversal load can [1], [2]. As shown in Figures 5.15 and 5.16, birefringence leads to polarization dependent loss in fiber Bragg gratings. Furthermore when a grating is subjected to transversal load, this effect leads to a modification in PDL evolution. Because birefringence value variation depends on applied transversal load. [2]

The transversal load effect is studied in literature as shown in Figure 5.17 that less than 250 N transversal force value can be measured based on monitoring PDL evolution. The result of the figure can be associated with figure 5.16 that after $1x10^{-4}$ birefringence value PDL amplitudes saturate and amplitude of PDL can't answer the load variation.

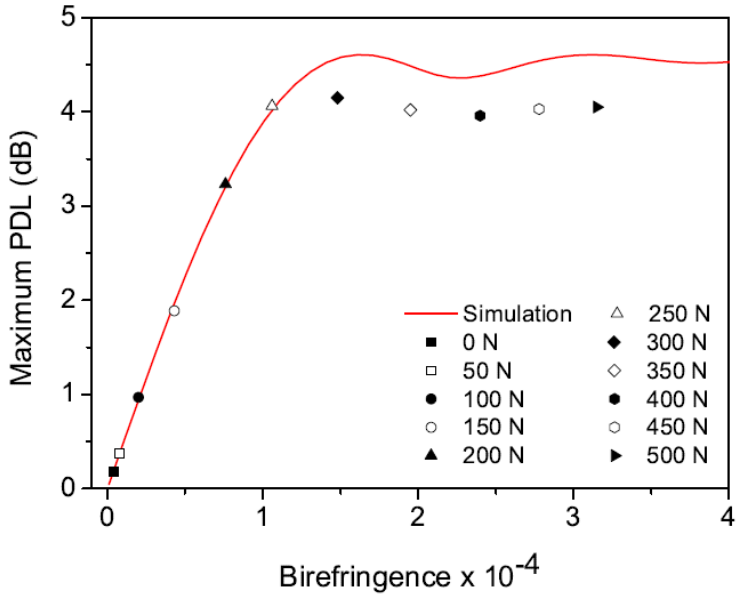

Figure 5.17. Evolution of maximum PDL value as a function of the measured transverse force value and reconstructed birefringence value [2]

The PDL evolution results of literature are good agreement with the presented study and show that the proposed approach in this thesis can be used to monitor transversal load on the structure in distributed or quasi-distributed manner.

CHAPTER 6

CONCLUSIONS

The goal of this thesis is to demonstrate the feasibility of an original fiber Bragg grating interrogation scheme which is able to obtain polarization properties of FBGs by using OFDR.

A theoretical model has been introduced and numerical simulations have been carried out to study the responses of uniform fiber Bragg grating interrogated by OFDR.

In first chapter of the thesis, fundamentals of fiber Bragg gratings are studied. The effect of grating parameters (length, grating period,...) on the reflection spectrum is analyzed using analytical formulas.

In the second chapter of the thesis, the state of the art covering various FBG interrogation methods is briefly presented. Optical Frequency Domain Reflectometry comes out to be a suitable technique for quasi-distributed sensor applications envisaged by this thesis. Therefore, after giving basic principles of OFDR, this chapter includes a mathematical analysis together with the numerical simulations of an OFDR system where a single FBG is used as the sensing element.

In chapter four, preliminary studies have been conducted in order to include the effect of the birefringence in the proposed model. Spectrograms have been obtained to study the power distribution along the FBG while taking both the polarization state of the input light beam and the birefringence of the FBG into consideration.

Chapter five contains the main added-value of the thesis. In this chapter, we propose an original scheme to interrogate PDL of a number of cascaded FBGs by the way of polarization sensitive OFDR. Then, we analyzed the PDL of the FBGs by the way of numerical simulations. Our simulation results have shown a very good agreement with the theoretical results.

In conclusion, our model and analysis have revealed the feasibility of an original scheme which is able to interrogate polarization dependent loss by optical frequency domain reflectometer.

The results provide an important guidance in designing novel fiber optic sensors utilizing fiber gratings as the sensing element and OFDR as the interrogation unit.

- **Perspectives**

The results of the thesis open the door to an interesting application area, namely strain sensors monitoring composite materials. The use of optical fiber sensing, particularly embedding of fiber Bragg grating (FBG) sensors into composite materials has been gaining growing popularity thanks to various advantages of FBGs. For the development of *smart structures*, fiber Bragg gratings brought about a great contribution in many engineering fields (civil, aerospace, renewable energy, …).

The use of composite materials in critical parts and high stress members (airplane wings, unmanned air vehicles, wind turbines…) has been exponentially growing thanks to their lightweight, superior strength, durability, and corrosion resistance. However, the unique mechanical properties of composite materials cannot be fully exploited without monitoring them when material is placed under constraints. This is because the behavior of composite materials under loading is different from metals and can rapidly degrade when internal damage occurs. It is therefore essential to monitor their behavior in the field or during manufacturing and prototyping for the purpose of improved performance, improved safety, and reduced cost.

The occurrence and growth of damage in composite elements can be detected by continually measuring the mechanical load, stress and strain inside the structures.

More than tens of fiber Bragg gratings can be cascaded in a single fiber. By combining the cascaded capability and compatibility with composite materials, optical fiber Bragg grating sensors are well suited to be embedded into composite materials without reforming their physical properties.

In literature, sensitivity of polarization properties of FBG to the transversal strain is demonstrated in recent publications [3] [4]. However, none of the previously demonstrated reports using FBG sensors could exhibit *quasi-distributed or distributed* measurement capability which significantly limits their implementations into composite materials. The novel interrogation technique that we proposed in this thesis can be implemented in many applications related to the strain monitoring of composite materials.

REFERENCES

[1] Erdoğan T., "Fiber grating spectra,'' Journal of Lightwave Technology, vol. 15, num. 8, pp. 1277–1294, 1997.

[2] Caucheteur C., "Realization of mechanical and chemical sensors based on the fiber Bragg gratings technology,'' Faculté Polytechnique de Mons, 2007.

[3] Zhang P., "High-resolution photon counting OTDR based interrogation of multiplexing broadband FBG sensors,'' PhD Dissertation Electrical and Computer Engineering Department, Blacksburg, Virginia, USA, 2003.

[4] Voisin V., Caucheteur C., Kinet D., Mégret P., Wuilpart M., " Self-referenced Photon Counting OTDR Technique for Quasi-distributed Fiber Bragg Gratings Sensors,'' IEEE Sensors Journal, 12, pp. 118-123, 2012.

[5] Fidanboylu K., Efendioğlu H. S., "Fiber optic sensors and their applications,'' 5th International Advanced Technologies Symposium (IATS'09), Karabük, Turkey, May 13-15, 2009.

[6] Francis To, So Yu, Shizhuo Yin, "Optical fiber sensors guide, Fundamentals & Applications,'' Micron Optics, August 22, 2009.

[7] Saleh B.E.A., Teich M.C., "Fundamentals of Photonics,'' Wiley & Sons, 2007.

[8] Yariv A., "Quantum Electronics,'' Wiley& Sons, 1989.

[9] Hartog H. A., "Distributed fiber optic sensors, Optical Fiber Sensor Technology,'' Chapman and Hall, London, 1995.

[10] Glisic B., "Distributed fiber optic sensing technologies and applications – an overview,'' ACI Special Publication, SP-292, art. no. 2 (18pp), 2013.

[11] Yu T. S. F., Yin S., "Fiber Optic Sensors,'' Pennsylvania State University, Pennsylvania, ISBN: 0-8247-0732-X, 2002.

[12] Othonos A., Kalli K., "Fiber Bragg gratings: Fundamentals and applications in telecommunications and sensing,'' Artech House, 1999.

[13] Kashyap R., "Fiber Bragg Gratings,'' 1990.

[14] Roths J., Sudan C., Kuttler R., Gerz C., "High Precision, Low-Cost Interrogation System for Fiber Bragg Grating Sensors,'' Munich University of Applied Sciences, DGaO Proceedings, 2005.

[15] Kreuzer M., "Strain measurement with fiber Bragg grating sensors,'' HBM, Darmstadt, Germany, HBM, Darmstadt, Germany, 2007.

[16] Smartfibres [website]. Avaible: www.smartfibres.com.

[17] Durana G., Kirchhof M., Luber M., Ocáriz I. S., Poisel H., Vázquez C., Zubia J., "Use of a Novel Fiber optical strain sensor for monitoring the vertical deflection of an Aircraft flap,'' IEEE Sensors Journal, Vol. 9, No. 10, 2009.

[18] Mishra V., Singh N., "Optical fiber gratings in perspective of their applications in Biomedicine,'' Central Scientific Instruments Organization, (CSIR), New Delhi, 2011.

[19] Glavind L., Olesen I., Skipper B., Kristensen M., "Fiber-optical grating sensors for wind turbine blades: a review,'' SPIE, Optical Engineering 52(3), 030901, 2013.

[20] Filograno M. L., Corredera P., Rodríguez-Barrios A., Martín-López S., Rodríguez-Plaza M., Andrés-Alguacil A., González-Herráez M., "Real time monitoring of railway traffic using fiber Bragg grating sensors,'' IEEE Sensors J. 12(1), 85–92 (2012).

[21] Vendittozzi C., Sindoni G., Paris C., Marmo P. P., "Application of an FBG sensors system for structural health monitoring and high performance trimming on racing yacht,'' Fifth International Conference on Sensing Technology, 2011.
[22] Lan Yi, "Geothermal Power Plant Monitoring Using FBG Temperature Sensors,'' A Micron Optics Case Study, Taiwan, 2012.

[23] Melle S., Liu K., Measure R., "A passive wavelength demodulation system for guided wave Bragg grating strain sensor,'' IEEE Photonics Technology Letters, vol. 4, no.5, pp.516-518, 1992.

[24] Davis M., Kersey A., "All- fiber Bragg grating strain sensor demodulation technique using wavelength division coupler,'' Electronics Letter, vol.30, no.1, pp. 75-77, 1994.

[25] Davis M., Kersey A., "Matched-filter interrogation technique for fiber Bragg grating arrays,'' Electronics Letter, vol. 37, no. 70, 1995.

[26] Xu M.G., Geiger H., and Dakin J., "Modeling and performance analysis of a fiber Bragg grating interrogation system using an acousto-optic tunable filter,'' Journal of Lightwave Technology, vol. 14, no. 3, 1996.

[27] Kersey A., Berkoff T., and Morey W., “Multiplexed fiber Bragg grating strain-sensor system with a Fabry-Perot wavelength filter,” Optics Letters, vol. 18, pp. 1370–1372, 1993.

[28] Kersey A., Berkoff T., and Morey W., “Fiber optic Bragg grating sensor with drift-compensated high resolution interferometric wavelength shift detection,” Optics Letters, vol. 18, issue 1, pp. 72–74, 1993.

[29] Beller, “OTDRs and backscatter measurements in fiber optic test and measurement,’’ Prentice Hall, 1998.

[30] Anderson R.D., Bell G.F., “Optical Time Domain Reflectometry- OTDR,’’ Tektonix, Inc, Willsonville, Oregon, 1997.

[31] Crunelle C., “Development of quasi-distributed and distributed fiber temperature sensors based on optical reflectometry techniques,’’ Faculté Polytechnique de Mons, 2007.

[32] Zhang P., Nunez H., Qi B., Pickrell G., and Wang A., “Optical time-domain reflectometry interrogation of multiplexing low-reflectance Bragg grating- based sensor system,’’ Optical Engineering, vol.42, no. 6, pp. 1597-1603, 2003.

[33] Valente B., Braga A., Ribeiro A., Regazzi R., Ecke W., Chojetzki C., and Willsh R., “Combined time and wavelength multiplexing technique of optical fiber grating arrays using commercial OTDR equipment,’’ IEEE sensors journal, vol.3, no.1, pp. 31-35, 2003.

[34] Eom T., Kim M., Lee B., and Park I., “Temperature monitoring system based on fiber Bragg grating arrays with wavelength tunable OTDR,’’ IEICE Trans. Electron., vol. E88, no. 5, pp.933-937, 2005.

[35] Zheng J., “Analysis of optical frequency-modulated continuous-wave interference,’’ Applied Optics, vol.43, no.21, pp. 4189-4197, 2004.

[36] Derickson D., Fiber Optic Test and Measurement, Prentice Hall PTR, 1998.

[37] Yüksel K., “Development of an optical frequency domain reflectometer and applications to the interrogation of fiber Bragg gratings,’’ Faculté Polytechnique de Mons, 2011.

[38] Childers B., Froggatt M., Allison S., Moore T., Hare D., Batten C., Jegley D., “Use of 3000 Bragg grating strain sensors distributed on four eight-meter optical fibers during static load test of a composite structure,’’ Proceeding of SPIE vol. 4332, 2001.

[39] Duncan R., Childers B., Gifford D., Pettit D., Hickson A., and Brown T., "Distributed sensing technique for test article damage detection and monitoring,'' Proceeding of SPIE Fiber Optic and Laser Sensors XIV conference, 2002.

[40] Abdi A., "Structural monitoring with fiber Bragg grating strain sensor array and optical frequency domain reflectometry,'' The University of Arizona, 2005.

[41] Richard L., Parker A., Ko W., Piazza A., "Real time in flight strain and deflection monitoring with fiber optic sensors,'' Space Sensor and Measurement Techniques Workshop, 2008.

[42] Igawa H., Ohta K., Kasai T., Yamaguchi I., Murayama H., Kageyama K., "Distributed Measurements with a long gauge FBG sensor using optical frequency domain reflectometry,'' Journal of Solid Mechanics and Materials Engineering, vol. 2, no. 9, 2008.

[43] Hernday P., Fiber Optic Test and Measurement: Polarization Measurements, Chapter 6, Prentice Hall, N. J. 1998.

[44] Rogers A., Essentials of Optoelectronics, Chapman and Hall, 1993.

[45] Azzam R., Bashara N., Ellipsometry and Polarized Light, North- Holland, 1977.

[46] Kumar A., Ghatak A., "Polarization of light with applications in optical fibers,'' Optical Engineering, v. TT90, 2011.

[47] Newport, "Polarization control and measurement for optical fibers,'' Application Note, Spectra Physics, 2004

[48] Linze N., Wuilpart M., Tihon P., Verlinden O., "Design of an optical-fiber accelerometer based on polarization variation due to crushing of the fiber,'' 10th International Conference on Vibration Problems, Springer Proceedings in Physics, Vol. 139, 2011.

[49] Belhadj N., LaRochelle S., Dossou K., "Form birefringence in UV exposed photosensitive fibers computed using a higher order finite element method,'' Optics Express, vol. 12, pp. 1720–1726, 2004.

[50] Erdogan T., Mizrahi V., "Characterization of UV-induced birefringence in photosensitive Ge-doped silica optical fibers,'' Journal of the Optical Society of America B, vol. 11, pp. 2100–2105, 1994.

[51] Bette S., Caucheteur C., Wuilpart M., Megret P., “Theoretical and experimental study of differential group delay and polarization dependent loss of Bragg gratings written in birefringent fiber,’’ Optical Communications, 269, pp. 331-337, 2007.

[52] Wuilpart M., Caucheteur C., Bette S., Megret P., Blondel M., “Polarization properties of uniform fiber Bragg gratings written in highly birefringent fibers.’’ Optical Communications, 247, pp. 239-245, 2005.

[53] Caucheteur C., Bette S., Olcina R., Wuilpart M., Sales S., Capmany J., Megret P., “Transversal strain measurements using the birefringence effect in fiber Bragg gratings.’’ IEEE Photonics Technology Letters, vol. 19, no. 13, 2007.

[54] Murayama H., Kageyama K., Uzawa K., Ohara K., and Igawa H., “Strain monitoring of a single-lap joint with embedded fiber-optic distributed sensors,’’ Structural Health Monitoring, 2011.

[55] Wada D., Murayama H., Kageyama K., Igawa H., Uzawa K., Omichi K., and “Simultaneous distributed measurement of strain and temperature by polarization maintaining fiber Bragg grating based on optical frequency domain reflectometry,’’ Smart Material Structures. 20, 2011.

[56] Wada D., Murayama H., “Analytical investigation of response of birefringent fiber Bragg grating sensors in distributed monitoring system based on optical frequency domain reflectometry.’’ Optics and Lasers in Engineering, 52, pp. 99–105, 2014.

APPENDIX A

COUPLE MODE THEORY

Let us consider a fiber Bragg grating formed within the core of an optical fiber with an average refractive index n_{core}. The refractive index profile along the longitudinal axis of the optical fiber z can be expressed as,

$$n(z) = n_{core}(z) + \delta n(z)\left(1 + \nu(z)cos\left[\frac{2\pi}{\Lambda}z + \phi(z)\right]\right) \qquad (A.1)$$

where

- δn (z) is the average refractive index modulation (typical values lie between 10^{-5} and 10^{-3});
- ν (z) represents the visibility of the interference fringes (0<v<1);
- Λ (z) is the periodicity of the refractive index modulation;
- ø (z) represents the phase variation inside the fiber grating.

Equation (A.1) allows to define different kinds of fiber gratings since the amplitude, periodicity and phase of the refractive index modulation evolve along the grating length.

In the ideal-mode approximation to coupled-mode theory, the transverse component of the electric field assumed as a superposition of the ideal modes labeled j (i.e., the modes in an ideal waveguide with no grating perturbation), so that monochromatic wave equation is mathematically obtained as [1],

$$\vec{E}_t(x,y,z,t) = \sum_j\left[A_j(z)\exp(i\beta_z) + B_j(z)\exp(-i\beta_{z)}\right].\vec{e}_{jt}(x,y)\exp(-i\omega t) \qquad (A.2)$$

where $A_j(z)$ and $B_j(z)$ are slowly varying amplitudes of the j^{th} mode traveling in the +z and –z directions, respectively. The transverse mode fields might describe the cladding or radiation modes.

When the modes are orthogonal in an ideal waveguide, there do not occur energy exchange, the presence of a dielectric perturbation causes the modes to be coupled such that the amplitudes A_j and B_j of the j^{th} mode evolve along the z axis:

$$\frac{dA_j}{dz} = i\sum_k A_k\,(K_{kj}^t + K_{kj}^z)\exp\left[i(\beta_k - \beta_j)z\right] + i\sum_k B_k\,(K_{kj}^t - K_{kj}^z)\exp\left[-i(\beta_k + \beta_j)z\right] \quad (A.3)$$

$$\frac{dB_j}{dz} = -i\sum_k A_k\,(K_{kj}^t - K_{kj}^z)\exp\left[i(\beta_k + \beta_j)z\right] - i\sum_k B_k\,(K_{kj}^t + K_{kj}^z)\exp\left[-i(\beta_k - \beta_j)z\right] \quad (A.4)$$

$K_{kj}^t$are the transverse coupling coefficients between modes j and k can be calculated by using overlapping integrals:

$$K_{kj}^t(z) = \frac{\omega}{4}\iint_\infty dxdy\Delta\varepsilon(x,y,z)\vec{e}_{kt}(x,y).\vec{e}_{jt}^*(x,y) \quad (A.5)$$

where $\Delta\varepsilon$ (x, y, z) is the perturbation of the electrical permittivity. $\Delta\epsilon$ can be approximated to $2n_{core}\delta n$ when $\delta n \ll n_{core}$. The longitudinal coefficients $K_{kj}^z(z)$ are analogous to K_{kj}^t but generally K_{kj}^z (z) $\ll K_{kj}^t(z)$ for fiber modes so that these coefficients are commonly neglected.

In most fiber gratings, the induced refractive index change is approximately uniform across the core and zero outside the core. So the two coupling coefficient, σ stands for the 'DC' coupling coefficient (average over one period) and κ is the 'AC' coupling coefficient are obtained as:

$$\sigma_{kj}(z) = \frac{\omega n_{core}}{4}\delta n_{dc}(z)\iint_{core} dxdy\vec{e}_{kt}(x,y).\vec{e}_{jt}^*(x,y) \quad (A.6)$$

$$\kappa_{kj}(z) = \frac{\nu}{2}\sigma_{kj}(z) = \frac{\omega n_{core}}{4}\delta n_{ac}(z)\iint_{core} dxdy\vec{e}_{kt}(x,y).\vec{e}_{jt}^*(x,y) \quad (A.7)$$

Thus the general coupling coefficient will be defined:

$$K_{kj}^t(z) = \sigma_{kj}(z) + 2\kappa_{kj}(z)\cos\left[\frac{2\pi}{\Lambda}z + \phi(z)\right] \quad (A.8)$$

By this theory, a series of differential equations of the first order presenting the amplitude variation resultant of the mode coupling of the different modes propagating along the optical fiber is obtained. For a uniform fiber Bragg grating which has uniform and periodic perturbation has an analytical solution and occurs coupling between a mode of amplitude A(z) and an identical mode propagating in the opposite direction of amplitude B(z).

As a result of the calculations, the coupled mode theory gives following equations:

$$\frac{dR}{dz} = i\hat{\sigma}R(z) + i\kappa S(z) \tag{A.9}$$

$$\frac{dS}{dz} = -i\hat{\sigma}S(z) - i\kappa R(z) \tag{A.10}$$

Finally amplitudes R(z) and S(z) are defined as:

$$R(z) = A(z)\exp\left(i\delta z - \frac{\emptyset}{2}\right) \tag{A.11}$$

$$S(z) = B(z)\exp\left(-i\delta z + \frac{\emptyset}{2}\right) \tag{A.12}$$

In these equations the parameters are defined by the following relationships:

Self coupling coefficient $$\hat{\sigma} = \delta + \sigma \tag{A.13}$$

AC coupling coefficient $$\kappa = \frac{\pi}{\lambda}\upsilon\delta n \tag{A.14}$$

Tuning rate $$\delta = \beta - \frac{\pi}{\Lambda} = 2\pi n_{eff}\left(\frac{1}{\lambda} - \frac{1}{\lambda Bragg}\right) \tag{A.15}$$

DC coupling coefficient $$\sigma = \frac{2\pi}{\lambda}\delta n \tag{A.16}$$

$$\alpha = \sqrt{\kappa^2 - \hat{\sigma}^2} \tag{A.17}$$

For a uniform fiber Bragg grating, the parameters ˆσ, σ and κ do not depend on the variable z. The system of differential equations is thus solved by specifying appropriate boundary conditions. The first condition considers that the incident light is normalized to 1 so that R(0)=1. The second condition sets S(z)=0 since the backward-going wave does not exist further than the grating length L. With these two conditions, the following results are obtained:

$$R(z) = R(0)\left[\cos(\alpha z) + i\frac{\hat{\sigma}}{\alpha}\sinh(\alpha z)\right] + S(0)i\frac{\kappa}{\alpha}\sinh(\alpha z) \quad \text{(A.18)}$$

$$S(z) = S(0)\left[\cos(\alpha z) - i\frac{\hat{\sigma}}{\alpha}\sinh(\alpha z)\right] - R(0)i\frac{\kappa}{\alpha}\sinh(\alpha z) \quad \text{(A.19)}$$

The amplitude evolution of the incident and reflected waves along the grating can be presented in the matrix form as shown in equation A.20,

$$\begin{bmatrix} R(0) \\ S(0) \end{bmatrix} = \begin{bmatrix} T_{11}\ T_{12} \\ T_{21} T_{22} \end{bmatrix} \begin{bmatrix} R(z) \\ S(z) \end{bmatrix} \quad \text{(A.20)}$$

Elements of transfer matrix are determined as:

$$T_{11} = \cosh(\alpha L) - \frac{i\delta\sinh(\alpha L)}{\alpha} \quad \text{(A.21)}$$

$$T_{12} = -\frac{i\kappa\sinh(\alpha L)}{\alpha} \quad \text{(A.22)}$$

$$T_{21} = \frac{i\kappa\sinh(\alpha L)}{\alpha} \quad \text{(A.23)}$$

$$T_{22} = \cosh(\alpha z) + \frac{i\delta\sinh(\alpha L)}{\alpha} \quad \text{(A.24)}$$

These coefficients of the matrix will help us to determine reflection and transmission coefficients belong to Bragg grating.

APPENDIX B

THEORY OF FMCW INTERFERENCE

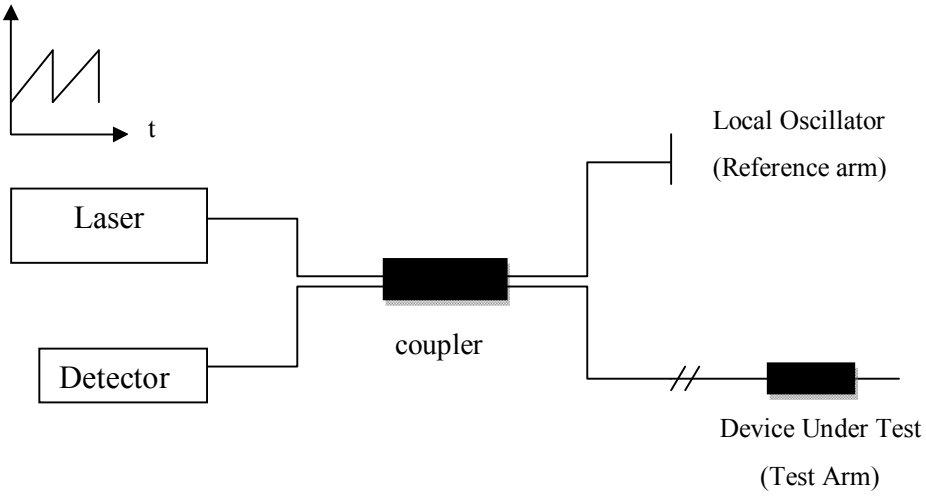

Figure B.1 Basic C-OFDR scheme

As shown in figure probe signal is launched into the system and divided into two optical path as reference and test arm [33].

The probe signal is a continuous wave coming from frequency modulated light source and complex electric field of the probe signal can be expressed as,

$$E(t)=E_0\exp(j\text{ø}(t)) \tag{B.1}$$

where E_0 is the amplitude of electric field and ø(t) is the phase component. The conversion from time domain to wavenumber domain is started with the equation,

$$t = \frac{2z}{v_g} = \frac{2n}{c}z \tag{B.2}$$

where n is the effective refractive index of the optical fiber.

The angular frequency which is the first derivative of phase component is defined as,

$$\omega(t) = \frac{d\phi}{dt} \tag{B.3}$$

$$\omega(z)\frac{2n}{c} = \frac{d\phi}{dz} \tag{B.4}$$

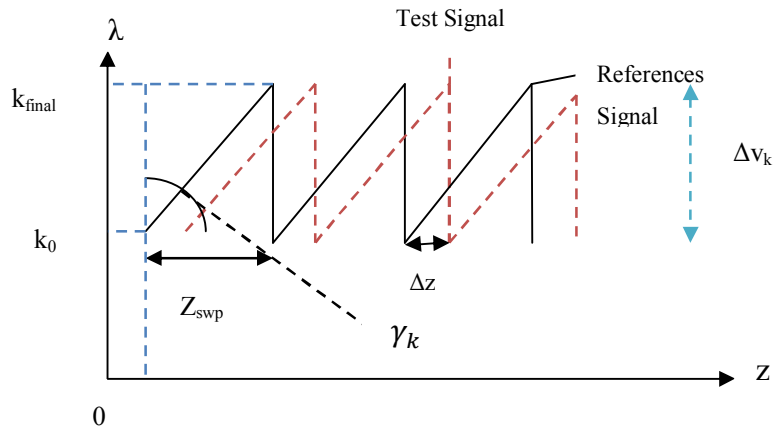

Figure B.2. Test and reference signal interferency scheme

Using sawtooth-wave optical frequency modulated interference which affects the beat term of the interference signal generates periodically ramped waveform due to the two interfering wave's optical frequency [35].

As the angular frequency of the probe signal's optical frequency swept linearly in time and can be expressed as,

$$\omega(t) = 2\pi(\gamma_v t + \omega_0) \tag{B.5}$$

The angular frequency can be written as,

$$\omega(z) = 2\pi(\gamma_k \frac{2nz}{c} + \nu_0) \tag{B.6}$$

where ω_0 is the initial angular frequency, ν_0 is the initial optical frequency and γ_v is the tuning rate in Hz/s and γ_k is the tuning rate in $1/m^2$.

$$\gamma_v = \frac{\Delta\nu}{T_{swp}} \quad ; \quad \gamma_k = \frac{\Delta\nu_k}{Z_{swp}} \tag{B.7}$$

where T_{swp} is the period of modulating signal in time domain and Z_{swp} is the period by means of distance.

So the phase component will be converted as,

$$\emptyset(t) = \int_0^t \omega(u)du + \emptyset_0 \tag{B.8}$$

$$\emptyset(z) = 2\pi \int_0^z \left(\frac{2n}{c}\gamma_k u + \nu_0\right)\frac{2n}{c}du \tag{B.9}$$

Finally the phase will be,

$$\emptyset(z) = \left(\frac{4\pi n^2}{c^2}z^2\gamma_k + \frac{4\pi n}{c}\nu_0 z\right) \tag{B.10}$$

So the electric field of reflected signal from local oscillator ($E_{ref}(z)$) is expressed as,

$$E_{ref}(z) = E_{0ref}\exp\left(j\emptyset(z)\right) \tag{B.11}$$

$$E_{ref}(z) = E_{0ref}\exp\left(\left(\frac{4\pi n^2}{c^2}z^2\gamma_k + \frac{4\pi n}{c}\nu_0 z\right)\right) \tag{B.12}$$

The electrical field of reflected signal from device under test (from discrete reflections- $E_{test}(z)$) is expressed as,

$$E_{test}(z) = E_{0test}\exp\left(j\emptyset(z-L)\right) \tag{B.13}$$

$$E_{test}(z) = E_{0test}\exp\left(\left(\frac{4\pi n^2}{c^2}(z-L)^2\gamma_k + \frac{4\pi n}{c}\nu_0(z-L)\right)\right) \tag{B.14}$$

The intensity of interference signal computed at the detector is the sum of individual electrical fields and can be defined as,

$$D(z) = \left|E_{ref}(z) + E_{test}(z)\right|^2 \tag{B.15}$$

$$D(z) = \left[E_{ref}(z) + E_{test}(z)\right]\left[E_{ref}(z) + E_{test}(z)\right]^* \tag{B.16}$$

The obtained interference signal can be described as,

$$D = \cos\left(2n_{eff}kL\right) \tag{B.17}$$